



Departament d' Enginyeria Química
Escola Técnica Superior d'Enginyeria Química
Universidad Rovira i Virgili

ENGINEERING BIOCOMPATIBLE SURFACES FROM THE NANO TO THE MICRO SCALE

Presented by Verónica Saravia Silvera

ENGINEERING BIOCOMPATIBLE SURFACES FROM THE NANO TO THE MICRO SCALE

Thesis committee:

Prof. Azadel Fabregat
Universitat Rovira i Virgili, Spain

Prof. Ricard Garcia Valls
Universitat Rovira i Virgili, Spain

Prof. Radostina Georgieva
Le Charite, Germany

Dr. Torsten Reese
Centro de Investigación Cooperativa en Biomateriales (CICbiomaGUNE), Spain

Dr. Jaume Folch
Universitat Rovira i Virgili, Spain

External evaluators (requirement for the mention of “European Doctor”):

Dr. Rumen Krastev
Max Planck Intitute of Colloids and Interfaces, Germany

Dr. Kathryn Melzak
University of Crete, Greece

Thesis advisors:

Dr. Susana Rodriguez Couto
Universitat Rovira i Virgili, Spain

Dr. José Luis Toca Herrera
Centro de Investigación Cooperativa en Biomateriales (CICbiomaGUNE), Spain

Dr. Petros Lenas
Universidad Complutense de Madrid, Spain

Els signants fem constar que el present treball que porta per títol:

Engineering biocompatible surfaces from the nano to the micro scale,

i que presenta na Verónica Saravia Silvera per optar al grau de Doctora per la Universitat Rovira i Virgili, ha estat realitzat sota la nostra direcció i que tots els resultats presentats i la seva anàlisi són fructu de la investigació realitzada per l'esmentada doctoranda.

I perquè s'en prengui coneixement i tingui el efects que correspongui, signem aquest certificat.

Dr. Susana Rodríguez-Couto
Universidad Rovira i Virgili
Tarragona

Dr. José Luis Toca-Herrera
CICbiomaGUNE
San Sebastián

Dr. Petros Lenas
Universidad Complutense
Madrid

Tarragona, 9 de julio de 2008

Acknowledgement/Agradecimientos

First of all, I would like to thank the members of the panel, Dr. Azael Fabregat, Dr. Ricard Garcia, Dr. Radostina Georgieva, Dr. Torsten Reese, and Dr. Jaume Folch, and the external evaluators Dr. Kathryn Melzak and Dr. Rumen Krastev.

Ahora repasando estos años de doctorado, tengo mucha gente a la que agradecer, ya que entre tantas idas y venidas... muchos me han ayudado. En primer lugar, me gustaría agradecerle a mis supervisores: a Petros por mostrarme el mundo de la ingeniería de tejidos, el que desconocía y que no dejará de fascinarme, y por su apoyo incluso desde Madrid; a José por permitirme continuar con el doctorado, trabajando y colaborando con centros de primer nivel, y especialmente en esta última fase por las “aclaradoras” conversaciones, ayuda y paciencia; y a Susana por permitirme colaborar en sus proyectos y darme la tranquilidad que necesitaba para culminar el doctorado.

Haciendo un repaso cronológico... durante los primeros años estuve fundamentalmente en el laboratorio de Bioquímica en Reus, gracias al apoyo del Dr. Paternáin, trabajando especialmente con Jaume, al que tengo que agradecer su ayuda e interés (hasta último momento!). Además en la facultad conocí muchos colegas que me hicieron muy fácil el trabajar por allí. En Tarragona, un “muchas gracias” a toda la gente del BBG, NBG y especialmente en el Servei de Recursos Científic a Mercè y a Mariana por su apoyo durante largas horas de AFM y SEM. No quiero olvidarme de mencionar a la Dra. Anna Ardèvol e Isabel Quesada, que me socorrieron cuando me quedé sin células con las que trabajar.

Agradezco al Dr. Andreas Fery por darme la oportunidad de trabajar e integrarme en su grupo de investigación en el MPI.

Fuera del laboratorio, imposible olvidarme de Nuria Juanpere, siempre con paciencia contestando las preguntas y solucionando los problemas, incluso esos de último momento y sin dejar de lado la amabilidad.

Y por último, lo fundamental, la amistad de los colegas del doctorado de la URV, del MPI, del CICBiomaGUNE (especialmente la segunda planta), Laura G, Irama, Laura P, Mihaela, y la incondicional compañía de mi familia.

Abstract

Different surfaces with defined functionalities have been constructed with synthetic polyelectrolytes, using the layer-by-layer technique and soft lithography. At the nanoscale, an enzyme (laccase) was covalently immobilised on a gold/PEI/GA layer, preserving its activity. The immobilisation was studied with a quartz crystal microbalance with dissipation monitoring and its activity assayed with a spectrophotometer.

Besides, bacterial proteins (SbpA, SbpA-EGFP and SbpA-STV) were adsorbed on polyelectrolytes multilayers. The combination of soft-lithography with a protein resistant polyelectrolyte (PLL-g-PEG) led to the construction of micro-structured surfaces of functional bacterial proteins. Surface wettability, fluorescence and atomic force microscopy (AFM) were used to characterise those interfaces.

Increasing the complexity, attachment of HepG2 cells on polyelectrolytes was studied. Cell adopted different morphologies depending on the hosting underlying polyelectrolyte as observed by transmission, scanning electron and atomic force microscopes. The adhesion and spreading of the cells that were monitored with QCM-D and transmission microscopy, and assayed with crystal violet, showed a higher affinity of the cells toward the adlayer formed on PEI, PAH and PLL in comparison with PSS and PLL-g-PEG. Force spectroscopy studies with AFM showed higher repulsion between PSS surfaces and the cell surface, and different local cell mechanical properties between cells attached to PEI and PSS.

Resumen

Las interfases juegan un papel relevante en la mayoría de los fenómenos científico-técnicos. A modo de ejemplo, la catálisis, los procesos electroquímicos como corrosión, el auto-ensamblaje de proteínas, y la estimulación celular, ocurren en interfases. En los últimos años, grandes progresos en la capacidad de diseñar y caracterizar las interfaces, han contribuido significativamente en el desarrollo de nuevos materiales.

En particular, la ingeniería de biomateriales busca obtener materiales biológicamente activos, ajustando las propiedades químico-físicas (y topográficas) de la superficie de interés. Esto incluye la incorporación de (biomacro)moléculas tales como proteínas, polisacáridos, lípidos, o polímeros sintéticos, generalmente a través de procesos de adsorción física, de interacciones específicas o de enlace covalente. Uno de los desafíos más importantes en la bioingeniería es la fabricación de estructuras supramoleculares regulares que incluyan biomoléculas que preserven su actividad.

Un método para construir estructuras supramoleculares, es el de adsorción capa tras capa. Esta técnica se basa en la adsorción alternada de macromoléculas de carga opuesta. La técnica permite el control nanométrico en el eje vertical, sin embargo otras técnicas se deben usar para manipular la estructura superficial (ejes x e y). Una alternativa posible es utilizar litografía blanda, un método que se usa actualmente para transferencia de biomoléculas sobre superficies siguiendo estructuras geométricas. Ambos métodos, capa tras capa y litografía blanda, se pueden combinar para construir superficies microestructuradas con una química superficial definida.

La absorción de proteínas en interfaces es un tema muy importante en bioingeniería y en medicina. Las proteínas son la maquinaria principal de muchos procesos en la naturaleza, realizando funciones protectoras, de catálisis y reconocimiento específico. Se sabe que las proteínas pueden desnaturalizarse cuando se adsorben en las superficies, perdiendo su funcionalidad biológica.

Considerando la adsorción de proteínas, las proteínas bacterianas S, son sistemas muy interesantes ya que se auto-ensamblan formando cristales en 2-D sobre muchos tipos de superficies. La proteína S (nativa) sirve de capa protectora ya que forma parte de la pared celular de las bacterias. Una importante ventaja biotecnológica que presentan, es la posibilidad de fusionarla con otras biomoléculas. En la última década, se han invertido esfuerzos en desarrollar proteínas S de fusión a través de la ingeniería de

proteínas. Varias proteínas S de fusión se han obtenido, por ejemplo: proteína fluorescente verde (SbpA-EGFP), con estreptavidina (SbpA-STV), entre otras, que se utilizan actualmente como material base para la fabricación de biosensores.

Las lacasas, son enzimas que catalizan la oxidación de un gran número de polifenoles y sustancias aromáticas. La importancia de esta enzima está en su amplia aplicación a diferentes sectores industriales relacionados con la alimentación, papel y textil. Además, se debe resaltar que más recientemente se ha reportado la aplicación de la lacasa en el desarrollo de biosensores, lo que requiere una alta actividad, estabilidad y reproducibilidad en la inmovilización. La adsorción inespecífica y el enlace covalente son algunos de los métodos que se han usado para la inmovilización de la lacasa con diferentes grados de eficiencia. La inclusión de la lacasa en multicapa de polielectrolitos ha sido propuesta con el fin de incrementar la estabilidad conformacional y actividad.

De la capacidad para generar superficies biocompatibles depende asimismo el éxito de la terapia en la medicina regenerativa, en la que la interacción célula-superficie y el crecimiento celular sobre dichas superficies son aspectos científico-tecnológicos cruciales. En la adhesión celular intervienen interacciones del tipo inespecífico (electrostáticas y de van der Waals) e interacciones específicas (por ejemplo mediadas por integrinas). La fuerza de adhesión celular está íntimamente relacionada con interacción entre el receptor y el cito-esqueleto. Las interacciones mediadas por integrinas inducen la formación de contactos focales, lo que lleva a que la célula se extienda sobre la superficie y a cambios en el cito-esqueleto, lo que afecta sus propiedades mecánicas.

La línea celular hepática cancerosa, HepG2, se ha empleado en estudios relacionados con el cáncer, así como en estudios de citotoxicidad e incorporación en dispositivos extracorporales para suplir funciones hepáticas, ya que a pesar de su transformación mantienen ciertas funciones de los hepatocitos normales. Debido a esto, incrementar el conocimiento de cómo reaccionan estas células frente a distintos sustratos, es relevante por ejemplo, para su incorporación en distintos dispositivos.

En este trabajo se han generado superficies biocompatibles con interfases en las que se inmovilizó lacasa y se adsorbieron proteínas (de fusión) bacterianas.

En primer lugar, la inmovilización de la lacasa, consistió en unirla covalentemente a un sustrato formado por capas de oro/poli(etilénimina)/glutaraldeído. Se demostró que la enzima conserva su actividad catalítica en la presencia de ABTS. Posteriormente a la

inmovilización se adsorbió PAH y PSS sobre la enzima. Sin embargo, el efecto del polielectrolito sobre su actividad es todavía una pregunta abierta que se abordará en trabajos futuros, ya que el ABTS también interacciona con los polielectrolitos.

Se usó litografía blanda para construir superficies estructuradas, en las que se adsorbieron proteínas (de fusión) S, generando superficies funcionales en escala nanométrica dentro de microestructuras. Esto se pudo realizar utilizando un polielectrolito que contiene PEG. Se utilizaron tres tipos de proteína bacteriana, cada uno de ellos con distintas propiedades biológicas. La proteína SbpA que actúa como en la naturaleza como barrera protectora manteniendo la forma de la bacteria (y también como superficie antibacteriana) mantiene su estructura cristalina (similar a la que se encuentra en la bacteria). La segunda proteína es recombinante, rSbpA-EGFP, mantiene su fluorescencia después de adsorberse en la superficie estructuradas, como se observó por microscopía de fluorescencia. Finalmente, el heterotetrámero de proteína S con estreptavidina (rSbpA-STV) mantuvo la afinidad específica por la biotina. Se debe destacar que la posibilidad de manipular la distribución de la proteína en escala micro es un requerimiento básico para el desarrollo de biosensores.

En lo que se refiere a la interacción célula/superficie, se encontró que las células HepG2 adoptan diferente morfología dependiendo de sustrato al que se adhieren. Mientras polielectrolitos positivos (PEI, PAH, PLL) adsorben moléculas que inducen la expansión celular, PLL-g-PEG (interfase neutra e hidrofílica) y PSS (polielectrolito negativo) no favorecieron la expansión celular. Aprovechando la baja afinidad celular del PLL-g-PEG, y combinándolo con la afinidad las técnicas de estructuración de superficies, fue posible confinar la adhesión y crecimiento de las células a diseños transferidos al sustrato.

El proceso de adhesión celular fue seguido en función del tiempo con QCM-D y microscopía de transmisión, y testado con cristal violeta. Una interesante pregunta que deber ser investigada en el futuro es la relación entre la carga superficial y los puntos de adhesión local. Por ejemplo, medidas de QCM-D revelan que las células no son detectadas cuando se depositan sobre PSS (lo opuesto sucede cuando se adhieren sobre PEI) aunque se mantiene adheridas.

AFM complementa el estudio y confirma que las células se extienden sobre PEI, presentando una altura máxima de aproximadamente 9 μm , mientras que la forma redondeada de las células sobre PSS mantienen una altura máxima de 12 μm . Esto se reflejó también en las propiedades mecánicas de la célula, las células sobre PSS son más

“blandas” que las células que crecen sobre PEI. Finalmente, la funcionalización de las puntas de AFM con polielectrolitos mostró que las puntas recubiertos con PSS experimentaron una repulsión mayor que los recubiertos con PEI cuando se aproximaban a la superficie celular. Se encontró que la máxima adhesión de las puntas del AFM a la superficie celular es independiente de la carga aplicada y de su recubrimiento, para un tiempo nulo de residencia de la punta sobre la superficie celular. La máxima adhesión observada fue de 750 pN para un tiempo de residencia de residencia de 3 s.

Algunas preguntas permanecen abiertas en lo que se refiere a la ingeniería y al nano-control de las biosuperficies, así como las propiedades mecánicas y manipulación celular. Este trabajo muestra que proteínas funcionales pueden depositarse sobre superficies que no impiden su funcionamiento biológico. Un desafío futuro en esa dirección es la manipulación de proteínas y deposición de péptidos para alcanzar diferente funcionalidad en la misma superficie. Queda mucho trabajo por realizar en relación con las propiedades mecánicas de la célula, ya que no hay un modelo físico claro que lo aborde sin excesivas simplificaciones. Otra pregunta ambiciosa por investigar es la conexión entre la mecánica celular y el ciclo de vida celular.

Table of contents

ABSTRACT	VIII
RESUMEN	IX
TABLE OF CONTENTS	XIII
ABBREVIATIONS	1
CHAPTER I	3
<i>INTRODUCTION</i>	3
I.1. BACKGROUND INFORMATION	3
I.2. SURFACE CHEMISTRY MODIFICATION	4
I.3. SURFACE PATTERNING	5
I.4. PROTEINS AT INTERFACES	6
<i>I.4.1. Bacterial proteins</i>	7
<i>I.4.2. Laccase</i>	8
I.5. CELL-SURFACE INTERACTION	9
I.6. OBJECTIVE AND OUTLINE	10
CHAPTER II	13
<i>MATERIALS AND METHODS</i>	13
II.1. MATERIALS	13
<i>II.1.1. Substrates</i>	13
<i>II.1.2. Coating materials</i>	13
<i>II.1.3. Microcontact printing materials</i>	15
<i>II.1.4. Biomolecules</i>	15
<i>II.1.5. Buffers and solutions</i>	17
II.2. METHODS	17
<i>II.2.1. Layer-by-layer coating</i>	17
<i>II.2.2. Surface patterning: PLL-g-PEG microcontact printing</i>	18
<i>II.2.3. Protein immobilisation</i>	19
II.2.3.1. Bacterial protein	19
II.2.3.2. Laccase	19
II.3. BIOMOLECULE ASSAYS	19
<i>II.3.1. Protein assay</i>	19
<i>II.3.2. Laccase activity</i>	19
II.4. INSTRUMENTAL TECHNIQUES	20
<i>II.4.1. Microscopy</i>	20
II.4.1.1. Bright field microscopy and phase contrast	20
II.4.1.2. Fluorescence microscopy	20
II.4.1.3. Scanning electron microscopy (SEM)	22
II.4.1.4. Atomic force microscopy (AFM)	23
<i>II.4.2. Contact angle measurements</i>	24
<i>II.4.3. Visible-UV spectrophotometer</i>	25
<i>II.4.4. Quartz crystal microbalance</i>	25
II.5. CELL CULTURE TECHNIQUES	27
<i>II.5.1. Cell culture</i>	27
II.5.1.1. Cells	27
II.5.1.2. Chemicals	27
II.5.1.3. Culture conditions	28
<i>II.5.2. Protocols</i>	28
II.5.2.1. Cell defrost	28
II.5.2.2. Cell frost	28
II.5.2.3. Subculture	29
II.5.2.4. Direct cell count with trypan blue	29
II.5.2.5. Viability with tetrazolim salt (MTT)	29
II.5.2.6. Cell attachment with crystal violet	30

CHAPTER III	31
<i>BUILDING FUNCTIONAL SURFACES</i>	31
III.1. INTRODUCTION.....	31
III.2. RESULTS.....	34
III.2.1. <i>Polyelectrolyte multilayer assembly</i>	34
III.2.2. <i>Contact angle</i>	36
III.2.3. <i>Polyelectrolyte patterning</i>	37
III.2.4. <i>Surface functionalisation</i>	37
III.2.4.1. <i>Laccase immobilisation and interaction with polyelectrolytes</i>	37
III.2.4.2. <i>S-layer proteins patterning on polyelectrolyte multilayers</i>	42
III.2.4.3. <i>Cell culture on polyelectrolyte multilayers</i>	45
III.2.4.4. <i>Cell patterning</i>	46
III.3. DISCUSSION.....	47
III.3.1. <i>Protein adsorption on polyelectrolyte multilayers</i>	47
III.3.2. <i>Laccase immobilisation and interaction with PEs</i>	49
III.3.3. <i>Patterning of SbpA and fusion proteins by polyelectrolyte microcontact printing</i>	50
III.3.4. <i>Cell culture on PE and patterning</i>	52
III.4. CONCLUSION	52
CHAPTER IV	55
<i>CELL INTERACTION WITH BIOCOMPATIBLE SURFACES</i>	55
IV.1. INTRODUCTION.....	55
IV.2. RESULTS.....	57
IV.2.1. <i>Cell viability</i>	57
IV.2.2. <i>Cell shape changes with time</i>	58
IV.2.3. <i>Cell adhesion vs time</i>	60
IV.2.4. <i>QCM-D: Frequency and dissipation change vs. time</i>	61
IV.2.5. <i>QCM-D with window chamber</i>	66
IV.3. DISCUSSION.....	68
IV.4. CONCLUSION	75
CHAPTER V	77
<i>AFM PROBING SURFACE-CELL INTERACTIONS AND MECHANICAL PROPERTIES</i>	77
V.1. INTRODUCTION.....	77
V.2. RESULTS.....	80
V.2.1. <i>Measurements with Si₃N₄ tip</i>	80
V.2.2. <i>Tip functionalised with PEs</i>	85
V.3. DISCUSSION.....	92
V.4. CONCLUSION	94
CHAPTER VI	95
<i>CONCLUSION AND OUTLOOK</i>	95
REFERENCES	97
CURRICULUM VITAE	107

Abbreviations

- AFM- Atomic force microscopy
ABTS- 2,2'-azino-bis-(3-ethylbenzothiazoline-6-sulphonic acid)
BSA- Bovin serum albumin
DMEM- Dulbecco's Modified Eagle's Medium
DMSO- Dimetilsulfoxide
DUV- Deep ultraviolet
ECM- Extra-cellular matrix
FBS- Foetal bovine serum
FITC- Fluorescein Isothiocyanate
GA- Glutaraldehyde
LbL- Layer-by-layer
Mw- Molecular weight
MTT- Methylthiazol tetrazolim salt
PEs- Polyelectrolytes
PAH- Poly(allylamine hydrochloride)
PBS- Phosphate buffer solution
PEI- Poly(ethylenimine)
PEM- polyelectrolyte multilayer
PLL- Poly(l-lysine)
PLL-g-PEG- Poly(l-lysine)-graft-(polyethyleneglycol)
PDMS- Polydimethylsiloxane
PR- Photo resistant material
PSS- Poly(sodium 4-styrenesulfonate)
QCM-D- Quartz crystal microbalance with dissipation monitoring
SbpA- S-protein from *Bacillus sphaericus* CCM 2177
SbpA/EGFP- Recombinant S-layer green fluorescent fusion protein
SbpA/STV- Tetramer streptavidin S-layer fusion protein
SEM- Scanning electron microscopy
STV- Streptavidin
TRITC- Tetramethyl Rhodamine Iso-Thiocyanate
 μ CP- Microcontact printing

Chapter I

Introduction

I.1. Background information

Surfaces and interfaces play an important role in a wide variety of phenomena, such as catalysis, electrochemical process, and cell signalling [1; 2]. Therefore in the last years, a dramatic progress in the ability to tailor and characterise surfaces, has significantly contributed to the development of Biomaterials and Surface Science, allowing the fabrication of new materials with defined interfacial properties down to the nanoscale.

The fact that most biological reactions occur at interfaces shows that nature evolved in such a way that molecular systems take advantage of surfaces. Some of those advantages are that surfaces provide high accessibility and high surface area geometries to enhance reaction rates. Besides, the formation of unique microenvironments can enhance specific affinities and reactions. Also, the mobility in the plane has low energy barriers what can facilitate complex reactions such as clustering and conformational changes. In addition, surface energy minimisation can orient specific structures to interfaces, and self-assembly processes on surfaces not only can orient but also space molecules with precision. Finally, molecular recognition is readily implemented at surfaces [2]. Furthermore, nature holds the largest knowledge about hierarchical supramolecular structures, making it a source of inspiration for new design strategies. This is the reason why many scientist are trying to discover and/or mimic the procedures that govern self-assembly in nature, in order to develop new materials with biotechnological activity [3].

Current surface biological technology applications involves among others implant biomaterials, affinity chromatography, surface diagnostics, cell culture surfaces and biosensors development [2].

One of the important challenges in surface bioengineering is the fabrication of robust and regular supramolecular structures, tuning the chemical and topographical properties

of the surface, in order to include functional biomolecules, which preserve their activity and/ or induce the desired biological process.

I.2. Surface chemistry modification

Building supramolecular structures with a bottom-up approach has been possible due to the ability to successively incorporate molecules on surfaces. Besides, the incorporation of not only natural (proteins, phospholipids) but also synthetic molecules (silanes, thiols, and dendrimers) has allowed building systems with original properties.

A mayor advance in material fabrication technology has been the development of self-assembly methods. Self-assembly on solid surfaces has been observed for phospholipids [4], silanes [5], n-alkyl thiols [6], proteins [7] and polyions multilayer systems[8]. These resulting surfaces provide well-defined structures that can be ordered or not, with defined chemistries that can be systematically varied. Therefore, they can be used as platforms to incorporate biomolecules. The immobilisation of biomolecules can be done by non-specific adsorption or covalent immobilisation, but with little control on the superficial distribution, orientation or activity. Other option is the immobilisation through specific interaction such as with: antibodies, histiding tag, or biotin/streptavidin, which improves the control of orientation and activity [2].

A method to build supramolecular structures in a bottom-up step fashion, which has been widely used in the laboratory during the last decade, is the layer-by-layer technique (LbL) [9; 14]

This technique is based on the alternate adsorption of oppositely charged macromolecules (and the entropy gain through ion release, after the layer adsorption) as shown in figure I-1. Up to date, polyelectrolytes have been the principal building blocks of LbL technique, although there should be no restriction in applying such procedure to other molecules. It has been found that different parameters, such as polymer molecular weight and concentration, ionic strength, surface and polymer charge density, influence the building-up of the polyelectrolyte multilayer. The LbL technique has served to get insight about different scientific and technological issues: in 2-D as support for protein recrystallization [15], for enzyme protection [16; 17], trapping of magnetic particles [18], and in 3-D in drug delivery systems [19].

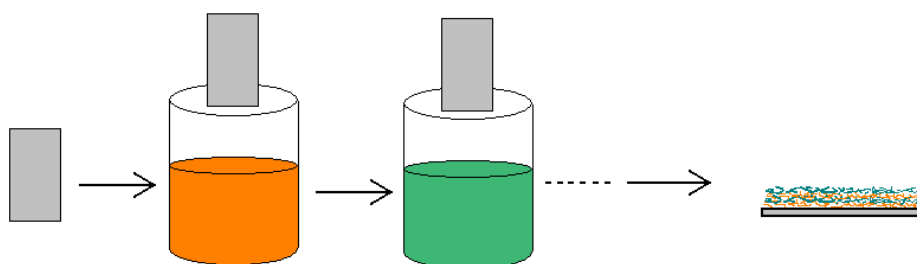


Figure I-1: Scheme of the procedure to build a multilayer with the layer by layer technique. The alternate adsorption of oppositely charged macromolecules results in a polyelectrolyte multilayer which surface properties mostly depend on the last adsorbed layer.

The LbL technique permits nanometrical control in the vertical axis. However, other approaches should be used to be able to manipulate the surface structure (x and y axis).

I.3. Surface patterning

The importance of being able to selectively distribute different functionalities on a surface is not only relevant to basic studies (e.g. cell behaviour is determined by surface chemistry and geometry) but also technological (production of high-through-put-arrays and biosensors).

Among the most used methods are photo-lithography and soft-lithography. The photo-lithography process involves the spin coating of a thin layer of UV-sensitive polymer called photoresistant (PR) on the substrate, followed by the surface irradiation with UV light through a mask and the PR development. The deposition of a layer of a bioactive molecules or the etching of the exposed substrate, followed by the PR lift off, unmask the protected areas and thus a pattern surface is obtained [20]. The application of the basic idea of photolithography is not restricted to the change of properties of a photoresistant materials, it can also be used to create patterns due to the modification UV chemical labile species that can be activated upon UV irradiation to bind target molecules or to de-active by DUV [21; 22]. In general those technologies require the use of expensive-clean room facilities, and sometimes are not suitable for biomolecules [23].

Soft lithography on the contrary is more biocompatible, and it covers a number of techniques with the common feature that at some stage of the process an elastomeric (“soft”) material is used to create the chemical structures [23].

Microcontact (μ CP) is part of this family. μ CP is a simple and cost-effective method, which neither requires clean room facilities nor absolutely flat surfaces. It is flexible with regards to both the choice of substrate and material to be transferred during imprinting, and it offers a way to create complex patterns (yet with some geometrical constraints) on surfaces [24; 25]. Besides, μ CP does not harsh chemically or physically the sample of interest. All printing take place in ambient conditions, and all post-printing steps occur in aqueous solutions that do not change the physicochemical state of the biomolecules [26]. In the process, an elastomeric stamp is formed by casting a polymer, (poly-dimethyl siloxane, PDMS) over a microstructured master. After curing, the stamp is removed. PDMS stamp can be used directly after peeling, or it can be modified to make its surface hydrophilic depending on the molecule to be pattern. The next step is the inking of the stamp, which is followed by the actual stamping procedure. The final step is generally the backfilling of the non-stamp areas with a second molecule. Optionally the stamped backfilled surface can be further modified. A wide variety of molecules have been patterned with microcontact printing, such as thiols, phospholipids, proteins, and polyelectrolytes [27; 28; 29; 30]. It should be pointed out that both methods, LbL and μ CP, can be combined to build microstructured surfaces with a defined chemistry [31].

I.4. Proteins at interfaces

Proteins are the main machinery of nature, performing or mediating different functions such as protective sieves, catalysis, and specific recognition [32]. It is known that proteins tend to denature when adsorb on surfaces, losing their biological function. The main challenge in bioengineering is the fabrication of surfaces that preserve protein functionality.

The fact that the protein surface is complex (hydrophobicity and charge) complicates the prediction of how a protein will interact with a substrate. Several studies reported that surface energy influences protein adsorption: proteins adsorb easily on hydrophobic

surfaces [33]. Norde suggested that proteins also might adsorb on surfaces due to an increase in entropy caused by a loss in protein's secondary structure [33]. He also pointed out that external protein residues are the ones that most likely interact with the solid surface, although interior groups might be exposed through conformational changes.

As mentioned before, different protein immobilization processes can be applied by tuning the surface chemistry, depending on the protein and its function.

1.4.1. Bacterial proteins

Bacterial S-layers are commonly found at the outermost cell envelope of prokaryotic organism, and have the ability to assemble into monomolecular arrays on the supporting envelope layer. In bacteria, they act as protective coats, molecular sieves, ion traps, and structures involved in cell surface interactions (in some *archaea* were identified as contributor to virulence when presented on pathogens cell wall). They are generally composed of a single protein with a molecular mass ranging from 40-170 kDa. It has been demonstrated that during bacterial growth, the surface properties of the protein subunit (charge distribution, hydrophobicity, specific interactions with components of the supporting envelope) direct the correct orientation during the replenishment of the S-layer in the lattice. S-layers usually are not covalently attached to the cell surface, so they are isolated in the presence of dissociating agents [34]. After extraction and purification, S-proteins are very interesting systems since they also self-assemble forming 2-D crystals (S-layers) on many type of surfaces as shown in figure I-2 [35], varying crystal domains size, protein layer thickness and surface electrical properties [36]. Interesting wise is that the driving force is different for every surface, e.g. they recrystallise on hydrophilic mica [37] on anionic polyelectrolyte [15] and also on hydrophobic terminated thiols [36]. Thus, the self-assembly mechanism is still not well understood, and may act as a paradigm for theoretical protein adsorption predictions. An important biotechnological advantage of bacterial S-proteins is that they can be fused with other biomolecules maintaining their functionality. In the last decade research has been devoted to the development of S-fusion proteins by means of protein engineering.

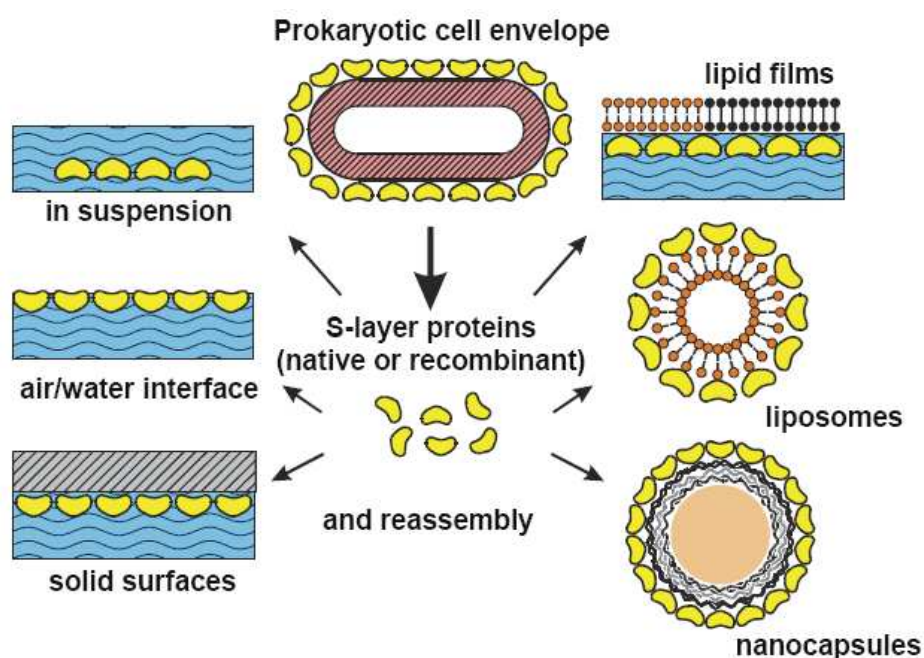


Figure I-2: Bacterial proteins monomers are capable of self-assemble on different interfaces (reproduced from [38]).

Several S-layer fusion proteins have been made, e.g. enhanced green fluorescent protein (EGFP) [39], streptavidin (STV) [40], the chain camel antibody (cAb-Lys3) [41], Fc-binding Z-domains [42] and birch pollen allergen (Bet v1) [43]. These proteins are currently used as building blocks for biosensor fabrication at nanoscale.

1.4.2. Laccase

Laccases, are copper containing redox enzyme, that belong to a small group denominated blue oxidases [44]. Laccases catalyse the oxidation of a broad range of polyphenols and aromatic substrates with the concomitant reduction of oxygen to water [45]. Most laccases have four copper atoms that are distributed in different binding sites, and play an important role in the enzyme catalytic mechanisms. In a typical laccase reaction, a phenolic substrate is oxidised giving rise to an aryloxyradical, which is converted to a quinone in a second oxidation stage. The quinone and the free radical undergo non-enzymatic coupling reactions leading to polymerization [44].

Laccases are produced by a wide variety of microorganisms, specially fungi and some bacteria [44] as an extracellular enzyme. The importance of this enzyme can be stated

by its application in different industrial sectors such as pulp, paper, textile and petrochemical industries mainly in waste-water treatments, and also for soil contamination due to herbicides and pesticides. Besides its use in cosmetics, chemical synthesis and biosensor have been reported [46]. The application in biosensor development requires an immobilization procedure yielding an active and stable enzyme in a reproducible way. Adsorption and covalent binding are some of the methods used for laccase immobilisation, with different degrees of efficiency. Specially for biosensor development, cross linked laccase crystals [47] and covalent immobilization on self-assembly monolayer of DSP:C4SH (Dithio-bis(succinimidyl propionate):(butanethiol) on gold, are two successful methods for its immobilization [48].

1.5. Cell-surface interaction

Understanding how surface chemistry and material structure can be used to control cell adhesion is a major aim for the development of biocompatible material for implants and in regenerative medicine. A central goal of modern bioengineering is the development of biomaterial that directs the biological healing response, leading not to isolation but to integration. These materials would interact with cells through a well-defined array of bio-recognition sites designed to direct cells behaviour through the desired cellular pathways of healing. The structure and function of many biological receptors have been determined along with their mechanism of cell binding and activation [2]. Receptor-mediated cell adhesion is an essential component of many biological responses including growth, differentiation, and motility [49].

The first step for cell-surface interactions is driven by non specific interaction (electrostatic, van der Waals). Once the cell is close enough to the surface, depending on the characteristic of the surface, specific interactions can mediate cell/surface interaction [50; 51]. Specific cell/substrate interactions are mediated by cell membrane bound receptors, in particular integrins, a family of heterodimeric transmembrane proteins that are linked to the cytoskeleton on the cytoplasmatic side of the membrane. Adhesion strength is closely related to receptor-cytoskeleton coupling. The integrins establish a mechanical link not only between the membrane and the ECM substrate but also between the ECM and the cytoskeleton [23]. Besides, interactions mediated by integrins lead to the formation of focal adhesion complexes (FAC), which induce

spreading and changes in the cytoskeleton of the cells. The mechanical tension between the various interconnected assemblies in the extracellular matrix and the cytoskeleton play an important role in determining cell shape and structure [52].

An integrating understanding of cell structure and mechanics is necessary for elucidating many fundamental aspects for cell behavior, from motility to differentiation and development. The cytoskeleton, a biopolymer network formed by filamentous actin, intermediate filaments and microtubules, together with filament cross-linker, motor and regulatory proteins determine the mechanical properties of cells [53]. Several approaches to model the cell structure have been proposed. The continuum approach treats the cell as comprising materials with certain continuum material properties. Even when it does not provide insight into detailed molecular mechanical events, it is a simple approach and more straightforward to use in computing mechanical properties of the cells if the biomechanical response at the cell level is what is needed [54].

HegG2 cell line is an hepatoma cell line that has been used for cancer research [55; 56; 57]. These cells maintain part of the normal metabolic capacity of hepatocytes, what make them a useful tool for high-throughput in vitro toxicity assays, as well as in the development of bioartificial livers [58; 64].

1.6. Objective and outline

In this PhD thesis we have engineered biocompatible surfaces using the layer-by-layer technique and soft-lithography. This simple approach permitted to functionalise surfaces from the nano to the micro scale. At nanoscale, four different proteins were adsorbed (recrystallized) on patterned polyelectrolyte surfaces preserving their functionality. The transition to micro scale was carried out by increasing the complexity of the system through adsorption of cells. Although the cells adopted different shapes depending on the host surface, cytotoxicity studies revealed that they were alive showing different mechanical properties in a first approximation.

Briefly, Chapter 2 contains all the relevant information about the experimental procedures. Chapter 3 is devoted to protein adsorption on planar and (patterned) polyelectrolyte surfaces; in this chapter the reader will find how AFM, QCM-D, and

fluorescence microscopy were used to characterise protein function and structure. Chapter 4 presents qualitative data of the interaction of HepG2 cells with (biocompatible) polyelectrolyte surfaces, this phenomenon was mainly studied with QCM-D coupled with a vertical microscope, and other standard methods. Chapter 5 shows the tentative of quantifying the cell/polyelectrolyte interactions, the mechanical properties of cells, and the local interaction of the tip coated with polyelectrolytes. Finally, a chapter summarizing the conclusions and future outlook is presented.

Chapter II

Materials and methods

II.1. Materials

II.1.1. Substrates

The substrates used were silicon wafers (Siegert Consulting e.K, Aachen, Germany), borosilicate glass slides, gold-coated quartz crystals for quartz crystal microbalance with dissipation (QCM-D) measurements (Q-Sense, Västra Frölunda, Sweden), and polystyrene tissue culture 96-well plates.

II.1.2. Coating materials

The polyelectrolytes (PEs) applied for substrate coating were poly(ethyleneimine) (PEI, Mw~ 750 kDa), poly(sodium-4-styrenesulfonate) (PSS, Mw~70 kDa), poly(allylamine-hydrochloride), (PAH, Mw~70 kDa), poly(L-lysine) solutions 0.01% (PLL, Mw~70-150 kDa) and 0.1% (Mw:150-300 kDa) (SigmaAldrich). Poly(L-lysine)-graft-(polyethylene glycol)co-polymer (PLL-g-PEG (20)-[3.5]-PEG(2)), PLL(20)-g[3.5]-PEG(2)/ TRITC (Tetramethyl Rhodamine Iso-Thiocyanate) was purchased from Surface Solutions (Zurich, Switzerland). PLL-g-PEG is a co-polymers with PLL backbone of molecular weight of 20 kDa, with a grafting ratio of lysine/PEG of 3.5, and PEG chain molecular weight of 2 kDa. PLL-g-PEG was fluorescently labelled with rhodamine by attaching TRITC to the PLL backbone. The basic structures of the PEs are shown in figure II-1.

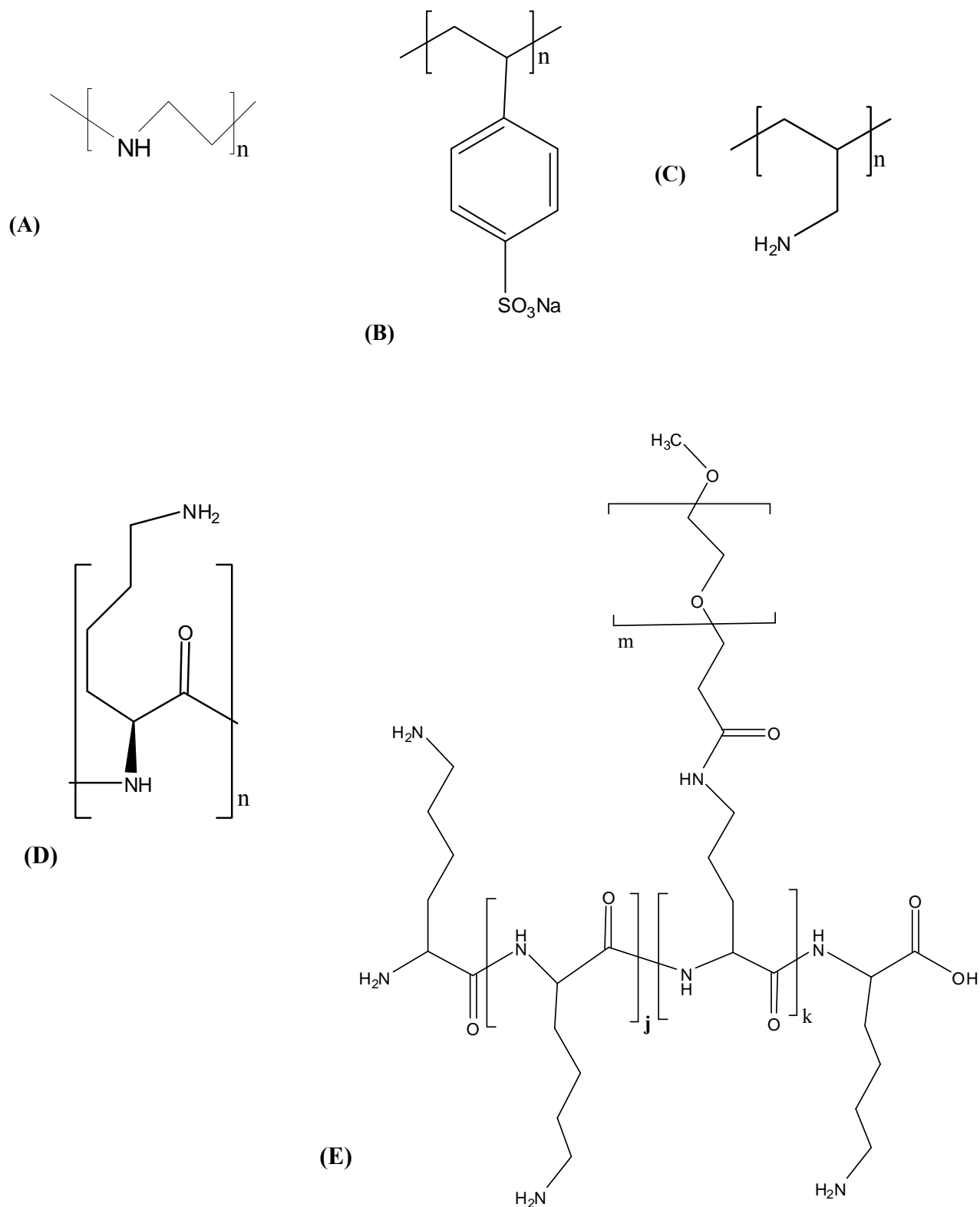


Figure II-1: Polyelectrolyte molecular structure: (A) PEI; (B) PSS, (C) PAH, (D) PLL; (E) PLL-g-PEG: $m \sim 45$, $j/k = \text{grafting ratio} = 3.5$

II.1.3. Microcontact printing materials

The silicon master used for moulding the stamps for protein patterning (GeSim, Germany) were kindly provided by Prof. H. Möhwald (Interfaces Department at the Max Planck Institute, Golm, Germany). The silicon masters for cell patterning were purchased from CIC microGune (Donostia, Spain).

The stamps were made of polydimethylsiloxane (PDMS) base silicon elastomer Sylgard 184 and the curing agent (Dow Corning Midland, MI).

II.1.4. Biomolecules

Biotin-4-FITC with a $M_w=644.70$ was purchased from Molecular Probes, Invitrogen Detection Technologies (Eugene, Oregon, USA).

The bacterial cell surface protein was provided by Prof. U. B. Sleytr (Centre for Nanobiotechnology, BOKU, Vienna, Austria). The bacterial cell surface layer protein (SbpA) was isolated from *Bacillus sphaericus* CCM 2177. Culture condition, extraction and purification was carried out as described by Sleytr *et al.* [65]. The recombinant S-layer green fluorescence fusion protein (rSbpA-EGFP) was isolated and purified from a transformed *E. coli* culture, in which the sequence coding gene for the rSbpA-EGFP production was introduced as explained by Ilk *et al.* [39]. The heterotetramers of rSbpA-STV fusion protein were obtained after a refolding procedure of a mixture of the protein rSbpA-STV (monomer) and an excess of core streptavidin as described by Moll *et al.* and Huber *et al.* [40; 66].

Laccase was provided by S. Rodriguez (ETSEQ, URV, Tarragona). It was produced by *Trametes pubescens* (MB 89) from the collection of the Institute of Applied Microbiology, University of Agricultural Science (Vienna, Austria) and was maintained on 3% malt extract agar (MEA) plates at 4 °C and sub-cultured every three months. *T. pubescens* was immobilized on nylon sponge discs (4.5 cm in diameter and 0.7 cm thick) as shown in figure II-2 (Scotch Brite[™], 3M Company, Spain; density 1,65 kgm⁻³; superficial area: 960 m⁻¹, hydrophobic). Before immobilization, the nylon sponge discs were pretreated according to Linko [67] by boiling for 10 min and washing thoroughly

three times with distilled water. Then, they were dried overnight at room temperature. Three plugs of 0.7 cm diameter of *T. pubescens* grown on MEA plates were placed in 250-ml Erlenmeyer flasks containing 100 ml medium and one disc of nylon sponge. The medium composition was: 10 g l⁻¹ glucose, 15 g l⁻¹ yeast extract, 0.9 g l⁻¹ (NH₄)₂SO₄, 2 g l⁻¹ KH₂PO₄, 0.5 g l⁻¹ MgSO₄·7H₂O, 0.1 g l⁻¹ CaCl₂·2H₂O and 0.5 g l⁻¹ KCl in 0.1 M citrate-phosphate buffer (pH=4.5) and 0.5 g l⁻¹ thiamine. The culture medium was sterilized at 121°C for 20 min. After cooling, the thiamine previously sterilized by filtration (0.22 μm) was added to the medium. The flasks were incubated at 30°C and 100 rpm on a rotatory shaker.

Culture broth was collected at the maximum laccase activity (10 days, 200 U l⁻¹), centrifuged (8000 g, 15 min) and ultra-filtrated in 20 ml-Vivaspin tubes (Sartorius AG, Göttingen, Germany) with a membrane cut-off of 10 kDa. The resulting crude extract showed a specific activity of 1.44 U mg⁻¹ (total protein 250 mg l⁻¹ and laccase activity 360 U l⁻¹). The experiments were performed with this crude extract.

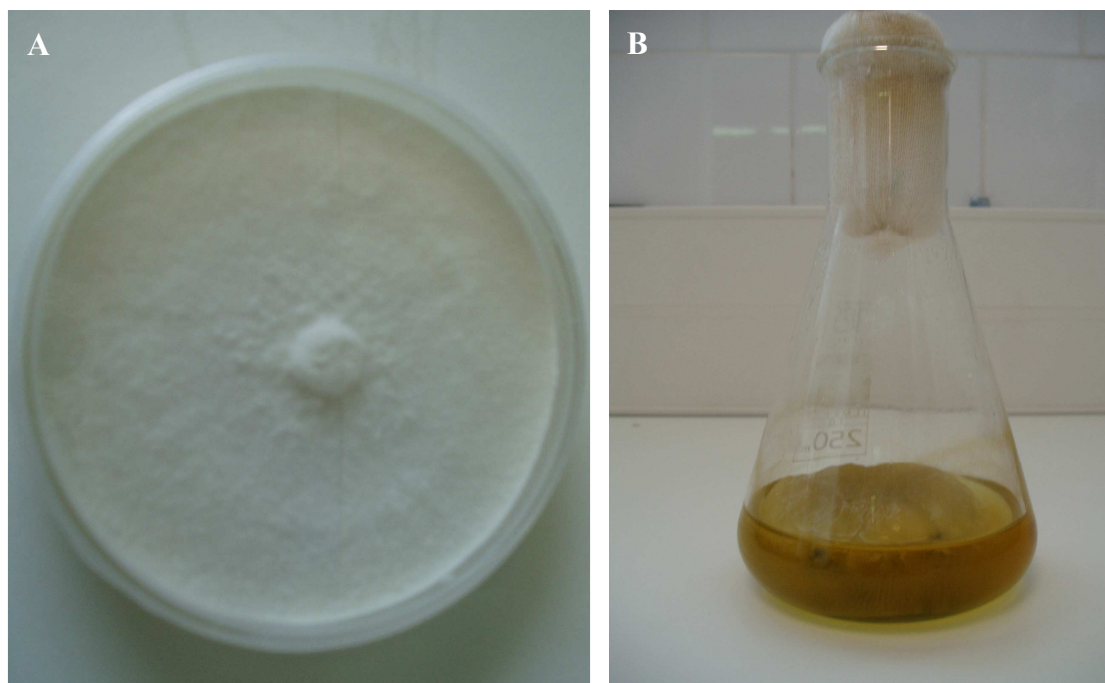


Figure II-2: Culture of *T. pubescens*, (A) in petri dish on 3% MEA, (B) on a nylon sponge disc under submerge fermentation condition.

II.1.5. Buffers and solutions

The solutions composition and names are presented in table II-1.

Table II-1: Buffers composition

<i>Name</i>	<i>Composition</i>	<i>Concentration</i>	<i>pH</i>
HEPES	HEPES	10 mM	7.4
TRIS	TRIS	0.5 mM	9
	CaCl ₂	10 mM	
PBS	NaCl	8g/l	7.4
	Na ₂ HPO ₄	1.15g/l	
	KCl	0.2 g/l	
	KH ₂ PO ₄	0.2 g/l	
Succinate buffer	C ₄ H ₆ O ₄	25 mM	4.5

MiliQ water with a resistivity of 18.2 MΩcm was used to prepare aqueous solutions, for contact angle measurements and washing steps (if the contrary is not specified).

II.2. Methods

II.2.1. Layer-by-layer coating

Glass and silicon wafers were cleaned with ethanol (96%) for 15 minutes in ultrasonic bath, followed by 5 minutes in air-plasma cleaner (Harrick PDC-32G-2, pressure: 0.5 mbar). RCA method was also used for cleaning. The samples were immersed in 5:1:1 H₂O:H₂O₂:NH₄OH solution for 15 minutes at 60-70°C. The clean substrates were coated with polyelectrolytes using the layer-by-layer technique described by Decher [8]. PEI was used as precursor layer. PEI concentration was 10⁻³ M in water. PSS and PAH

solution were 10^{-3} M in 0.5 M NaCl. PLL-g-PEG was adjusted to 1 mg/ml concentration with HEPES.

A similar procedure was applied to 96-well culture plates. 200 μ l of PE solution was added to each well, allowed to adsorb for 20 minutes and washed 3 times with water before proceeding with next layer.

II.2.2. Surface patterning: PLL-g-PEG microcontact printing

PDMS base silicon elastomer Sylgard 184 and the curing agent were mixed in a 10:1 mass ratio, and degassed in vacuum. The mixture was spread over the master, degassed again, and cured for 12h at 60°C. The PDMS was cut, peeled off from the master, and the resulting PDMS stamp hydrophilized in an air-plasma cleaner (Harrick PDC-32G-2, pressure: 0.3-0.4 mbar, 1 min). The solution of the PLL-g-PEG was spread on the stamp. After 15 minutes, the stamp was briefly rinsed with water and dried with nitrogen. The stamping procedure is shown in Figure II-2. The inked stamp was brought into contact with clean and dried substrate with or without coating for 30 seconds and then removed. The final structured surface was carefully rinsed with water.

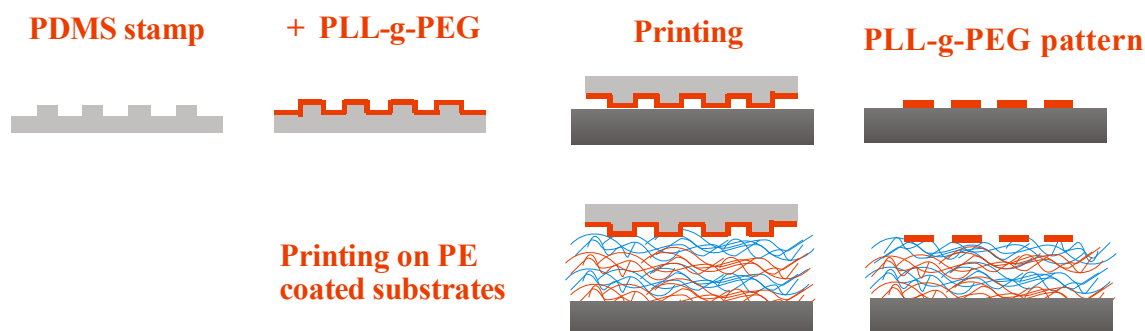


Figure II-3: Scheme of the patterning process. PDMS stamps were moulded from silicon masters and their surface hydrophilized by 60-second air plasma treatment. PLL-g-PEG was adsorbed on the stamp and transferred to the substrates by putting the stamp in close contact with the substrates for 30 seconds [30; 31].

II.2.3. Protein immobilisation

II.2.3.1. Bacterial protein

SbpA, rSbpA-EGFP and heterotetramers of rSpbA-STV were adjusted to 0.1 mg ml^{-1} protein in TRIS buffer. The protein adsorption was carried out by immersion of the substrates in the protein solution overnight.

II.2.3.2. Laccase

Laccase (benzenodiol: oxygen oxidoreductases, EC1.10.3.2) extract was diluted to a total protein concentration of 0.1 mg/ml and was immobilised on PEI coated-gold QCM crystals by cross-linking with glutaraldehyde (2.5 % in water).

II.3. Biomolecule assays

II.3.1. Protein assay

The concentration of protein was determined as described by Bradford using the reagent commercialized by Bio-Rad ((Richmond, USA) [68]. Bovine serum albumin (BSA) was used as a standard.

II.3.2. Laccase activity

Laccase activity was determined according to the method of Niku-Paavola et al. with ABTS (2,2'-azino-di-[3-ethyl-benzothiazoline-(6)-sulphonic acid]) as a substrate [69]. The reaction mixture (in a total volume of 1.5 ml) contained 1150 μl enzyme diluted to buffer (25 mM succinic acid, pH 4.5) and 350 μl 20 mM ABTS. The reaction was monitored at room temperature by measuring the change in absorbance at 436 nm ($\epsilon = 29.3 \text{ mM}^{-1}\text{cm}^{-1}$) for 2 min. One activity unit was defined as the amount of enzyme that oxidised 1 μmol of ABTS per minute and the activities were reported as UI^{-1} .

II.4. Instrumental techniques

II.4.1. Microscopy

II.4.1.1. Bright field microscopy and phase contrast

In bright field microscopy the sample is illuminated with white light, and the image is build up after collecting the transmitted light through the sample. Phase contrast microscopy is an optical microscopy illumination technique, invented by Frits Zernike in 1930s, in which small phase shifts in the light passing through a transparent specimen is converted into amplitude or contrast changes in the image. The human eye retina detects the changes in intensity energy, but the detection of changes in phase are not easily observed. In order to make phase variations observable, it is necessary to combine the light passing through the sample with a reference so that the resulting interference reveals the phase structure of the sample. In phase contrast microscopes, rings inserted into the optical path introduce the necessary phase shift. Specimens such as cells and bacteria are unable to produce sufficient contrast for interesting regions to be visible under bright field illumination conditions unless stained (and therefore killed). The difference in densities and composition within these objects however often give rise to changes in the phase of light passing through them. The use of phase contrast technique makes these structures visible and then allows their study with alive specimens.

Phase contrast images were taken with a Leica CTR6000 with controller DMI6000B and a Leica camera DFC300FX.

II.4.1.2. Fluorescence microscopy

Fluorescence and phosphorescence are particular cases of luminescence, which is the emission of ultraviolet, visible or infrared photons from an electronically excited species. In the case of fluorescence (a transition between two singlet states), the molecules are excited after adsorbing a photon of wavelength (λ_1) from its ground electronic state to a higher one with various vibrational states (a process that takes about

10^{-15} s). The excited molecule loses energy (internal conversion) reaching the lowest vibrational state of the excited electronic state (after ca. 10^{-12} s). From this (thermally equilibrated) excited state the emission of a photon of longer wavelength (λ_2) is emitted, being the typical fluorescence lifetime of ca. 10^{-8} - 10^{-9} s.

The basic components of a fluorescence microscope are the light source, the excitation filter, the objective, the dichroic mirror (or dichromatic beamsplitter), the emission filter, and the detector (figure II-3). The specimen is illuminated with light of a specific wavelength (or wavelengths), which is absorbed by the fluorophore (fluorescent molecule). The much weaker emitted fluorescence is separated from the excitation light through the use of an emission filter. To improve the signal-to-noise ratio, the excitation light and the fluorescence must be completely separated. The selection of the filters and dichroic mirror to match the excitation and emission spectra characteristics of the fluorophore, together with the use of high-quality optical filters are essential requirements for fluorescence microscopy.

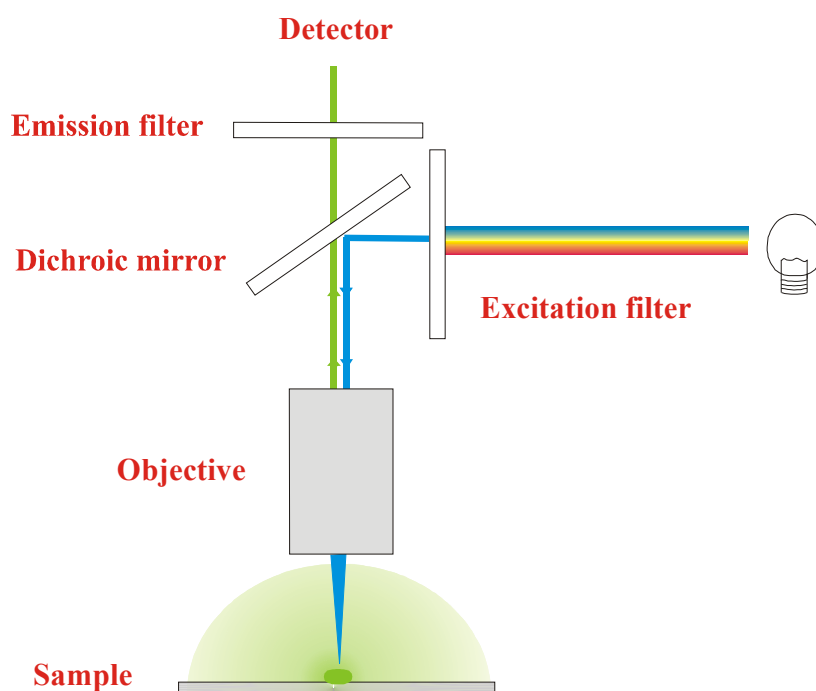


Figure II-4: Fluorescence microscope scheme. For the imaging of the fluorophore presents in the sample, the correct pair of excitation and emission filters has to be set.

Fluorescence microscopy imaging of polyelectrolyte patterns were carried out with a Zeiss Axiovert 200 (Zeiss, Germany) with an Axiovert LDA-Plan 10X, light source was

Hg vapour lamp. A Zeiss Axiocam HR high-resolution monochromatic camera was used. The rSbpA-EGFP samples were imaged with a Zeiss Axioskop 2 plus with a Hg vapour lamp and a Hamamatsu Colour Chilled 3CCD camera. The heterotetramers-biotin-4-fluorescein pictures were taken with a Zeiss Axiovert 200 (Zeiss, Germany), with a Hg vapour lamp and a Zeiss Axiocam HR high-resolution monochromatic camera. Two filter sets were used for the observation of fluorescently molecules labeled with rhodamine and EGFP. A Zeiss filter set with a band pass of 534-558 nm for excitation light, and a long pass at 590 nm, was used to observe the rhodamine emission. The other filter set with a band pass for excitation light of 450-490 nm, and a band pass of 515-565 nm for emission light was used to observe EGFP.

II.4.1.3. Scanning electron microscopy (SEM)

Scanning electron microscopes are currently used to achieve high-resolution images of a sample surface due to the short wavelength of the electrons. The electrons are emitted by an incandescent cathode source and are accelerated through either electrostatic or magnetic field lens, with energy of ca. 100 keV. After the primary electron beam hits the surface of the sample, secondary electrons of about 50 eV energy are produced. Due to their low energy they can escape only from a very shallow region at the sample surface offering a good image resolution.

The need of high vacuum and sample conductive surfaces (to avoid specimen charging) imposes some limitation in the use of SEM. The environmental SEM (ESEM) retains the advantages of a conventional SEM, but reduces those requirements. High vacuum conditions are required in the electron gun and throughout the column, where gas molecules can scatter electrons and degrade the beam. In the ESEM, the column is still high vacuum, but the chamber may sustain higher pressures. Another difference is the detector, which can work in non-vacuum environments using the principle of gas ionisation.

A Jeol 6400 scanning electron microscope and a FEI Quanta 600 (ESEM) from the Scientific and Technical Services of the Rovira i Virgili University (Tarragona, Spain) were used in this work.

II.4.1.4. Atomic force microscopy (AFM)

The atomic force microscope is a scanning probe microscope that permits the study of conducting and insulating surfaces. It was developed by Binnig, Quate and Gerber in 1986 [13], few years after the invention of the scanning tunnelling microscope (STM). AFM is not only a tool to image topography with nanoscale resolution; it can also provide information on local material properties such as elasticity, hardness, adhesion, and surface charge densities by means of force-distance curves. Besides, it can be used to study samples in air as well as in liquid. For these reasons, AFM has become a useful tool in different fields of research such as surface science, material engineering and biology.

Basically, AFM measures the force between a small tip, built with micro-fabricated techniques, and the specimen surface using a free-moving cantilever as shown in figure II-4. The force is measured by monitoring the deflection of the cantilever using in most cases an optical lever. The optical lever operates by reflecting a laser beam on the cantilever, which strikes a position-sensitive photo-detector. Then, the vertical deflection of the cantilever is measured as a change in the signal from the photo-detector. If one is acquiring an image, a feedback loop maintains a constant force between tip and sample. The image contrast arises because the force between the tip and sample is function of both tip-sample separation and the material properties of the tip and sample. Then, the vertical deflection of the cantilever can be assigned to each point of the surface, and a topographic image of the sample is obtained. If one is interested in acquiring a force-distance curve, at a certain point of the sample the deflection of the cantilever is recorded while approaching and retracting the tip from the surface. The combination of imaging and force-curve acquisition results in topography and material properties characterization condensed in one AFM experiment [14].

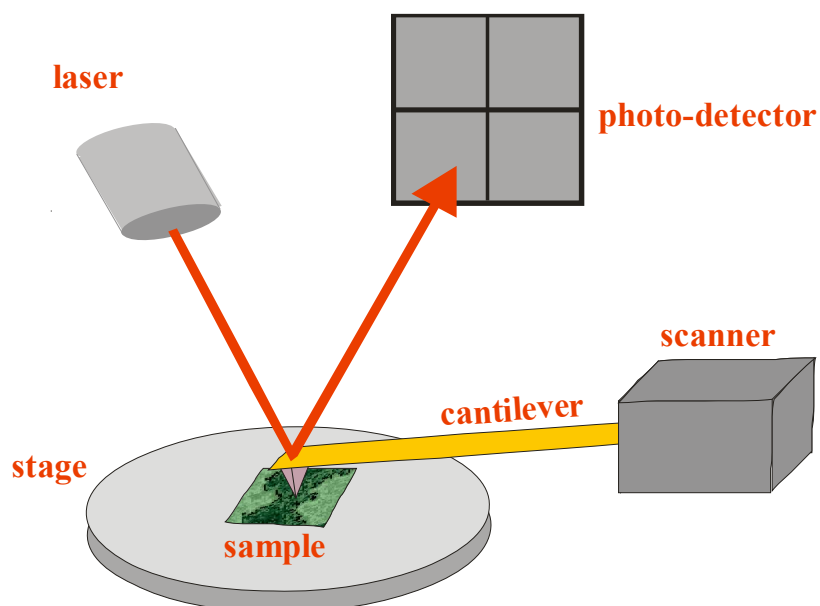


Figure II-5: Cartoon showing the physical principle of an AFM. The force between a tip situated at the end of a cantilever and the sample surface is measured by monitoring the deflection of the cantilever using a laser beam. The vertical deflection of the cantilever is measured as a change in the signal from the photo-detector.

Bacterial S-proteins were imaged with a Nanowizard®AFM from JPK (Berlin, Germany) in contact mode under liquid with a Si_3N_4 cantilever (Veeco, California, USA) with a nominal spring constant of 0.1 Nm^{-1} , using the same conditions reported in [38].

Cell experiments were done with a NanoWizard®AFM II form JPK (Berlin, Germany) in contact mode using Si_3N_4 tips with a nominal spring constant of 0.01 Nm^{-1} (Veeco, Santa Barbara, USA) in the $400 \mu\text{l}$ liquid chamber with PBS at room temperature.

II.4.2. Contact angle measurements

Contact angle analysis is normally used to investigate the wetting properties of a given surface. The contact angle (θ) can be defined as the angle at which the liquid/vapour interface meets the solid surface [16]. The contact angle gives a qualitative description of the force balance between the molecules within the droplet versus the attraction or repulsion those droplet molecules experience towards the surface molecules. The contact angle is specific for any given system and is determined by the interactions

across the three interfaces. Figure II-5 shows a scheme for two different wetting behaviours. The contact angle is not limited to a liquid/vapour interface; it is equally applicable to the interface of two liquids or two vapours.

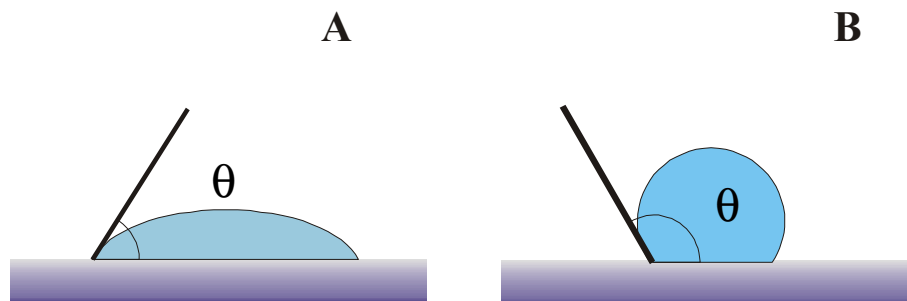


Figure II-6: Different surface wettability. (A) Shape of a water droplet on a hydrophilic surface, (B) water droplet on hydrophobic surface.

The wetting properties of adsorbed PE and proteins were carried out using a Kruess System (Hamburg, Germany). Measurements were performed at room temperature using MiliQ water and a 0.1 mm diameter needle.

II.4.3. Visible-UV spectrophotometer

The absorption of light by matter can be described by the Beer-Lambert law [17], which states that

$$A = \alpha \cdot l \cdot c$$

where A is absorbance, α is the absorption coefficient, l is the path length, and c the concentration of the absorbing species in the sample. The law is not valid at high concentrations, especially if the material is highly scattering.

II.4.4. Quartz crystal microbalance

The quartz crystal microbalance (QCM) is able to measured mass loads reaching a resolution down to ng/cm^2 . QCM operation can be done in vacuum, in gaseous environment or in liquid. Among others, QCM has been used to study thin polymer films and protein deposition [70; 71], and also cell adhesion [72].

In the 90's, Rodahl *et al* developed the QCM with dissipation (QCM-D), a technique that enables to quantify not only the deposited mass but also to characterise the viscoelastic properties of the film [73]. The basic set-up for QCM with dissipation (QCM-D) is shown in figure II-7. A single AT-cut quartz that is sandwiched between a pair of electrodes deforms when an electric field is applied due to the piezoelectric properties of the quartz.

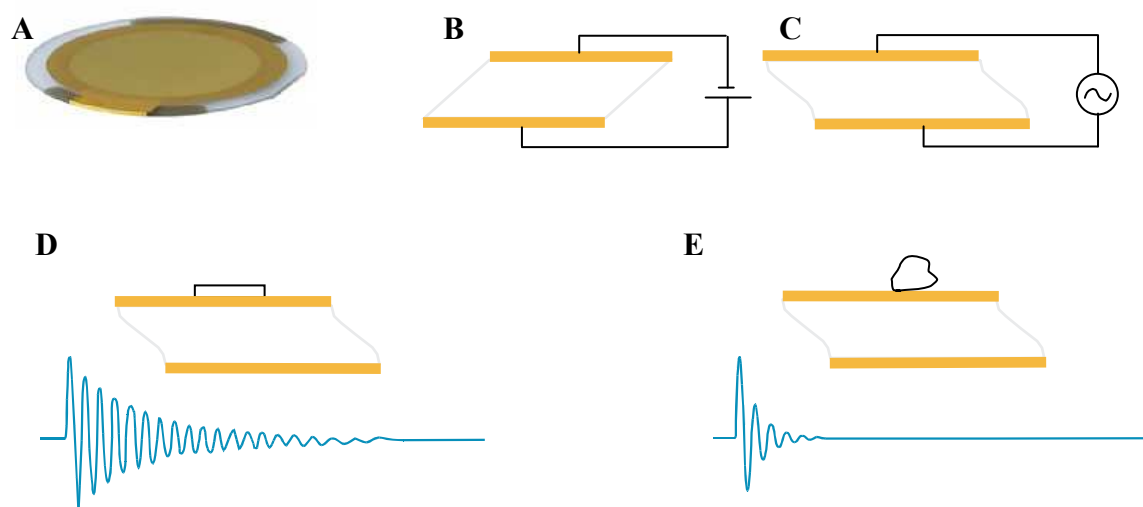


Figure II-7: QCM-D working principle (A) 5MHz AT-cut quartz crystal, (B) the application of an electric field across the piezoelectric quartz results in shear motion of the crystal, (C) resonance in the shear motion can be excited applying an alternating current of appropriate frequency. (D, E) After cutting the driving circuit, the decaying oscillation of the crystal is monitored. Attachment of a rigid mass (D) or soft mass (E) leads to different responses (taken from Q-Sense, www.q-sense.com).

If an alternating current of the appropriate frequency is applied, it oscillates at its resonance frequency (f_0), which is determined by the thickness of the crystal (d) and the speed of shear waves in quartz (v_Q). When the crystal is loaded, the changes in the resonance frequency as a function of loading of a quartz crystal is not the only type of information that can be gained from QCM-D. Frictional energy losses originating from the contact of the crystal with the surrounding medium can be used to gather additional information on the material on the crystal. The QCM with dissipation (QCM-D) measures changes in frequency as well as energy losses. To do so, the crystals are excited intermittently, and the decay of the oscillations is measured as a function of time. The temporal change in the crystal's movement, $A(t)$, can be fitted by

$$A(t) = A \cdot \exp(-\pi D t) \cdot \sin(2\pi f t + \phi)$$

and frequency, f , and the dissipation, D are calculated as function of time. When a rigid mass is attached to the crystal, there will only be a decrease in f , while when a viscoelastic mass is attached, an increase in D will be also obtained.

Different methods have been proposed to determine both mass increase and characteristic of the film [71] but it has been recognised that in certain situation where the viscoelastic properties of the film can be disregarded, and considered as a rigid film.

The increase in frequency on a crystal can be modelled using the Sauerbrey equation [18], which states that the change in the resonance frequency of the crystal before and after loading is directly proportional to the mass of the overlayer. Several restrictions have to be taken into account: i) the frequency decrease due to loading must be smaller than 2% of the resonance frequency of the bare crystal, ii) Second, the adsorbed mass must be distributed homogeneously on the sensor surface, iii) there must be no slip between the crystal and the coupled overlayer, and iv) the overlayer must be rigid (that is, no viscoelastic deformation can occur).

II.5. Cell culture techniques

II.5.1. Cell culture

II.5.1.1. Cells

Human hepatoma cell line (HepG2) was kindly provided by the Biochemistry Department of the Rovira i Rovira University (Tarragona, Spain). The cells were frozen, suspended in cell freeze media, and stored in liquid nitrogen tank until use. All experiments were performed using cells with a maximum of 20 passages.

II.5.1.2. Chemicals

The basal medium used was Dulbecco's Modified Eagle's Medium (DMEM, GIBCO), which concisely consist of glucose, essential aminoacids, vitamins and salts. It was

complemented with 10% foetal bovine serum (FBS, GIBCO), which incorporates growth factors, lipids, hormones and minerals; 1% non-essential amino-acids 100X (GIBCO) which are glycine, L-alanine, L-asparagine, L-aspartic acid, L-glutamic acid, L-proline and serine, 1% penicillin-streptomycin 100X (GIBCO) and a 2,5% of 0,16 M solution of L-glutamine (SIGMA).

Other products used were trypsin-EDTA 10X (0.5% Trypsin, 5.3 mM EDTA•4Na, GIBCO), 3-[4,5-dimethyliazol-2-il]2,5-difenil-tetrazolium bromide (MTT, SIGMA), and dimetil sulfoxide (DMSO, SIGMA), crystal violet (Aldrich), and 25% in water glutaraldehyde (MERCK).

II.5.1.3. Culture conditions

The cell culture was carried out in a CO₂ incubator at 37°C, 5% of CO₂ in air, and in a humidified atmosphere.

II.5.2. Protocols

II.5.2.1. Cell defrost

Cells were kept in N₂(l) until use. To start the culture, one ampoule was defrosted by addition of warm DMEM (37°C). DMEM was slowly added to the cryotube and was transferred to 15-ml tube. Once completely defrost, it was centrifuged at 1000 rpm for 3 minutes. The supernatant was discarded and more DMEM was added to completely eliminate the DMSO. It was again centrifuged for 3 minutes at 1000 rpm and the medium discarded. Finally, cells were resuspended with complete medium and transferred to a tissue culture flask for culturing.

II.5.2.2. Cell frost

Freezing media was composed of 50% DMEM, 40% FBS and 10% DMSO. The mixture FBS-DMSO was added drop-wise to the cells suspended in DMEM while kept in ice. The temperature decreased 1°C per minute and it was left overnight at -80°C. Cells were transferred to N₂(l) until use.

II.5.2.3. Subculture

Cells in flasks were observed under phase contrast microscopy on alternating days to inspect the state of the cells, and subculture three times a week (80% confluence). Cells were rinsed twice with phosphate buffer solution (PBS). The PBS was removed and trypsin formed by a 1:10 dilution of 10X trypsin in PBS, was added to the flask and incubated for 3-5 minutes at 37°C. FBS was added to stop the action of trypsin. The cell suspension was removed from the flask and placed in centrifuge for 3 minutes at 1000 rpm. The supernatant was removed and replaced with complete media to suspend the cells. These cells were seeded on tissue culture flasks to expand the culture (1:3) or counted in order to be used for further experiments.

II.5.2.4. Direct cell count with trypan blue

Trypan blue is a dye that is taken up by dead cells, but excluded by living cells. A 1:1 dilution of the cell suspension and dye was used to count the cell in a hemacytometer. Less than 1% dead cells were found in all the experiments.

II.5.2.5. Viability with tetrazolim salt (MTT)

This method is based on the colour change that MTT tetrazolim salt undergoes from yellow to dark insoluble formazan caused by the activity of various dehydrogenase enzymes in the cells. The tetrazolim ring is cleaved in active mitochondria, and so the reaction occurs only in living cells.

The assay was performed with cells seeded on 96-well plates. 10 µl of 5mg/ml MTT solution in PBS was added to each well, and incubated for 3 hours at 37°C. The medium was discarded and 100 µl of DMSO was added to dissolve the crystals formed. The absorbance was read at 550 nm. The viability is expressed as % of the viability of the cells in the control assay.

II.5.2.6. Cell attachment with crystal violet

96-well coated plates (see section 2.2.1.1) were seeded with cells 50000 cells/well and allowed to attach for 45, 120, 240 min and overnight. In order to remove in a gently way the media without detaching the cells, the plates were submerged slowly in a basin with PBS to completely fill the wells. They were covered and inverted in order to allow the cells not adhered to sediment. The media was removed and the above procedure repeated. After washing the wells twice with PBS, cells were fixed with 50 μ l of 2.5 % glutaraldehyde solution in water for 20 minutes. The plates were rinsed twice with H₂O and 50 μ l of 0.1 % crystal violet solution in H₂O was added. After 20 minutes, the plates were washed 3 times with water and allowed to dry at 37°C overnight. 50 μ l HCl 0.1 M was added and the absorbance measured at 630 nm within 3 minutes.

Chapter III

Building functional surfaces

III.1. Introduction

Polyelectrolyte multilayers (PEM) built by layer-by-layer technique have been extensively studied over the last years, resulting in a wide variety of current and potential applications [8]. This technique can be used to construct thin films with different functionalities, or to functionalize surfaces with substantial different properties of those of the underlying substrates. The multilayering process is achieved by the alternate adsorption of oppositely charged polyelectrolytes. Different parameters influence the building-up of the polyelectrolyte multilayer, such as polymer molecular weight and concentration, ionic strength, surface and polymer charge density [8; 12]. But once the building conditions are set, the PEM assembly is highly reproducible.

One of the biggest advantages of polyelectrolytes (PEs) technology is the versatility. PE can be applied on a wide variety of substrates and different surfaces characteristics can be obtained depending on the PEs used [9; 10]. Integrating proteins on/or in the PE multilayer, different functionalities ranging from DNA to specific recognition entities, can be incorporated to the surface [11; 13; 74].

Besides, by means of a soft-lithographic technique such as microcontact printing, it is possible to obtain surfaces where a PE is deposited following a desired feature with micrometers dimensions on a opposite charge PE surface [24; 75]. At this point, several selective immobilisation driven by electrostatic force has been reported [76].

In this work we get advantage of the protein resistant property of the PLL-g-PEG to create protein patterns. Excluded volume effects, steric repulsion and screening of interfacial charges between the proteins in solution and the PEG-modified surface might be responsible for the resistance to adsorption [77; 78].

Proteins can be immobilised on a surface by unspecific physical adsorption, covalent binding or through specific interactions.

Adsorption of proteins takes place almost instantaneously after a surface comes into contact with a protein solution. Considering the use of polyelectrolytes coated surfaces, the protein-polyelectrolyte interactions can arise from (1) electrostatic forces, (2) hydrophobic effects, (3) Van der Waals forces, and (4) dipolar or hydrogen bonds [79; 80]. It is generally accepted that the surface charge plays a major role, given the apparent range and strength of electrostatic forces. However, proteins are persistent adsorbers because of the other interactions mechanisms [79].

Covalent protein immobilisation often begins with surface modification and/or an activation step. Two activation steps commonly used are based on carboxylic acid or amine moieties that through the reaction with coupling agents such as glutaraldehyde or carbodiimide, chemically anchors the biomolecule through its amine groups [44].

Finally, the use of biotin-strept(avidin) system is an example of specific interaction systems that can be used as bridge between a surface and the biomolecule of interest. The highly specific interaction between biotin and strept(avidin), and feasibility to introduce biotin in a target biomolecule without affecting the activity, lead to other possible method to modify surfaces through biotinylated molecules [81].

Each of the methods offers advantages and disadvantages that depend on several factors. In general, chemical immobilisation methods tend to disturb the native structure of the protein due to the covalent bonds formed as a result of immobilisation. By contrast, such covalent linkages provide strong stable attachment. However, the adsorption typically perturb the protein structure much less depending on its rigidity [44].

The success or failure of biomaterials implanted *in vivo* depends on the initial cellular response that is mediated by the concentration, composition, and conformation of adsorbed proteins at the implant surface. *In vitro* and *in vivo* studies carried out to evaluate the biocompatibility of different polyelectrolytes with different cell types have been reported [14; 82-87]. During *in vitro* studies if cell culture medium contains serum, the surfaces adsorb a non defined mixture of proteins. Among serum proteins, there are extracellular matrix proteins that are known to contain specific peptide sequences recognised by membrane receptors, such as integrins. Integrins, a family of heterodimeric transmembrane proteins that are linked to the cytoskeleton on the cytoplasmic side of the membrane, establish a mechanical link not only between the

membrane and the ECM but also with the cytoskeleton [51]. In most cell types, certain essential biochemical signals are triggered by integrins upon attachment, and without attachment the cell undergoes apoptosis. Cell attachment and spreading depend on these types of interactions, thus depends on the surface characteristics.

The first protein used in this work was laccase, a copper-containing redox enzyme that catalyses the oxidation of a broad range of polyphenols and aromatic substrates, coupled to the reduction of O_2 to H_2O without need of cofactors [45]. Applications of laccases have been reported in food, pulp, paper, and textile industry, and also in biosensor development [46]. Some uses require the immobilisation of the enzyme on solid supports by adsorption, covalent attachment, entrapment, etc, on several substrates [44]. Especially for biosensor development, highly active, stable and reproducible immobilisation of laccase is required. Different configurations for laccase immobilisation on polyelectrolyte multilayers, self assembly monolayers have been proposed [46]. Besides, polyelectrolyte interaction with laccase immobilised on Al_2O_3 carriers seemed to increase the stability and activity [17].

Other proteins used in this work are S-layers. S-layers are bacterial cell surface (glyco) proteins that have the intrinsic property to self-assemble on surfaces of a broad spectrum of materials (including PEM), forming 2-D crystalline structures with unit cell dimensions ranging from 3 nm to 30 nm [38; 88]. More than 30 years of research has been devoted to the development of S-layer technology with the aim to obtain nanometer ordered functional surfaces [88]. By means of protein engineering, it is possible to produce recombinant S-proteins integrating the biomolecule of interest. Several S-layer fusion proteins have been developed, e.g. enhanced green fluorescent protein (EGFP) [39], streptavidin (STV) [40], the chain camel antibody (cAb-Lys3) [41], Fc-binding Z-domains [42] and birch pollen allergen (Bet v1) [43]. The spatial nanometer control of the fused biomolecule is of importance for biosensor development, but also, for the production of that kind of devices it is necessary to combine the nano features with microstructure surfaces. Up to now, two techniques have been proposed for the micro and sub-micro patterning of S-layers, deep Ultra Violet (DUV) radiation [89; 90] and micro-moulding in capillaries [91].

Cell interaction with PEM was studied using a hepatoma cell line (HepG2 cells). This cell line has been used in cancer research, and since at certain level some hepatocyte

metabolic functions are still present, they are used in vitro toxicological studied [59; 61; 92].

In this chapter, we present the assembly of PEMs followed by QCM-D and contact angle measurements, which were functionalise through protein immobilisation and microcontact printing of PLL-g-PEG.

First, laccase immobilisation and evaluation of interaction PAH and PSS was studied by QCM-D measurements. Secondly, the feasibility and functionality of the micropatterning of SbpA proteins (SbpA, rSbpA-EGFP and rSbpA-STV) was study with contact angle measurements, fluorescence and atomic force microscopy.

Finally, HegG2 were culture on positively and negatively charge polyelectrolytes (PEI, PAH, PLL and PSS, PLL-g-PEG), and cell patterning was attempted.

III.2. Results

III.2.1. Polyelectrolyte multilayer assembly

The assembly of the polyelectrolyte multilayers was monitored by QCM-D. The change in frequency after each layer is plotted in figure III-1. PEI was the first layer with a $\Delta f = 10 \pm 2$ Hz and $\Delta D = 0.1 \pm 0.3 \times 10^{-6}$ after adsorption. Lately, PSS and PAH were adsorbed until a total of 4 layers.

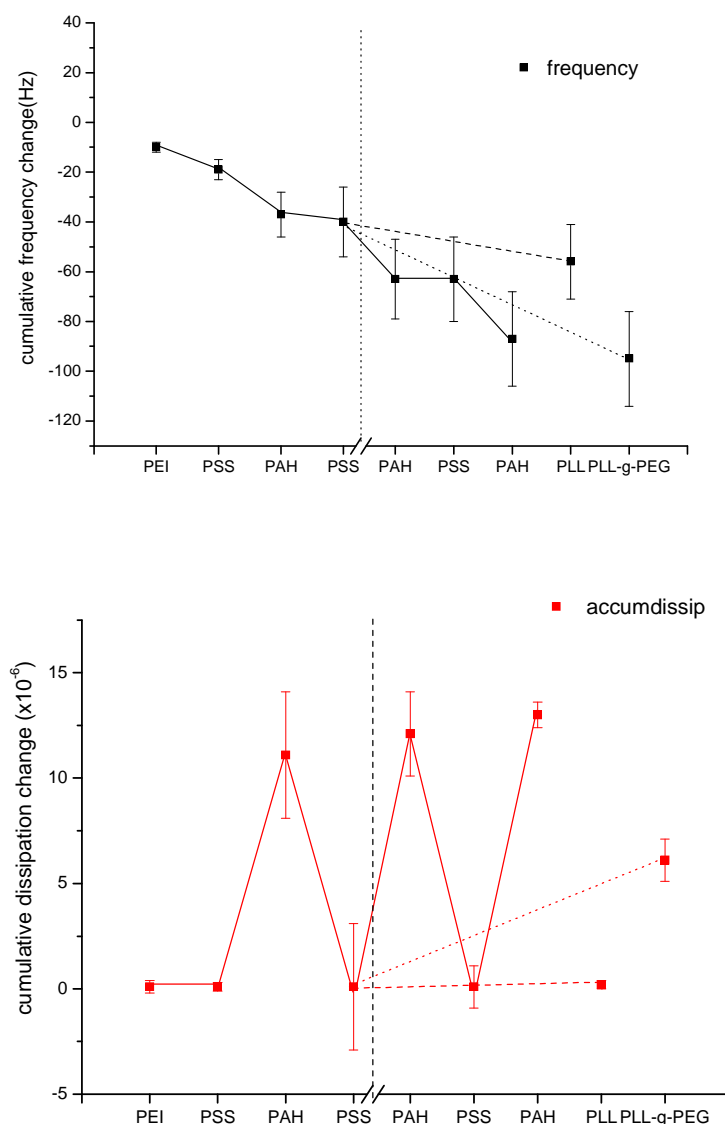


Figure III-1: Frequency and dissipation change during the layer-by-layer deposition on gold crystals. A continuous decrease in frequency was observed after deposition of every PE layer. The dissipation increased after PAH adsorption, but always decreased after PSS adsorption.

The change in frequency for PSS after PEI was of 9 ± 2 Hz and the dissipation remained close to 0. When the first PAH layer was adsorbed on PSS, the change of frequency was of 18 ± 5 Hz, and its deposition always led to an increase in dissipation of $10 \pm 3 \times 10^{-6}$. After the second layer of PSS, the frequency remained almost constant, with a $\Delta f = 3 \pm 2$ Hz and a $\Delta D = -10 \pm 3 \times 10^{-6}$. This behaviour repeats for the next PAH/PSS/PAH adsorption. After the second PSS layer, other 2 positive polyelectrolytes

were adsorbed in different experiments, PLL and PLL-g-PEG. After PLL, the frequency drop was of 16 ± 1 Hz and the dissipation increase $0.1 \pm 0.2 \times 10^{-6}$. The PLL-g-PEG adsorption led to the biggest change in frequency for only one layer, 55 ± 5 Hz, and the dissipation increase was $6 \pm 1 \times 10^{-6}$.

III.2.2. Contact angle

The contact angle of the polyelectrolyte surfaces was measured and the values obtained are presented in table III-1 and III-2. Silicon wafers and glass were cleaned with the RCA method, making the surface hydrophilic with a contact angle of $12 \pm 6^\circ$. The deposition of PEI made the surface less hydrophilic, with a contact angle of $48 \pm 22^\circ$. After the deposition of a PSS/PAH/PSS, the contact angle was measured again. The contact angle of PSS and PAH were similar on SiO_x , but slightly lower when measured on glass. The PLL presented a contact angle of $31 \pm 3^\circ$ on glass, and as expected the PLL-g-PEG surface presented a most hydrophilic surface, with a contact angle of $24 \pm 3^\circ$.

Table III-1: PE contact angle measurements on SiO_x

Surface	<i>Contact angle</i>
SiO_x	12 ± 6
PEI	48 ± 22
PSS	44 ± 5
PAH	44 ± 9
PLL-g-PEG	24 ± 3

Table III-2: PE contact angle measurements on glass

Surface	<i>Contact angle</i>
PSS	33 ± 5
PAH	38 ± 2
PLL	31 ± 3

III.2.3. Polyelectrolyte patterning

The patterning technique used was the micro-contact printing. It was possible to obtain different patterning features with different polyelectrolytes. Figure III-2 shows some examples obtained with fluorescently labelled PAH (PAH-FITC). Besides, PLL-g-PEG patterns were obtained. Backfilling of the pattern for PLL-g-PEG pattern with PAH and PLL were accomplished. In figure 2, RBITC-PAH was used to backfill the free PSS areas between the PLL-g-PEG stripes.

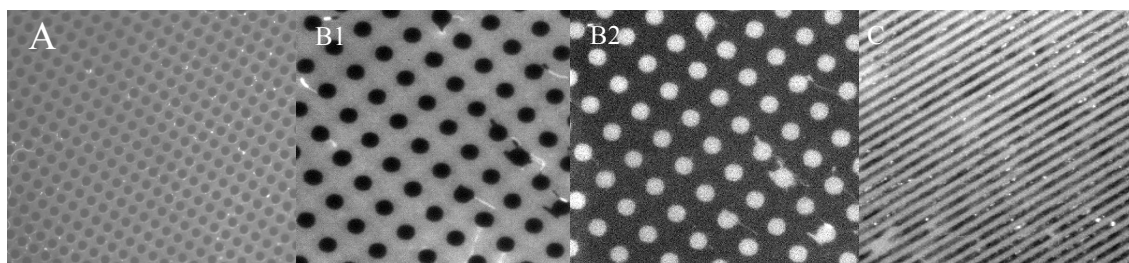
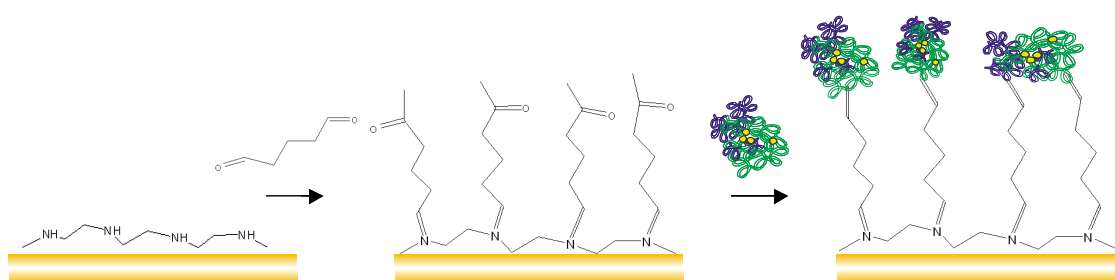


Figure III-2: Fluorescence microscope images of patterned surfaces. A) PAH-FITC is the complementary area of circles $D=10\ \mu\text{m}$, B1) RBITC-PAH stamped pattern and B2) FITC-PAH pattern obtained after backfilling the RBITC-PAH free areas, C) PLL-g-PEG pattern backfilled with RBITC-PAH.

III.2.4. Surface functionalisation

III.2.4.1. Laccase immobilisation and interaction with polyelectrolytes

Laccase was covalently immobilised with glutaraldehyde (GA) as shown in scheme III-1. GA first reacted with the amines of poly(ethyleneimine) (PEI) adsorbed on gold, and later with laccase.



Scheme III-1: Scheme of the laccase immobilisation on the gold crystals. First, GA reacts with the adsorbed PEI, and afterwards with laccase (relative sizes are not real, scheme not in scale).

The enzyme immobilisation process was followed by QCM-D as shown in figure III-3. The adsorption of PEI and the reaction with GA led to a compact layer with Δf and ΔD change of 10 ± 2 Hz and $0.1 \pm 0.3 \times 10^{-6}$, and 6 ± 1 Hz and $0 \pm 0.3 \times 10^{-6}$, respectively.

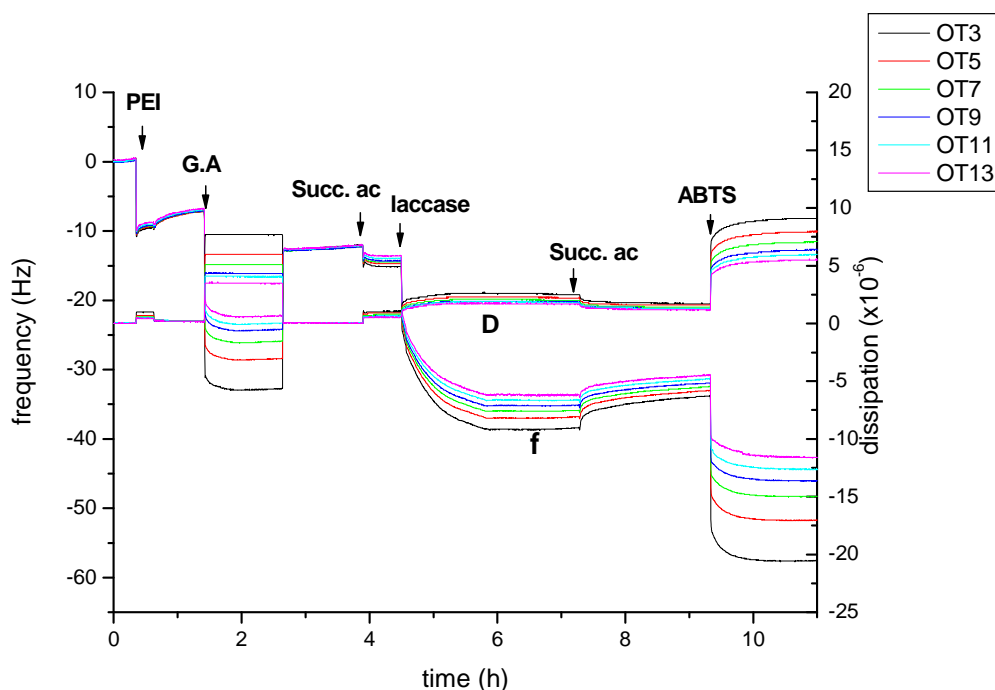


Figure III-3: QCM-D measurement of the laccase immobilisation. A decrease in frequency without significant change in dissipation was observed after adsorption of PEI and the covalent attachment of GA. The immobilisation of laccase led to a decrease in frequency of 24 Hz with dissipation increase of 1.2×10^{-6} .

Due to the fact that succinate buffer was used to dilute the laccase, prior to laccase immobilisation, this buffer was pumped through the QCM chamber. Before dilution, the

crude extract was centrifuged and filtered as explained in Materials and Methods. The protein concentration and activity of the diluted laccase were $270 \pm 20 \text{ mg l}^{-1}$ and $570 \pm 80 \text{ UI}^{-1}$. Laccase solution was injected in the chamber and after stabilisation, the change in frequency and dissipation were of $24 \pm 5 \text{ Hz}$ and $1.2 \pm 0.6 \times 10^{-6}$.

Table III-3: Immobilisation of laccase monitored with QCM-D

<i>3th overtone</i>	<i>$\Delta f/n$ (Hz)</i>	<i>ΔD ($\times 10^{-6}$)</i>
PEI	10 ± 3	0.2 ± 0.1
GA	6 ± 1	0 ± 0.3
Succinate buffer	4 ± 1	1 ± 0.4
Laccase	24 ± 5	1.2 ± 0.6

In order to check whether the change in frequency was due to immobilisation of active laccase, 2,2'-azino-di-[3-ethyl-benzo-thiazolin-sulphonate] (ABTS) was injected into the chamber and while recording frequency and dissipation change, the effluent was collected. After injecting succinate buffer solution to remove ABTS, the frequency and dissipation returned to their original values within the experimental error.

Since laccase oxidises ABTS to a dark green product, the presence of active laccase was confirmed by measuring an increase in the absorbance of the effluent. When the flow increased, the effluent absorbance decreased as shown in table III-4.

Table III-4: Effluent absorbance at different flows

Flow ($\mu\text{l min}^{-1}$)	Absorbance
10	0.028 ± 0.003
20	0.017 ± 0.001
30	0.011 ± 0.002

After laccase immobilisation, polyelectrolytes were adsorbed. The frequency and dissipation changes are reported in table III-5.

Table III-5: QCM-D measurements of PE deposition on laccase

<i>Polyelectrolyte</i>	Δf (Hz)	ΔD ($\times 10^{-6}$)
PAH 1	18 ± 3	2.3 ± 0.6
PSS 1	6 ± 2	-1.2 ± 0.5
PAH2	14 ± 2	-0.6 ± 0.4
PSS 2	6 ± 1	-0.1 ± 0.4

After the adsorption of PAH, PAH/PSS/PAH, and (PAH/PSS)₂, ABTS was pumped into the chamber to test if the enzyme was still active. In figure III-4, it can be observed that the PE on the laccase changed the shape of the adsorption curve.

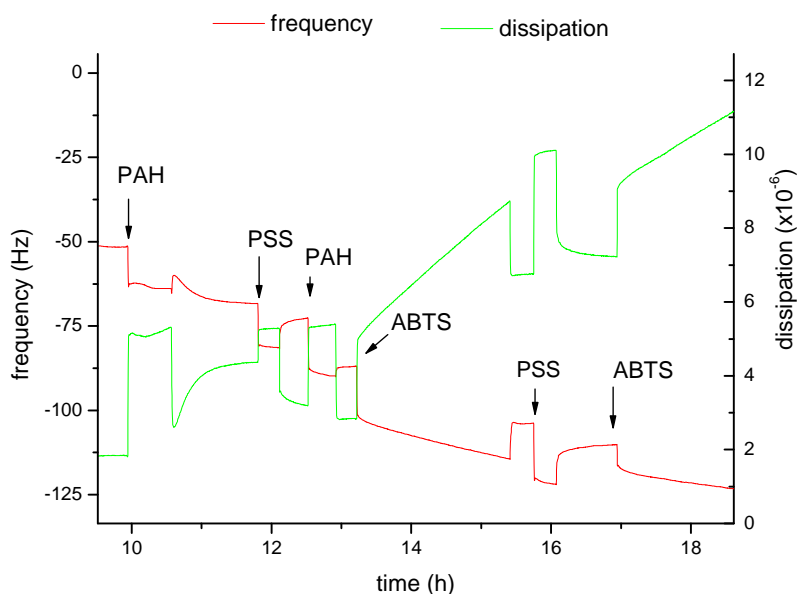


Figure III-4: Polyelectrolytes deposition on laccase. The PAH adsorbed on the previously immobilised laccase led to a decrease in frequency and increase in dissipation. After PSS adsorption there was a compactation of the layer, showed by a decrease in dissipation with a slightly decrease in frequency. After adsorption of another layer of PAH and PSS, ABTS was injected but no stable frequency nor dissipation was obtained in both situations.

Besides, after pumping succinate buffer solution to remove the ABTS, the frequency and dissipation did not returned to the values before ABTS injection.

Control experiments with only the polyelectrolyte multilayer layer with PAH and PSS as last layers are shown in figure III-5.

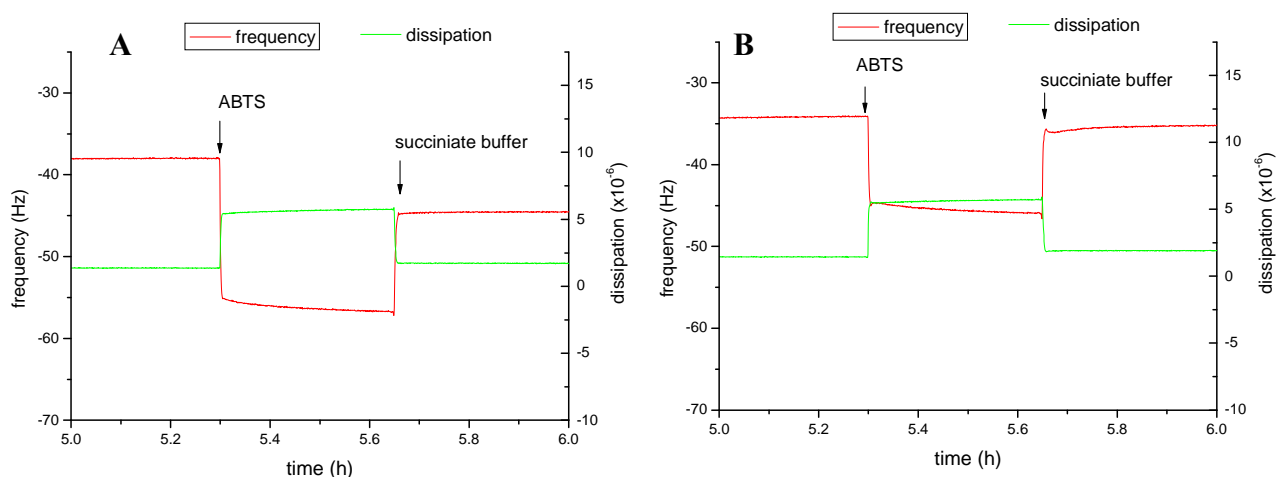


Figure III-5: ABTS adsorption on the polyelectrolyte multilayers. After building a polyelectrolyte multilayer with PEI/(PSS/PAH)₂ and PEI/(PSS/PAH)₂/PSS, ABTS was injected. (A) When the last layer was PAH a permanent decrease in frequency without change in dissipation was registered after washing with buffer, (B) when the last layer was PSS, the frequency and dissipation values almost returned to the values before ABTS injection.

Two multilayer systems were build with PEI/(PSS/PAH)₂ and PEI(PSS/PAH)₂ PSS. Afterwards ABTS was injected and the frequency and dissipation was monitored. In both cases a stable value of f and D were reached in less than 30 minutes. On one hand, after washing with buffer a 7 Hz frequency change was registered when PAH was the last layer, without significant dissipation change. On the other hand, no significant differences either in frequency or dissipation after buffer injection were observed when PSS was the last layer.

The remaining enzyme activity measured after polyelectrolyte deposition is presented in table III-6. The values presented are the ratio between the absorbance of out coming solution of the chamber after the polyelectrolyte deposition and the value obtained after laccase immobilization (100%).

Table III-6: Activity ratio (%) after and before polyelectrolyte adsorption

<i>Activity</i>	<i>PAH</i>	<i>PAH/PSS/PAH</i>	<i>(PAH/PSS)2</i>
%	93 ± 19	56 ± 21	89 ± 26

III.2.4.2. S-layer proteins patterning on polyelectrolyte multilayers

In order to pattern S-layer proteins applying microcontact printing, one of the polyelectrolyte on the surface has to resist to the adsorption of the protein. The ability of PLL-g-PEG to resist the adsorption of SbpA was tested first on plain surfaces by means of contact angle measurement as shown in figure III-6. When SbpA was adsorbed on SiO_x, the contact angle of water was 72 ± 11°. On the other hand, when PLL-g-PEG was the exposed surface, the contact angle was 24 ± 3°. The addition of SbpA on PLL-g-PEG did not change significantly the wetting properties of the PLL-g-PEG within experimental error (27 ± 7°).

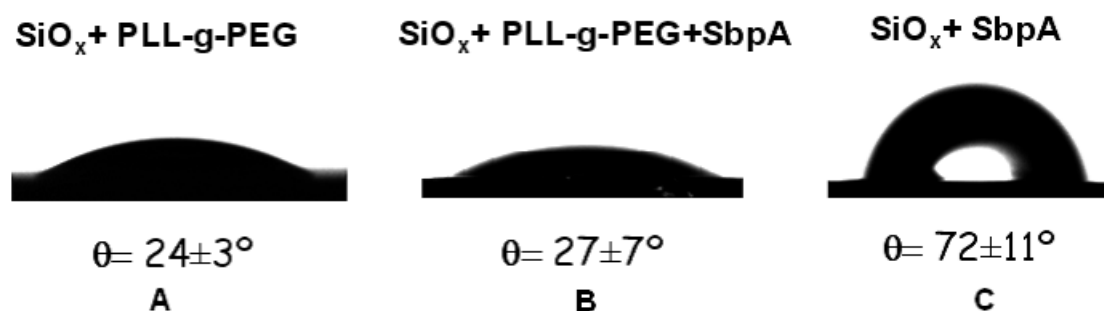


Figure III-6: Contact angle measurements (θ) of PLL-g-PEG and SbpA coated surfaces. Advancing contact angle measured on: (A) SiO_x/PLL-g-PEG, (B) SiO_x/PLL-g-PEG, and (C) SiO_x after being in contact with a 0,1 mg/ml SbpA solution overnight. No significant change in the contact angle value in (C) indicates that SbpA did not adsorb on PLL-g-PEG coated surfaces.

PLL-g-PEG pattern surfaces after incubation with SbpA were observed by atomic force microscopy as shown in figure III-7. Two different areas could be observed, and the feature corresponds to the 5- μ m width strips stamped. The pattern could be observed due to the difference in roughness between PLL-g-PEG and SbpA areas. The smoother surface corresponds to the place where SbpA recrystallised with a root means square

value (RMS) ranging from 0.2 to 0.5 nm, while the PLL-g-PEG area had a RMS from 1 to 1.5 nm. After zooming in the SbpA area down to a scan size of a $1 \mu\text{m}^2$ (Figure III-7B), the 2-D crystalline structure of the S-layer was resolved, with lattice parameters close to those found in bacteria. The S-layer shows a polycrystalline character with 10^4 nm^2 crystalline domains due to the randomly distributed nucleation sites that grew with different crystalline orientations.

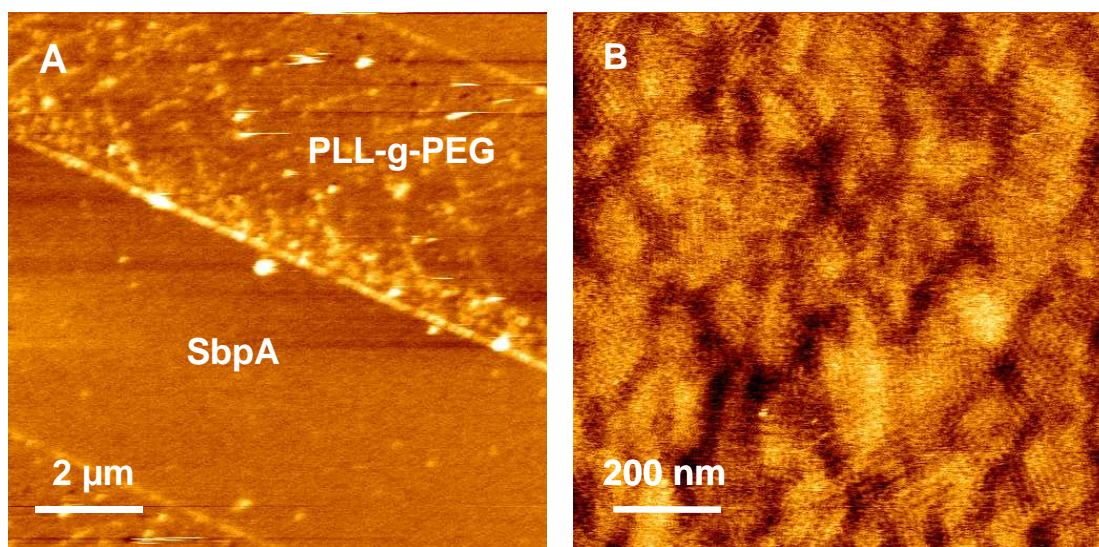


Figure III-7: AFM images of SbpA patterned surface. SbpA crystallized on PSS $5 \mu\text{m}$ strips (PLL-g-PEG free areas). (A) SbpA and PLL-g-PEG areas are clearly differentiated, (B) zoom in of the image shown in (A) of the SbpA zone. Note the SbpA crystalline structure with polycrystalline domains of about 10^4 nm^2 .

S-layer fusion proteins were also patterned. Figure III-8 shows the adsorption of rSbpA-EGFP by fluorescence microscopy on the micro structured surface. The pattern on the figure III-8A corresponds to the PLL-g-PEG rhodamine labelled. For the rSbpA-EGFP the direct observation of the green light emitted when excited at 490 nm confirmed the presence of the protein as shows figure III-8B. Both images complement each other, then the restriction of the adsorption of the rSbpA-EGFP to the PLL-g-PEG free areas was also confirmed.

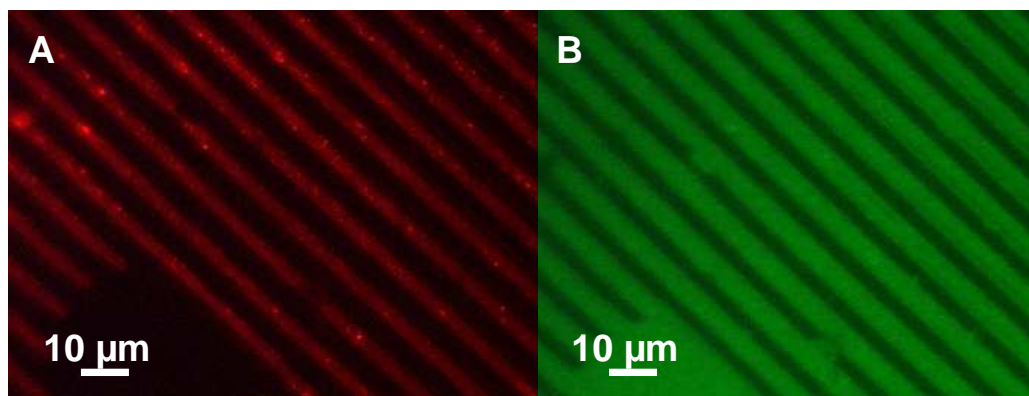


Figure III-8: Fluorescence microscopy image of rSbpA-EGFP pattern. Complementary images of patterned surface were obtained by changing the filter sets, due to the emission of (A) PLL-g-PEG rhodamine and (B) rSbpA-EGFP.

Figure III-9 shows the rSbpA-STV patterning after the binding of biotin-4-fluorescein to the heterotetramer units of the fusion protein. This S-layer fusion protein was adsorbed on the surface respecting the PLL-g-PEG pattern. Streptavidin was able to bind to biotin dissolved in solution, so the interaction streptavidin-biotin was not altered by the adsorption of the heterotetramer fusion protein (rSbpA-STV) on the micro patterned surface.

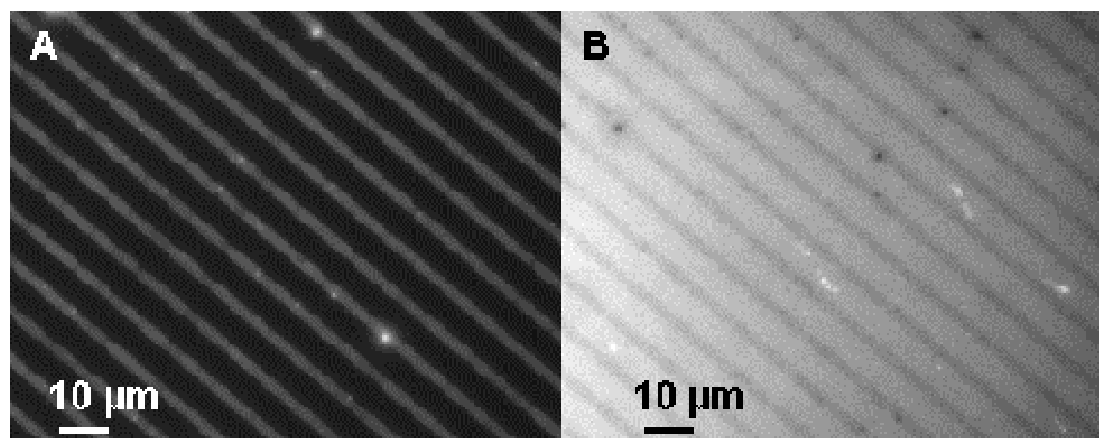


Figure III-9: Fluorescence microscopy image of biotin-4-fluorescein bound to SbpA-streptavidin pattern. After adsorption of heterotetramer SbpA-streptavidin on the PLL-g-PEG free areas, biotin-4-fluorescein bound to functional streptavidin on the surface. Two filters were used to identify the PLL-g-PEG rhodamine labeled pattern (A) and the Biotin-4-fluorescein bound to heterotetramer rSbpA-streptavidin (B). The difference in grey levels indicates the selective distribution of the biotin-4-fluorescein on PLL-g-PEG free areas.

III.2.4.3. Cell culture on polyelectrolyte multilayers

Usually cell culture medium formulation includes serum as a rich source of nutrients, which among others contains proteins, which adsorbs on the surfaces that contacts it. According to the PE last layer characteristics, different protein adsorption processes could take place. QCM-D was used to study the adsorption of proteins on different polyelectrolytes.

After coating the gold crystal with the PE, the temperature was increased up to 37°C and cell culture medium was pumped into the chamber. The temperature was increased to set the conditions closer to the physiological, because afterwards cell interactions were going to be studied (see chapter 4). The medium was allowed to interact with the surface until no significant changes were measured (approx. 1 hour). The final values for the adsorption of molecules from the medium are shown in table III-7.

Table III-7: Adsorption from culture media on the PE coated crystals

<i>Overtone 3</i>	<i>Culture medium</i>	
Substrate	$\Delta f_{\text{average}}$ (Hz)	$\Delta D_{\text{average}} \times 10^{-6}$
PEI	81 ± 5	10 ± 3
PAH	71 ± 2	6 ± 4
PLL	80 ± 7	10 ± 3
PSS	90 ± 12	6 ± 3
PLL-g-PEG	22 ± 8	6 ± 1

The Δf registered for the PEI, PAH and PLL were similar and indicate the presence of an adlayer between the polyelectrolytes and the medium. On all the polyelectrolytes except on PLL-g-PEG, the formation of a viscoelastic protein layer was obtained. PLL-g-PEG has the lowest value of Δf but with a comparable change in dissipation.

Cells adopted different morphology according to surface properties on which they were adsorbed. Figure III-10A shows cells attached to a PEM with PAH as last layer after 24 hours of culture.

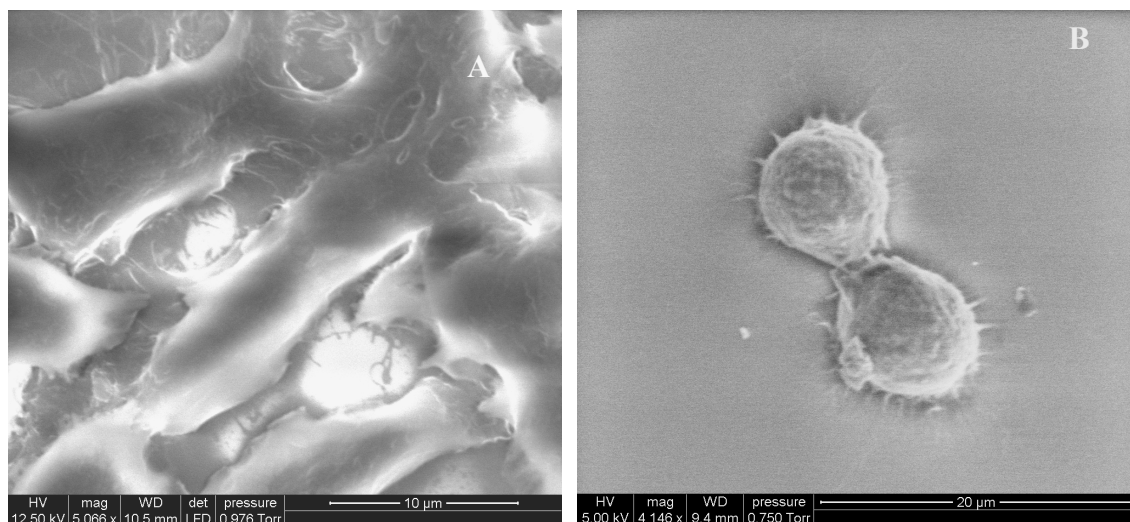


Figure III-10: SEM images of cells attached on PEMs (A) Cells are spread, adopting a flat morphology on PEMs ending with PAH, (B) cells remained quasi-spherical when the last PE layer was PSS.

It can be observed that the cells spread along the surface, with cell membrane protrusions. The same cell morphology was seen with PEI and PLL Figure III-10B shows cells cultured on PEMs PSS terminated. The cell membrane protrusions are smaller, and even when the cells are attached to the surface their shape is round. Cells growing on PLL-g-PEG adopted the same shape.

III.2.4.4. Cell patterning

After preparing different substrates with patterned surfaces, HepG2 cells were seeded on the patterned surfaces. It was observed that if the cells were allowed to attach for too much time, they did not follow the pattern and attached on the entire surface. In chapter 4 it is shown that the time that the cells require for attachment was different according to the polyelectrolyte used. Cells attached faster on PEI, PAH and PLL and more time was required for attachment on PSS and PLL-g-PEG. Then after seeding the cells, they had 3 hours to attach and after that time non-or loosely attached cells were removed by washing the substrates with cell culture medium. The cell pattern was obtained and it became clear after allowing the cells to grow as it shown in figure III-10. Even the cell confluence in the strip was almost 100%, the cells did not spread further away when the patterning was backfilled with PLL-g-PEG. This behaviour was clearer for the patterns with PLL/PLL-g-PEG.

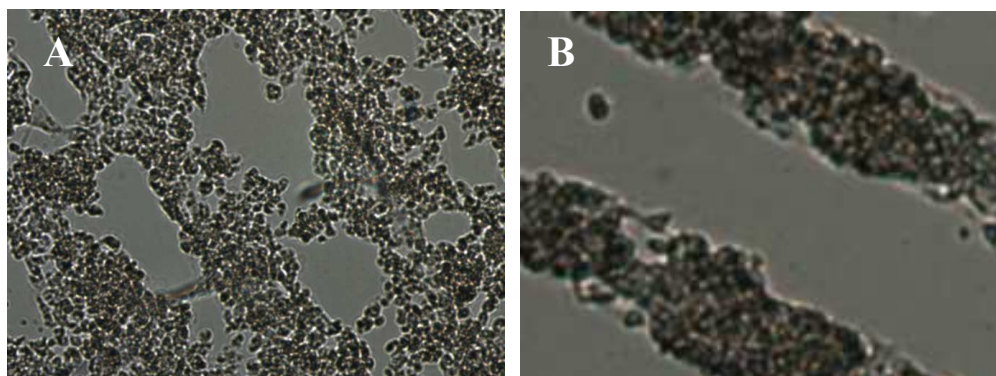


Figure III-11: Microscopy image showing cell patterning after 72 hours culture. (A) Cells growing on PLL patterned surface do not respect the patterning. (B) PLL patterned surfaces backfilled with PLL-g-PEG limited the cell growth only PLL strips.

III.3. Discussion

III.3.1. Protein adsorption on polyelectrolyte multilayers

We used QCM-D to follow the assembly and the viscoelastic characteristic of the multilayer system. After the adsorption of PEI, a non dissipative layer of PE was deposited, and all the overtones were almost overlapped. This means that the Sauerbrey relation can be used to determine the superficial mass density:

$$\Delta m = \frac{C \cdot \Delta f}{n}$$

with m: mass surface density, C: mass sensitivity constant and n: overtone number.

The mass surface density obtained for the PEI and associated water on the crystal was of $185 \pm 35 \text{ ng/cm}^2$. The adsorption of PSS on the PEI led also to a compact layer, with a surface density of $396 \pm 77 \text{ ng/cm}^2$. The increase of $167 \pm 33 \text{ ng/cm}^2$ was due to the adsorption of PSS and the water coupled to the PEs. After PAH deposition, the characteristics of the polyelectrolyte film were different since an increase of 10×10^{-6} showed that the last layer was not longer rigid or elastic, but viscoelastic. The fact that PAH adsorption resulted in a “fluffy film” due to an extended conformation of the PAH has been previously reported by Notley et al., and Ngnakam et al.[93; 94]. After PSS

adsorption, the dissipation decreased to almost the original value and the frequency did not change significantly. The decreased in dissipation showed the collapse of the PEM after adsorption of PSS. In spite of that, the fact that the frequency did not change could be due to the massive release of water of the “fluffy” layer, what resulted in a compact layer. Schmitt et al. [95] showed that even molecularly thin multilayer films have significant water associated with them, up to 27% for PSS-PAH, then a collapse could result in a significant expulsion of water from the multilayer without decrease in frequency in spite of the adsorption of PSS. The superficial mass density obtained after the deposition of the second PSS layer calculated with Sauerbrey relation was of $779 \pm 96 \text{ ng/cm}^2$. A similar behaviour was observed after the deposition of another bilayer, and the superficial density obtained was of $1190 \pm 130 \text{ ng/cm}^2$. Both bilayer depositions had a similar change in the superficial mass density. After the first bilayer, the superficial mass density increased in $361 \pm 54 \text{ ng/cm}^2$, and $415 \pm 34 \text{ ng/cm}^2$ after the second.

PLL was also adsorbed on PSS ending PEM giving a compact layer that corresponded to an increase in superficial density of $272 \pm 16 \text{ ng/cm}^2$.

The Sauerbrey relation cannot model the PLL-g-PEG adsorption due to the fact that the PEG brushes are a highly dissipative system. After injecting the PE, there was a huge change in frequency compared with the other polyelectrolytes due to the big molecular weight of the PEG that is attached to the PLL back bone and associated water. The increase in dissipation was expected, due to the dissipation introduced by the PEG brushes.

The contact angle measurements of the different surfaces were not significantly different except for the PLL-g-PEG, which was the one with lowest contact angle due to the highly hydrated PEG brush. PSS had a slightly lower contact angle than PAH, likely due to the sulphate groups facing the solution, and the aromatic rings orientating away from the surface [3].

III.3.2. Laccase immobilisation and interaction with PEs

PEI layer was used as a platform to covalently immobilise laccase through glutaraldehyde. Since the increase in dissipation compared with the change in frequency is less than 1/20, the Sauerbrey is still valid [96]. The superficial mass density for PEI was $200 \pm 40 \text{ ng/cm}^2$, GA $96 \pm 20 \text{ ng/cm}^2$ and crude laccase $430 \pm 80 \text{ ng/cm}^2$.

This value included not only immobilised laccase but other proteins species in the crude extract. The activity of the enzyme was confirmed with ABTS, which after flowing inside the chamber, was oxidised and detected spectrophotometrically. The measured activity decreased as the flow increased because the residence time inside the chamber decreased.

Afterwards, PAH and PSS were adsorbed on laccase. PAH was the first layer since the enzyme has an overall negative charge at the current pH. There was a change in frequency similar to the one observed when adsorbed on the compact PSS, but the dissipation did not increased as much as before. The interaction of the polyelectrolyte with the enzyme led to a more compact layer. After, PSS was adsorbed, the frequency decreased and a slight decrease in the dissipation was observed showing further compactation. After the next PAH adsorption step the frequency decrease was similar as before, but this time did not led to an increase in dissipation. The different behaviour of PAH adsorption compared with the observed on PSS multilayers, is probably due to the different nature of the underlying layer. It seems that there was a cross-linking of the PAH with the underlying molecules, what led to a decrease in frequency without increasing the dissipation. The presence of the enzyme showed that the coating with the polyelectrolytes led to a different type of interaction, resulting in a different behaviour (characterised by the evolution of the frequency and dissipation) when a PSS/PAH bilayer was adsorbed. Depending on the strength of those interactions, the activity of the enzyme could be affected.

The control experiments with both PEM terminating with PAH and PSS showed that ABTS adsorbs when the last layer is PAH. But when the last layer is a homogenous PSS layer, no ABTS remains on the surface. This is explained by the fact that ABTS is a negatively charge molecule.

When ABTS was injected into the chamber with polyelectrolyte coated laccase, the QCM-D response was different from the bare laccase. In spite of the polyelectrolytes, the shape of the f vs t or D vs t did not reached a stable value when in contact with ABTS solution. The polyelectrolytes seemed to be a diffusional barrier. Besides, after washing with succinate buffer, neither the frequency nor the dissipation returned to the values before injecting ABTS, even when the last layer was PAH or PSS. This could be explained if after the PSS coating a non-homogenous layer with positively charge area is available for the ABTS to adsorb.

When a first layer of PAH was deposited, the activity of the enzyme was not significantly affected. After the subsequent adsorption of PSS and PAH, the laccase activity was almost half the original value. But when PSS was the last layer, the activity seemed to recover.

Due to the fact the polyelectrolytes interacts with the enzyme and also with the substrate to measured the activity, complicates the analysis of the data. The apparent reduction of activity of the enzyme may be due to the interaction of the ABTS with the PAH, which interfere with the reaction between the laccase with the ABTS, but no due to a deactivation of the enzyme. Besides, the recovery of the activity after the second PSS layer could be due to a stronger interaction between PSS and PAH, what permits the ABTS to reach the enzyme. In order to clarify the influence of the PE on the activity of the laccase, other substrate or technique (such as electrochemical-QCM) could be used, in order to determine directly the enzyme activity without interference.

III.3.3. Patterning of SbpA and fusion proteins by polyelectrolyte microcontact printing

The main reasons for using polyelectrolytes as substrates were their compatibility with the adsorption/recrystallisation of bacterial proteins (S-layers), as well as their low cost and availability, together with the possibility of building structured surfaces with defined physico-chemical properties using the layer-by-layer technique. To be able to pattern SbpA applying microcontact printing the stamped polyelectrolyte has to have

different properties than the underlying layer. SbpA is known to be able to recrystallize on PEMs with PSS ending layer, even increasing their mechanical resistance with respect to silicon substrates [38]. On the other hand, PLL-g-PEG is a protein resistant PE, tested with proteins such as albumin, fibrinogen and myoglobin, on different metal oxides [77; 78]. The contact angle measurements confirmed that it also resists the crystallization of the SbpA. Once it was proved that SbpA does not adsorb on PLL-g-PEG, we proceeded with the patterning of the surface combining two well-known techniques: polyelectrolyte adsorption and micro-contact printing. The microcontact printing technique is fast, easy, inexpensive and compatible with the use of biomolecules. By AFM it was possible to distinguish between PLL-g-PEG and crystalline wild type SbpA. In order to introduce functionalities to the surfaces recombinant and fusion proteins were used. Patterning of rSbpA-EGFP was confirmed using fluorescence microscopy. rSbpA-EGFP covered all the areas where no PLL-g-PEG was present and it was active after adsorption meaning that its fluorophore remains intact. Besides rSbpA-STV adsorbed on the surface respecting the PLL-g-PEG pattern and remained functional since it was able to bind to fluorescently label biotin.

Even though the functionality of the both fusion proteins was shown, their crystalline state has not been addressed yet. The ability of recombinant S-layer proteins to recrystallize on pyruvylated secondary cell wall polymer (SCWP) has been studied. Truncated rSbpA₃₁₋₁₀₃₁ showed comparable self-assembly and SCWP binding properties as full-length rSbpA [97]. Besides, truncated S-proteins fused to EGFP [39], streptavidin [66], Fc-binding Z-domains [42] and birch pollen allergen [43] maintained their ability to reassemble on SCWP. In particular, the rSbpA-EGFP recrystallised and retained the fluorescence on peptidoglycan and on positively charged liposomes [39] and anionic polyelectrolytes [38]. Heterotetramer rSbpA-STV remained functional and recrystallized on plain gold chips and on gold chips pre-coated with thiolated SCWP (Huber et. al., 2006).

S-layer protein patterning was possible by micro-contact printing of PLL-g-PEG. Wild type SbpA was able to reassemble on the PLL-g-PEG free areas maintaining the crystalline parameters similar to those observed in the bacterial cell wall. Our work shows the potential of bacterial proteins (S-layers) as a “self assembling building block” since they are able to create biomimetic structures. We have proved that direct S-layer

patterning through protein passivating compound such as PEG is possible, mimicking the bacterial cell wall.

III.3.4. Cell culture on PE and patterning

When cells were seeded on the different surfaces, different morphologies were observed. Cells spread on PEI, PAH and PLL, but not on PSS and PLL-g-PEG. The positively charge polyelectrolytes seemed to adsorb proteins on which the cells spread. When cells were cultured on PSS, even when a protein layer was on the PE, its composition did not trigger cell spreading. A similar morphology was observed when the cells were adsorbed on PLL-g-PEG, where a lower amount of protein was adsorbed.

It is known that using culture medium complemented by serum, the attachment process of the cells is facilitated by the adsorption of proteins, resulting in cell spreading. Proteins such as concavalin A, fibronectin, laminin, vitronectin, ricin and chondronectin (present in serum) have been identified to mediate adhesion and spreading [51].

Due to the difference in adhesion properties, it was possible to direct cell adhesion to certain areas on the substrate. On one hand, if only a “favourable” PE was printed on the surface, most the cells attached to those areas, but afterwards they extended to non-printed areas. On the other hand, if PLL-g-PEG was adsorbed on the free areas after printing, the cells remained confined.

III.4. Conclusion

Different surfaces with defined functionalites were obtained. First, laccase was covalently immobilized on gold/PEI/GA layer and remain active as measured with ABTS. The adsorption of PAH and PSS on immobilized laccase was observed, and a cross-linking without significant changes in dissipation. The effect of the PEs on the activity of the enzyme is not clear, due to the ABTS interaction with the PEs.

Besides, it was proved that direct S-layer patterning through protein passivating compound such as PEG is possible. Three types of bacterial proteins were patterned, two of them fusion proteins with intrinsic biological functions. Furthermore, it was

shown that wild type SbpA maintained its crystalline structure as on the bacteria wall, rSbpa-EGFP and heterotetramer rSbpA-STV remained functional in the patterned surface. The ability to direct the micro-scale protein distribution is a basic requirement for future biosensor development.

Finally, HepG2 morphology was different according to the underlying PE. Positive polyelectrolytes adsorb molecules that trigger cell spreading. On the other hand, PLL-g-PEG (neutral and highly hydrated interface) and PSS (negative polyelectrolyte) does not favour spreading. Taking advantages of the lower affinity for PLL-g-PEG, cell attachment and confinement on PLL stamped strips was attained.

Chapter IV

Cell interaction with biocompatible surfaces

IV.1. Introduction

The ability to control the interactions of cells with surfaces is of major importance for the development of biocompatible materials. The surface chemistry, topography, and mechanical characteristics of the material modulate the cell behaviour [2; 23; 98; 99].

The mechanisms used by the cells to attach to surfaces are complex, and vary with the cell type and surface properties. The forces that are involved in the attachment can be divided in non-specific physical forces and specific interactions. Among non specific interactions are electrostatic forces, van der Waals and steric stability forces that result from hydrated layer of polymer of long chain polymer that are in the cell membrane (glycocalix). Non specific interactions act in a long range up to 100 nm, and are important in the initial approach of the cells to the substratum [51]. In 1978 Grinnell [100] proposed a relatively general process with different stages that leads to cell adhesion. It consists on four phases: protein adsorption, cell contact, attachment, and spreading. When the proteins adsorbed from the medium do not facilitate the attachment, cells secrete microexudate to aid the adhesion. If the surface has a favourable chemistry, the attachment is mediated by specific interactions that lead to the formation of focal adhesion points, which induce reorganisation of cytoskeleton and related proteins. Varying the concentration, composition and conformation of the adsorbed proteins or the peptide sequences responsible of the interaction, cell behaviour can be modulated [101; 102].

Polyelectrolytes are a versatile tool to tune surface chemistry [14; 83; 84; 87; 99]. In a multilayer system the interactions with the cells depend on the type of the outermost layer, number of layers in the film and the presence of proteins [83]. As mention in chapter 3, the adsorption of proteins takes place almost instantaneously after a solid surface comes into contact with a protein solution. The process of protein adsorption is

affected by the properties of the surface (surface energy), the nature of the protein (hydropathicity, charge and size), and the solution conditions [103].

Natural and synthetic polyelectrolytes have been tested as biocompatible materials for the ability to avoid or to promote adhesion [83; 85- 87].

Due to an increased interest in cell adhesion studies, new tools are being applied to increase current knowledge. Traditionally, cell adhesion studies are usually based on direct or indirect cell quantification. Direct cell counting or protein determination, or colorant up-take (crystal violet), are few examples. The characterisation of morphological features during attachment and spreading often employ time-lapse videomicroscopy and ultrastructural techniques. These methods are time consuming, labour intensive and sometimes subjective. Therefore, techniques that allows to monitor the attachment and spreading of cells quantitatively and in real-time are highly desirable [104]. As an answer to that, among others techniques, the quartz crystal microbalance (QCM) has been proposed as an indirect method to follow the kinetic of cell adhesion [105]. Until now, several studies have shown that the QCM can follow adhesion and spreading of initially suspended cells on different substrates such as polystyrene and metal surfaces: Ta, Cr, etc, with and without serum [106; 107]. Several studies have reported frequency shifts due to the presence of cells on the sensor [105; 108], which can be related with the number of cells adhered to the surface or to changes in degree of spreading [72; 109]. Besides, a cell layer influence shear displacement predominantly by damping, so increasing the energy dissipation [106]. The energy dissipation due to the cells on the crystal could be affected, for example, by the cell rigidity, which is influenced by the spreading and organisation of the actin cytoskeleton. Beside, the distance between the cell and the surface can also affect the dissipation of the system. Thus, considering the complexity and non-idealities of the cell adhesion process a theoretical approach to model the response obtained with the QCM is not available yet. In spite of that, the correlations reported among frequency change (Δf), dissipation change (ΔD) and cell attachment show the potential of the technique [105; 108; 110].

We used polyelectrolyte multilayers (PEM) with different ending layers, and study the adhesion of cells in serum containing medium. Optical microscopy, a spectrophotometer method and QCM-D were used to study how adhesion changes with time. The use of microscopy gave hints for the interpretation of the QCM results. The

viscoelastic characteristic of the systems composed by PEM, adsorbed protein, cells and confined medium is a system very difficult to model. In spite of its complexity, qualitative information about the different adhesion process was obtained.

IV.2. Results

IV.2.1. Cell viability

The viability of HepG2 studied with the MTT method was evaluated to determine if it was affected by interactions with the PEs coated surfaces. This method relates the activity of various dehydrogenase enzymes present in active mitochondria with an increase in absorbance measured at 550 nm. The viability is expressed as the % of the absorbance obtained for the cells growing on coated surfaces and a control (surface without PEs). The assay was performed after 24 and 48 hours of culture on PE surfaces. Figure IV-1 shows that there is no significant difference in the viability of the cells due to the presence of the polyelectrolyte on the surface.

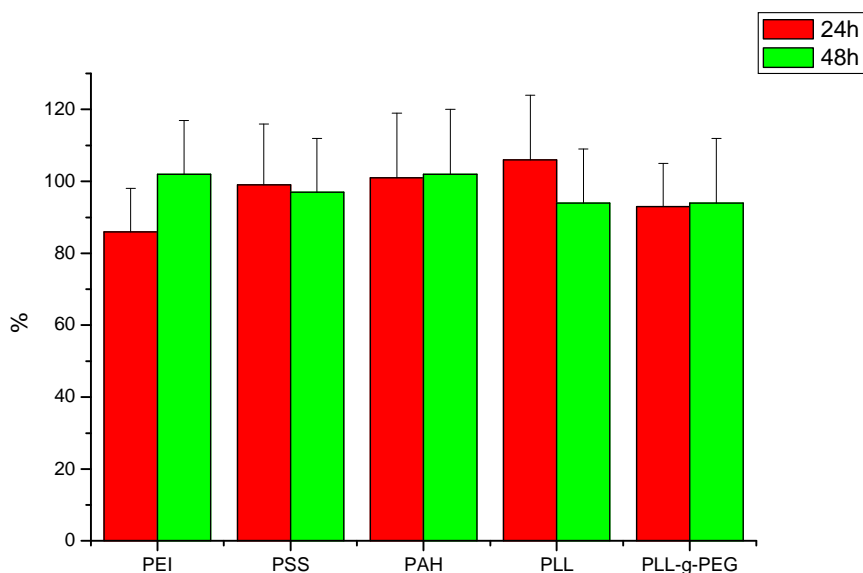


Figure IV-1: Cell viability on different coated surfaces. No significant difference in the viability of the cells was observed after 24 and 48 h. The error bars represent the standard deviation (n=4).

IV.2.2. Cell shape changes with time

In order to observe the cells during attachment, images were taken at 45 min, 1.5 h, 3h and 5 h, are shown in figure IV-2. When cells were seeded on PEI, after 45 minutes in contact with the surface, they remained attached to the surface even when the medium was agitated gently. Although they remained spherical, protrusions from the membrane started to appear in a couple of cells. After 3 hours, most of the cells presented these protrusions and some of them started spreading on the surface. This process kept going, as it is appreciate in figure 2 at 5h. After leaving the cells overnight, most of the cells were spread and “flat”. A similar behaviour was observed for the PAH and PLL.

When cells were seeded on PLL-g-PEG, they sedimented but they did not attached to the surface even after 1.5 hours (shaking the medium removed them from the surface). After 3 hours, most of the cells remained attached to the surface but no morphological changes were observed. After 5 hours protrusions started to appear, and become more clear after leaving the cells overnight. The cells on PSS behaved in a similar way.

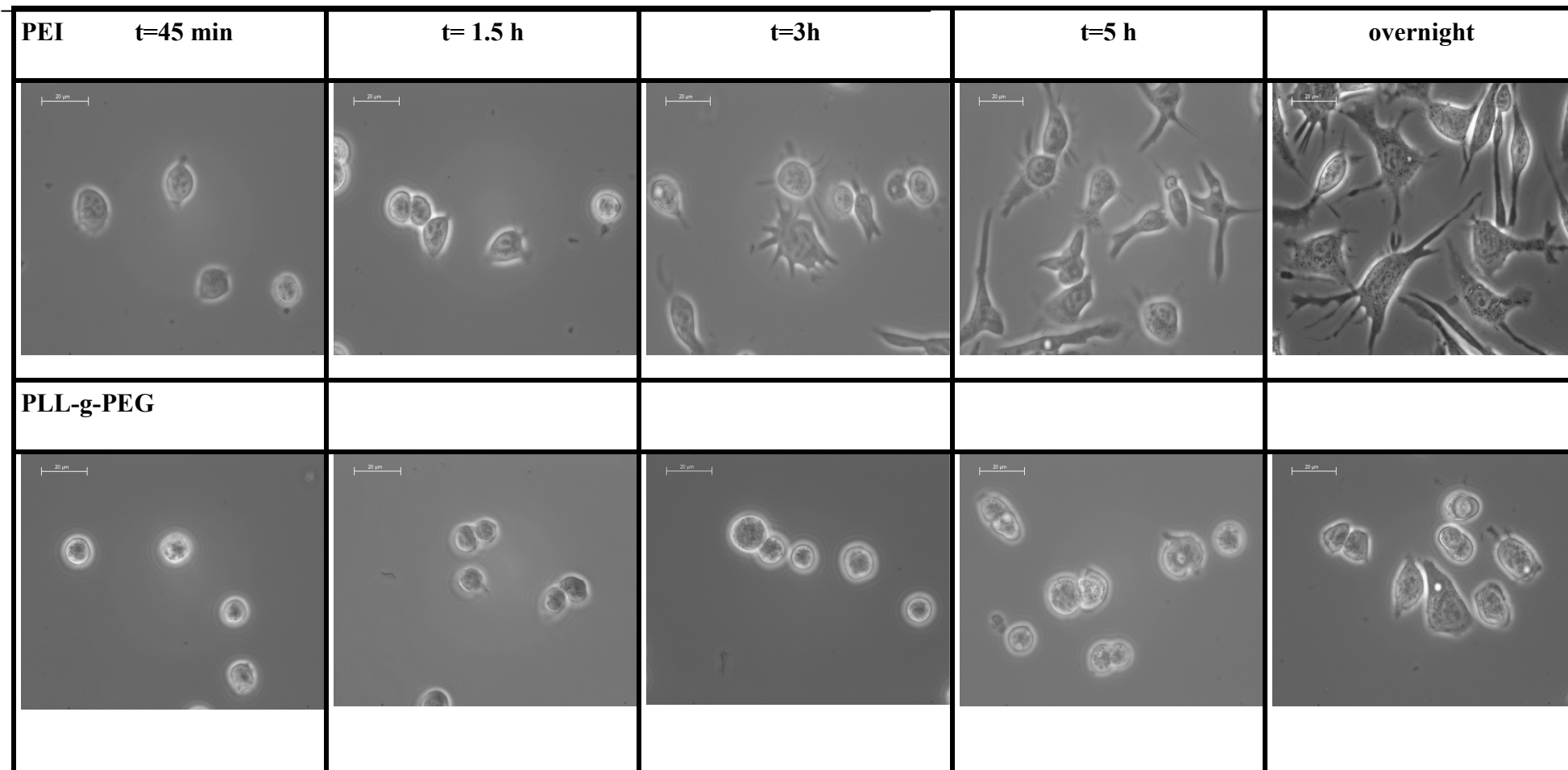


Figure IV-2: Phase contrast images of cells adhering to PEMs coated glass slides showing the morphology changes observed after different time intervals. **PEI:** After 45 min the cells were attached to the surface. Cell membrane protrusions started to form after 1.5 h and were clear after 3 -5 h. Cell spreading was observed overnight. **PLL-g-PEG:** No changes in morphology were noticeable after 3 h culture. After 5 hours protrusions started to appear in some cells, becoming more visible after setting the system (substrate/cell) overnight.

IV.2.3. Cell adhesion vs time

The amount of adhered cells was estimated by the assay with crystal violet (material and methods). It is an indirect way to quantify the cell number, and it is based on the uptake of crystal violet by the cells, which is released after cell lysis, and measured with a spectrophotometer. Figure IV-3 shows the absorbance measured at 630 nm, which correspond to the cells adhered on different substrates after 45 minutes, 2 and 4 hours, and overnight. Regardless the surface, with time more cells remained attached to the surface.

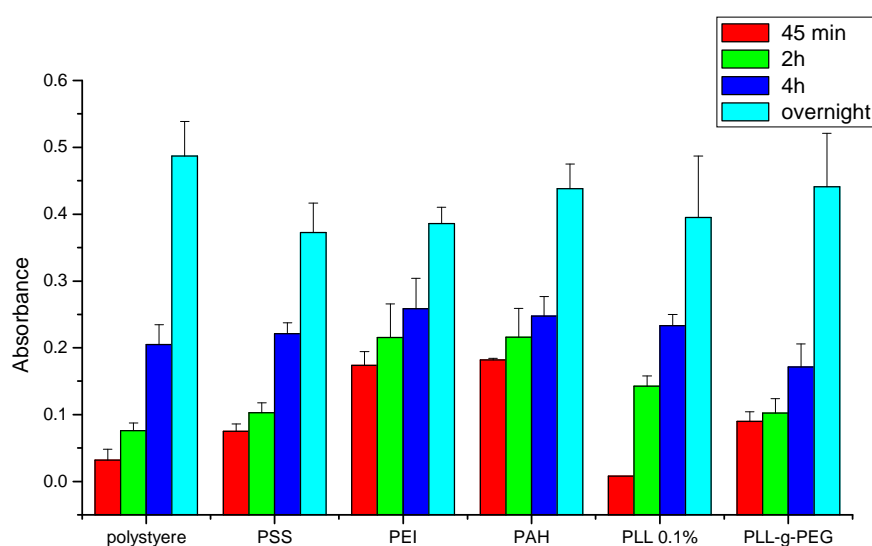


Figure IV-3: Cell adhesion measured with crystal violet. After 45 min PEI and PAH had the highest amount of cells adhered to PE coated surface. PLL, PSS and PLL-g-PEG had lower values but the differences among all diminished with time.

After 45 minutes PEI and PAH were the substrates that showed the highest affinity to the cells. Lower values were obtained for PSS, PLL-g-PEG, PS (polystyrene) and PLL. In the next 2 and 4 hours, the number of cells adhered increased but maintained the same tendency as before. After leaving the cells overnight all the surfaces had more cells and no significant differences among the substrates.

IV.2.4. QCM-D: Frequency and dissipation change vs. time

Cells were injected in QCM chambers, and frequency and dissipation changes were registered to monitor the adhesion process on PE coated crystals. Normalised frequency values (f/n) are shown. When only one overtone is presented, it corresponds to the 3rd. After coating the gold crystal with the PE, the temperature was increased up to 37°C and cell culture medium was pumped into the chamber and allowed to interact with the surface. Once a stable base line was attained (see chapter 3), a cell suspension with 1×10^6 cells/ml was pumped into the chamber. Control experiments (medium without cells) were carried out in parallel to evaluate the effects of the injection and the new adsorption of molecules from the medium on the crystal. After new culture medium was pumped, the maximum change of frequency and dissipation was of 5 Hz and 1×10^{-6} . Besides, the slope of the control experiment in all the different substrates had maximum values of 2 Hz h^{-1} and $0.5 \times 10^{-6} \text{ h}^{-1}$. Considering that the fabrication specification report that on clean non-coated standard Au crystal in water, the measurement should not drift more than 2 Hz h^{-1} and $0.2 \times 10^{-6} \text{ h}^{-1}$, this means that the changes registered with time are within the error of the apparatus.

Figure IV-4 shows the data recorded while monitoring cell attachment on a crystal coated with PEI. Immediately after the injection of the cells, there were a decrease in the frequency and an increase in the dissipation comparable with the values of control experiment. Afterwards, there was a continuous decrease in frequency, and an increase in dissipation. Looking at the evolution of the normalised frequency, it is observed that there is a continuous decrease, and the variation is smaller as the overtone number increase. Besides, there is a dissipation increase. This behaviour is related to the viscoelastic properties of the system and will be discussed further in the chapter (see discussion). The cells attaching on PAH and PLL presented a similar behaviour.

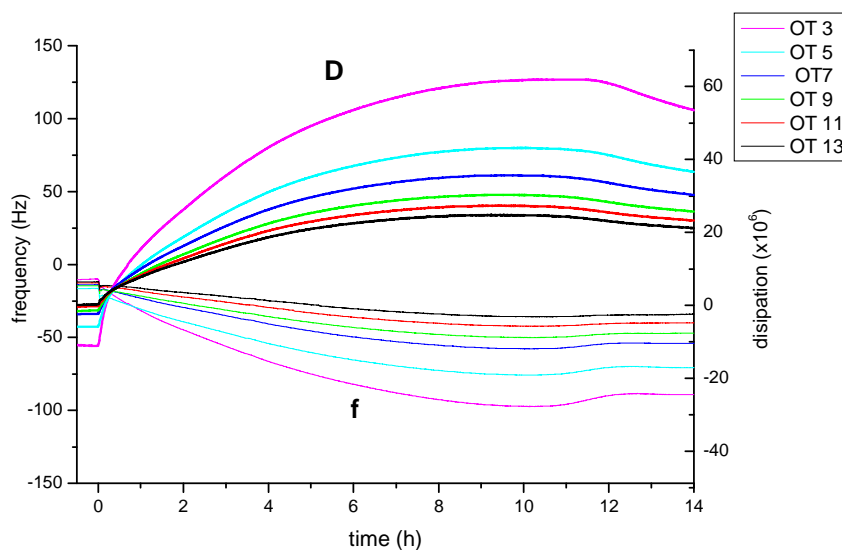


Figure IV-4: QCM-D measurements monitoring the cell attachment on PEI. The frequency values are normalised by the overtone number ($OT=n$) f_n/n . The change in frequency and dissipation decrease as the overtone number increases.

Even though the experiment replicates and experiments repetitions presented a similar qualitative behaviour, there were quantitative differences. For example, in some experiments a maximum in dissipation (minimum in frequency) was observed, but in others no maximum was reached until the end of the experiment. In table IV-1, the frequency and dissipation changes up to the end of the experiment, or until a maximum was reached, are presented.

Table IV-1: Maximum frequency and dissipation changes registered

<i>OT3</i>	Δf (Hz)	ΔD ($\times 10^{-6}$)	<i>Time</i> (h)
PEI	54 ± 13	30 ± 5	10
	50	46	max. 6
	34 ± 7	30 ± 3	15
	86	63	max. 11
	75	52	max. 10
	70	53	13
	48	36	max 4.5
PAH	65 ± 1	40 ± 1	9
	36	29	max. 2.5
PLL	51 ± 9	42 ± 7	10

The values of frequency and dissipation shifts ranged from 30-90 Hz and $30-65 \times 10^{-6}$ respectively, in 2.5 to 15 hours.

An alternative representation of QCM-D data are the dissipation vs. frequency plots, in which the time is implicit [106]. Advantages of this way to present the data are: I) different adsorption processes are detected since regions with similar $\Delta D/\Delta f$ become visible, and II) it is qualitatively independent of the number and spatial distribution of cells on the surface because the lateral sensitivity for f and D are the same.

Figure IV-5 shows the D vs. f plot for the 3rd overtone for a PAH coated crystal. It can be observed that there is a sharp change in D , followed by a decrease of the $\Delta D/\Delta f$ slope reaching a region in which was almost constant. This could be due to the disturbance introduced when injecting the cell suspension and the first period of cells interacting with the surface. Afterwards, a linear relation between D and f lasted for approx. 1 hour. A constant value of $\Delta D/\Delta f$ shows that during that period, the interaction of the cells with the crystal produced constant increase in frequency and dissipation. After that time $\Delta D/\Delta f$ diminished, and sometimes at the end of the experiment a decrease in dissipation was observed.

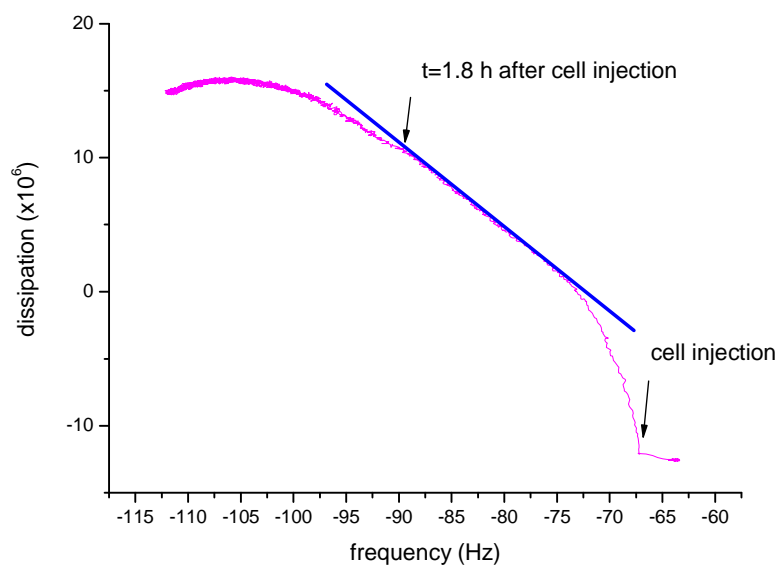


Figure IV-5: D vs. f plots evidence different adsorption process characterised with a similar $\Delta D/\Delta f$. For cells attaching on PAH coated surface, after cell injection the highest values of $\Delta D/\Delta f$ were observed, and after 0.4 hour the $\Delta D/\Delta f$ stabilised reaching a lineal region that lasted 1.4 hours.

Although D vs. f curve shape varied within substrate replicates and for different substrates, all of them have in common at least one lineal region with similar slopes for each substrate, as shown in table IV-2.

Table IV-2: Slope values obtained in the linear region in the D vs. f plots of the 3rd overtone for the different substrates

<i>Polyelectrolyte</i>	$\Delta D/\Delta f$ ($\times 10^{-6} \text{ Hz}^{-1}$)	<i>Time linear regression starts (h)</i>	<i>Duration (h)</i>
PEI	0.83	1.3	9 till end
	0.79	0.5	3 max (max 6)
	0.7	0.9	5 till end
	1.2 0.9	1.5	3 6 till end
	0.8 0.6	2.3	3.2 5 till end
	1.2 0.9	1.5	3.4 6 (max)
	0.75	1.4	8 till end
	0.72	1.4	8 till end
	1.0 0.7	0.5	0.6 2 max (max 4.5)
PLL	0.68± 0.02	2.1	8 till end
		1.8	8 till max
		2.1	8 till end
PAH	0.55±0.01	0.3	10 till end
		0.4	1.4 max (max)
		0.3	7 almost end

The highest variability for the PEI experiments could be due to the fact that when only one layer of polyelectrolyte is deposited, no homogenous surface is obtained, and then the adsorption of proteins is more variable compared with the PLL and PAH, where a more homogeneous surface is attainable after 6 layers of polyelectrolytes.

When PEI was adsorbed on the crystals, two different regions with constant $\Delta D/\Delta f$ were found. In the first period a $\Delta D/\Delta f = 1.0 \pm 0.2 \times 10^{-6} \text{ Hz}^{-1}$ and started in some cases after 0.5 until 2.3 hours, and lasted from 0.6 until 4 hours. The second period, with a lower $\Delta D/\Delta f = 0.8 \pm 0.1 \times 10^{-6} \text{ Hz}^{-1}$ lasted for 1.4-6 hours. When only a unique $\Delta D/\Delta f$ was fitted, the value was $0.77 \pm 0.05 \times 10^{-6} \text{ Hz}^{-1}$ and was present until the end of the experiment or a maximum was reached.

When PLL was the last PE layer, only one linear region with a slope of $0.68 \pm 0.02 \times 10^{-6} \text{Hz}^{-1}$ was observed, and it started 1.8-2.1 hours after the cell injection. For the PAH, a constant $\Delta D/\Delta t = 0.55 \pm 0.01 \times 10^{-6} \text{Hz}^{-1}$ started after 0.3-0.4 hours. Figure IV-6 shows an experiment in which cells are exposed to the adlayer on PSS coated crystal. There was a decrease in frequency of about 10 Hz within the first 30 minutes, and then it decreased at a rate of 2Hz/h. The change in dissipation was of 2×10^{-6} after the injection of the cells, and increasing afterwards to $0.3 \times 10^{-6} \text{h}^{-1}$. These values are similar to those obtained in the control experiments, with slightly higher frequency change, but lower dissipation change with time.

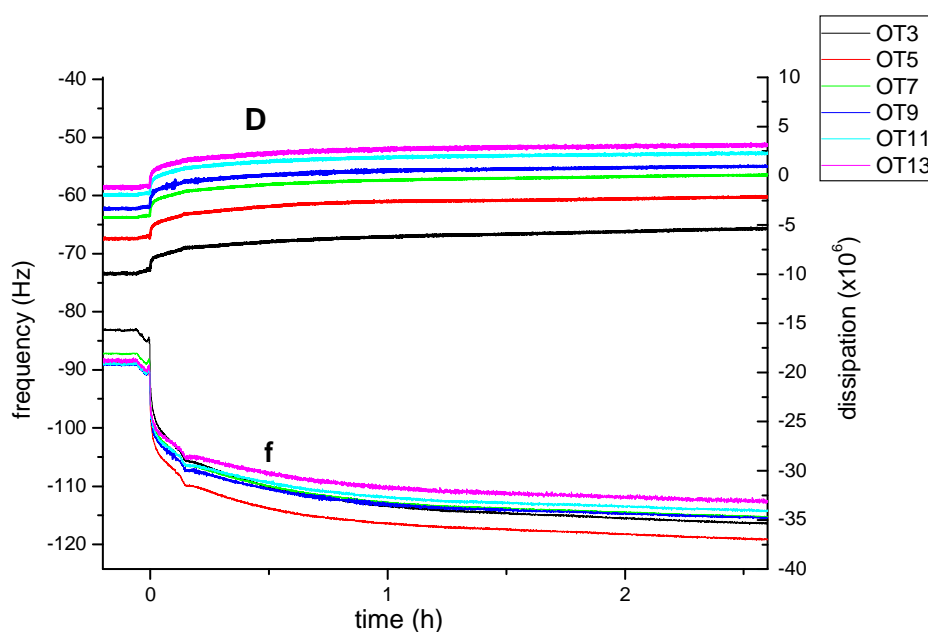


Figure IV-6: QCM-D measurements monitoring the cell attachment on PSS. After cell injection a decrease in frequency without significant change of the dissipation was registered. All the overtones registered a similar change.

The normalised Δf was similar for all the overtones and the change in dissipation was almost not detected (no difference with the blank). The results of the experiments on PLL-g-PEG were similar. The registered changes after 3 hours of injection are shown in table IV-3.

Table IV-3: Frequency and dissipation changes due to the cells on the adlayer formed after PSS and PLL-g-PEG surfaces contacted the culture medium, and after 3 hours of cell injection.

<i>Overtone 3</i>	<i>After 3 hours cell injection</i>	
<i>Substrate</i>	$\Delta f_{average} (Hz)$	$\Delta D_{average} \times 10^{-6}$
PSS	19 ± 1	3 ± 2
PLL-g-PEG	14 ± 3	4 ± 3

This behaviour is different from the one registered for the PEI, PAH and PLL. This data corresponds to the deposition of a more compact layer with no significant change with time in the period tested.

IV.2.5. QCM-D with window chamber

The figure IV-7 shows the set-up for the coupling of a reflection microscope with the QCM-D. This configuration allowed the recording of the frequency and dissipation changes simultaneously with the direct observation of what was on the crystal through the window in the chamber.

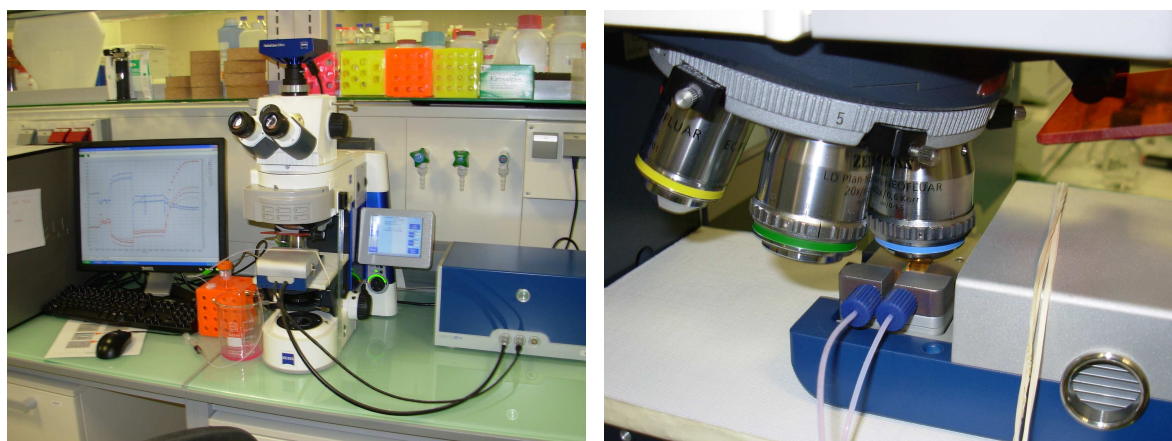


Figure IV-7: QCM-D system consisting in one module chamber with a window couple to a microscope. This system allows the direct observation inside the chamber with a reflective microscope while monitoring the frequency and dissipation changes.

The main difference with the previous set-up is that only one chamber is used, the volume above the crystal is of 100 μ l (2.5 times bigger), the injection of liquid was done

manually with a syringe at the end of the tubing, and there is no heat exchanger for the liquid entering the crystal chamber.

The experiments were carried out with three of the substrates tested: PEI, PAH and PSS. Figure IV-8 shows the frequency and dissipation measurements and the percentage of the surface that was covered with cells calculated from images processed with ImageJ 1.37v (NIH, USA).

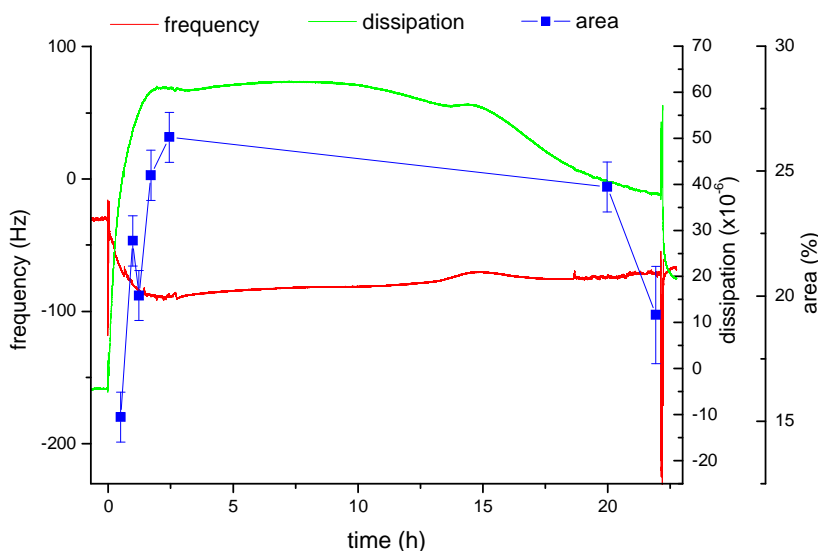


Figure IV-8: Changes in frequency and dissipation, and optical area evaluation of cells on a PEI coated crystal. The decrease in frequency and increase in dissipation was accompanied by the increase of the area of the cell, during the first hours after cell injection. Afterwards cells reduced their contact area, and a decrease in the dissipation and increase in frequency was measured.

For the PEI experiment, a fast increase in dissipation was observed after cell injection, with $\Delta D = 61 \times 10^{-6}$ reached after 1.4 hours. At the same time, the minimum value of frequency led to a $\Delta f = 54$ Hz. The percentage of area occupied by the cells increased during the first hours, and a decreased after leaving the experiment overnight.

The theoretical superficial cell density value considering that the cell diameter is approximately $10 \mu\text{m}$ (when cells are still rounded) is of 12%. After injecting 2 ml of the cell suspension the initial superficial cell density calculated was of 15%. After 0.3 hours, a linear relation $\Delta D/\Delta f = 0.9 \times 10^{-6} \text{ Hz}^{-1}$ lasted 1.1 h, before the maximum was reached.

A similar cell density was obtained for the experiment on PAH, with an initial value of 11%. The dissipation increased during the whole experiment and the frequency decreased. After 15 hours of cell injection, the $\Delta D = 59 \times 10^{-6}$ and $\Delta f = 77$ Hz. A lineal

relation of $\Delta D/\Delta f = 0.67 \times 10^{-6} \text{ Hz}^{-1}$ was fitted after 0.3 hours and lasted till the end of the experiment.

The experiment with PSS, as shows figure 10, behaved as in the prior set of experiments. First, after injecting the 2 ml of cell suspension, the superficial cell density was of 7%. Besides, during more than 20 hours experiment, the cells did not spread, as the almost constant % area shows. The dissipation change was of 2×10^{-6} in the first 6 hours, and afterwards remained almost constant.

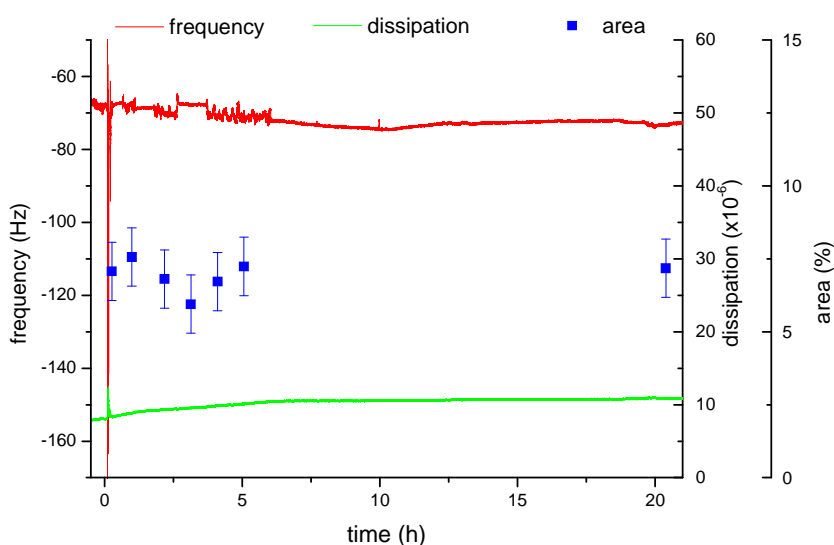


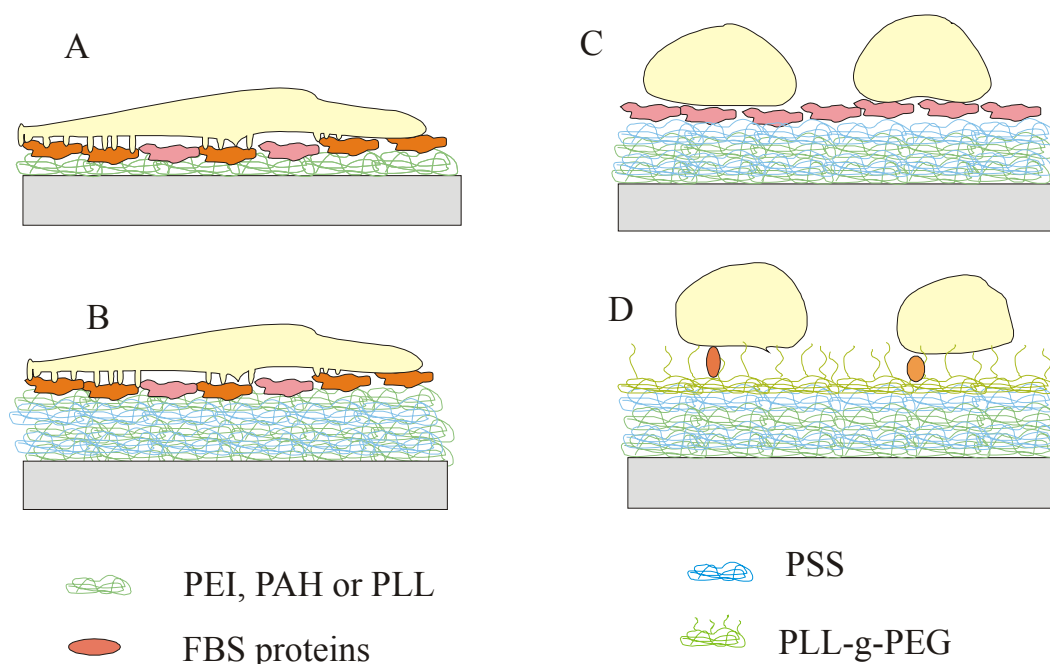
Figure IV-9: Changes in frequency and dissipation, and optical area evaluation of cells on a PSS coated crystal. After injection the cells did not significant spread, and the frequency and dissipation changes were of 4 Hz and 2×10^{-6} respectively.

IV.3. Discussion

In order to study the interaction of cells with the different surfaces, two complementary approaches were used. In the first one, we studied different characteristics of the cell as a whole. Their morphology on different surfaces was studied by optical microscopy. Besides, the cell viability on polyelectrolyte surfaces was assayed, as well as the adhesion as the amount of cells adhered on the different surfaces. The other, studying the outer part of the cell and local interactions, QCM-D and AFM were used (see next chapter). The interpretation of the results of these techniques was correlated by the information given by the more traditional approach to help its interpretation.

The interaction of cells with surfaces coated with the polyelectrolytes tested under serum containing media did not affect cell viability. The QCM measurements confirm

the presence of a layer of proteins on the surface, except in the case of PLL-g-PEG, which is known to be protein resistant (see chapter 3). The adsorption of polyelectrolytes followed by the deposition of proteins on the surface mediate the interaction of the cells without affecting their activity. In scheme IV-1, the different surfaces and cell adhesion are presented for better understanding of the result interpretation.



Scheme IV-1: Cell morphology on different surfaces. Cell spread on the protein layer adsorbed on: (A) PEI layer and (B) PEM ending with PAH or PLL. Cell attached but remained rounded on surfaces coated with PEM ending with (C) PSS and (D) PLL-g-PEG.

The properties of the resulting last layer determine the adhesion process. On one hand, when cells interacted with the proteins adsorbed on PEI, PAH and PLL (positive polyelectrolytes), they adhere in less than 45 minutes showing a similar behaviour. On the other hand, for the PSS and PLL-g-PEG, the cells seemed to float around on the surface for at least 3 hours until they attached. It seems that the cell contact with the surface, the first step for cell attachment, required more time. PSS is a negatively charged polyelectrolyte, then according to this observation the proteins adsorbed on it do not favour a fast contact with the cells, due to repulsion (cells glyocalix is generally negatively charged). On the other hand, the PEG brushes of the PLL-g-PEG diminish protein adsorption, and shield the positive charge of the underlying PLL backbone. Providing enough time, the cells adhered adopting a quasi-spherical shape without

spreading. Scheme V-1 shows that the presence or the absence of the protein layer is responsible for the different behaviours observed.

Crystal violet assay partially support those results. It seems that PEI and PAH had the biggest amount of cell attached to the surface after 45min and 2 h. Providing enough time, more than 4 hours, there was no significant difference among the number of cells adhered on any substrate. It is important to consider, that in this assay, what is measured is the quantity of cells that remain adhered after disturbing them by washing the surface. Ideally only unattached cells should be removed, but if the attachment were weaker than the shear force applied during that procedure, the cells would be washed away from the surface. That is one of the major weaknesses of this assay and source of error, since this force is controlled manually. It seems that the attachment strength of the cells after 4 hours was strong enough in all the surfaces to maintain the cells attached, and then no further difference were observed. These results are in agreement with microscopy images showing that PEI and PAH are the fastest to attach, but does not give more information. PLL had significantly lower values than could be expected considering that it is a positive polyelectrolyte. Although the cells on PSS and PLL-g-PEG do not spread, the adhesion was strong enough to avoid to be washed away from it.

QCM-D measurements show different responses for cells in contact with crystals coated with PEI, PAH and PLL or PSS and PLL-g-PEG.

For PEI, PAH and PLL, the decrease in frequency and the increase in dissipation were significantly higher than the values measured of the control experiments, when only medium without cells was injected. The normalised frequency varied with the overtone number, what together with the high values measured of the dissipation evidence viscoelastic behaviour of the system. The different overtones (OT) probe different depths, according to the decay length (δ):

$$\delta = \frac{2 \cdot \eta_{med}}{\sqrt{2 \cdot \pi \cdot f \cdot \rho_{med}}}$$

where the η_{med} is the viscosity of the medium and ρ_{med} is the density.

For 5 MHz crystal in water, the decay length decrease with the OT number as follows: 250, 145, 110, 95, 85, 75, 70 nm. The crystals were coated with a PEM with a thickness of 20-30 nm and on top a FBS protein layer with an estimated thickness of 30-40 nm.

Assuming these values valid for our experiments, the 13th overtone sense until slightly above the protein layer (except for PEI, only one layer), and for the other overtones further from the substrate. But cells attached to the crystal do not have a homogenous direct contact with the substrates. The distance between them depends on the cell type and substrate, and it could be up to a range 500 nm for BAECs (attachment barely detected with QCM) and epithelial cells with smaller distance with higher QCM responses [111]. On PEI coated crystals, as the overtone number increases, then sensing a shortest distance from the crystal, the change in f and D diminished due to the cell viscoelastic properties. The interaction with the surface seemed to be strong enough to maintain the cell close enough to the crystal surface to be sensed. Moreover, when cells attached on PEM ending in PAH, cells spread and with similar values of Δf and ΔD than on PEI, what shows that when the interaction between cell and surface were stronger, QCM-D was able to detect the cell attachment even when attaching on a PEM. Then, it seems that the different QCM-D response depended on the interactions nature between the cell and the molecules on the PEM, and it was not influence by the PEM thickness. Furthermore, it has been reported that the QCM response to cell attachment depends on the cell type, type of interaction, substrates and adlayer between crystal and cells [109]. Fredriksson et al. observed that cells attached but not spread on hydrophobic surfaces in serum containing medium presented a huge increase in D but not on f [106]. They suggested that since Δf is proportional to the cell-surface contact area, the unspread cell did not produce a significant change in frequency. They hypnotized that a receptor-mediated attachment or focal contact, even it is not extensive enough to stimulate spreading, might lead to significant dissipative processes in the acting part of the cytoskeleton. Wegener et al. showed that the presence of soluble RGD-related peptides can inhibited the adhesion by competition for the integrin domains what reduce the ability of the cell to firmly adhere to the surface, and made the presence of the cells near the surface undetectable for the QCM system (monitoring only the frequency change) [104]. Lord et al. used albumin coated surface to see the response resulting from cell-surface interactions with a non-adhesive surface, which showed little change in both f and D with QCM-D system, and cell adhered with a rounded morphology [112]. Then, it seems that the molecules adsorbed on PSS behaved as a non-adhesive surface.

Contrasting the QCM data behaviour with the microscopy images, we could try to interpret the QCM data with what is happening to the crystals and the cells. Besides

with the coupling of the optical microscope with the QCM-D was possible to confirm the observations in situ. Observing the D vs f plots, it is possible to identify 4 phases. The first one, immediately after cell injection, there was a sudden and sometimes erratic frequency increase that in some cases was partially recovered, with a slightly change in dissipation. It lasted from 3 to 20 minutes depending on the polyelectrolyte last layer. This could be due to the disturbance at the interface of the adsorbed FBS proteins from the medium due to the injection of new medium with the cells and when this period was longer, the first cell-substrate interaction. Afterward, there was a second phase where the $\Delta D/\Delta f$ ratio reached the highest values, and later started to decrease (this stage was not always present, especially on PEI) until it seemed to stabilise. The fact that after some time there is a clear increase in dissipation might indicate that the cells contacted the surface. The microscopy images showed that after 45 minutes, the first interaction with the surface results in cells already attached to the substrates without any further change in morphology. Then in this period, it could be said that after the medium disruption, the cells were able to contact the surface and start to interact. Similar results were reported by Fredriksson et al. who observed that CHO cells attached but not spread on hydrophobic surfaces in serum containing medium that presented a vertical D vs. f slope [106]. They suggested that since Δf is proportional to the cell-surface contact area, the unspread cell did not produce a significant change in frequency. In our experiments, both the dissipation and frequency change simultaneously, but at this phase the dissipation increase was more pronounced. The third phase is when the change in dissipation with respect to the frequency remained constant. It seems that the value of $\Delta D/\Delta f$ is characteristic of the substrate. The PEI has the highest value, followed by the PLL and PAH. Besides, the lineal relation started before for the PAH and PEI, and later for the PLL, that coincides with the apparent slower attachment observed with the crystal violet assay. Considering that the FBS adsorbed on PEI, PLL and PAH had different viscoelastic characteristics, whether $\Delta D/\Delta f$ values have a quantitative meaning in the attachment process is not certain. Since the cells attaching on QCM crystals give a complex response that integrate the presence of a protein layer, cell-substrate separation distance, and, presumably, the mechanical properties of the narrow cleft between cell and substrate, too many variables may affect the response, then quantification is difficult [111].

In the case of the PSS and PLL-g-PEG, a decrease in frequency and an increase in dissipation were observed after injection but comparable with the control experiments.

After cell injection, all the overtones run almost parallel to each other, together with almost no change in dissipation but more significant change in frequency. The fact that the overtones run parallel to each other, that is that the change in the normalised frequency is the same for all the overtones, implies that the Sauerbrey equation can be applied to study the system (considering that the dissipation value is also small). Then it seems that whatever was on the crystal behaves more like a rigid body, which corresponds to a compact protein layer rather than to a viscoelastic cell. When medium proteins were adsorbed on PSS a frequency shift of 86 ± 9 Hz and a dissipation increase of $7 \pm 1 \times 10^{-6}$ suggest that a thick protein layer is on top of the PE as scheme 1 shows. It is possible that after the medium injection, this layer was disturbed and led to a further absorption of proteins. It is known that the adsorption of proteins is a dynamic process, where smaller molecules are adsorbed faster, but bigger ones can replace them. Since this was registered after about 30 minutes of injection, and later almost no significant further changes were registered, it seems that after the cells were for 3 hours in contact with the coated crystal, the attachment was not detected. The experiment performed using the QCM-D coupled to the microscope confirmed that after even 20 hours, the cells on the crystal remain round, and without significant change of frequency. It has been proposed that during cell attachment, the change in frequency is dependent on the contact area. Since the cells remain rounded when in contact with PSS protein layer, it could be that the contact area is not big enough to be detectable, since the cell will not spread. But the fact that the dissipation did not increase does not agree with the dissipation increase reported when cells attach on surfaces. It seems the protein layer on PSS do not mediate strong enough interactions to be detected with QCM-D. A similar explanation is given for the PLL-g-PEG but for a different reason. The scheme 1 shows that the amount of protein absorbed was less with a $\Delta f = 13 \pm 3$ Hz and then if the proteins mediate the interaction, no enough amount of interactions were present to be able to detect adhesion.

When we compared the QCM data with the microscopy images, we tried to put in relation different images with different regimens of interaction observable in QCM plots. But it is important to remark that the complexity of the process is such that during measurement cells are suspended or attaching and/or spreading at the same time, and the QCM response is a “kind of average” of all.

The coupling of the microscope with the QCM gave us the possibility to confirm that what was observed in the petri dishes was also happening inside the chamber in spite of

the different conditions in both environments. Besides, other parameters that probably affect the results were detected. For example, the flow rate and amount of volume injected can affect the cell density on the crystal depending on the substrate. When injecting cells on PEI coated crystal, it was observed that the amount of cells on the crystal increased while the cell suspension was being injected, due to the fast adhesion of the cells on the crystal. In this case, the initial cells occupied the 15% of the total surface. On the other hand, when PSS was injected half of the cells were seeded on the crystal in spite of the fact that the same procedure was followed. Higher cell density leads to higher values of changes of frequency and dissipation. Higher cell number and unequal distribution on the surface may be reasons for different f and D curves with time, but this does not affect the qualitative behaviour of D vs. f curves. Apart from that, the differences among experiments with the same surface but different cell batch, could be due to different conditions of the cell membrane due to different handling during for e.g. trypsinization, obtaining initially different rate of adhesion.

In the case of the PEI experiment where QCM-D was coupled with a microscope, it was clearly observed that the cell area reduction (cell detachment) after 10 hours from cell injection, led to dissipation decrease and slightly frequency increase. If the cells were viable, they should remain adhered, so this behaviour showed that in this case the cell viability could have been affected. This could be due to the lack of nutrients or presence of toxins, for example due to the contamination with microorganisms. Considering that for the experiment with PAH, where the initial cell density was similar, the cells remained apparently viable during 15 hours, nutrient depletion seems not to be a problem. To diminish the risk of cells suffering nutrient depletion or contamination, the length of the experiment should be considered. As shorter is the experiment, both risk diminish, but also the information obtained may be different. If just the attachment of the cells is under study, the extension of the assay does not have to be long. If the spreading is studied, then longer experiments are required, and then aseptic conditions should be kept in order to assure the integrity of the cells during the assay. Besides, considering the microscopy pictures, the total spreading of the cells is observed after leaving the cells overnight.

IV.4. Conclusion

The cell viability was not affected after the cells were seeded on the different polyelectrolyte multilayers (PEM) with different ending layers.

The protein layer on PEI, PAH and PLL mediates strong interactions what lead to adhesion and spreading of the cells that was observed by microscopy, assayed with crystal violet and detected with QCM-D.

A slower attachment and no cell spreading were observed on the protein layer on PSS. The weaker interaction between the cells and the protein layer were not detected by QCM-D. Since PLL-g-PEG is a protein resistant polyelectrolyte, there was almost no protein layer on it, and then no mediators were present, what made the adhesion slower and not measurable by QCM-D. Even though model that fit cell-crystal interaction is not yet available; the QCM-D is a promising tool to follow the adhesion, spreading as well as detachment processes. Besides, when couple with a microscope the data interpretation becomes more direct.

Chapter V

AFM probing surface-cell interactions and mechanical properties

V.1. Introduction

AFM has become a standard tool to examine surface topography [113; 114], to study structural and functional biological systems [115; 116], to measure adhesive forces between the tip and the sample surface [117; 118], and to quantify interactions between biomolecules [119; 120].

As mentioned in chapter 4, cell adhesion is of fundamental importance to many biological processes. The use of atomic force microscopy on cells has been reported using mainly two different configurations. One possibility is to perform the measurements on cells cultured on a surface, using cantilevers with different types of probes, from standard tips to colloidal probes, with or without functionalisation [121]. The other is to attach a cell to the cantilever and perform the measurement on functionalised substrates or cells [122]. The first configuration is used to study mechanical properties of the cells as well as adhesion, while the last one is mainly used to study adhesion. One advantage of the direct measurement with cells, is that the receptors are studied in their physiological environment, which ensures their proper representation at the cell surface [122].

Cell adhesion is controlled by a complex interplay of short range (lock and key) forces mediated by cell surface receptors, short and long range nonspecific interactions, and membrane elasticity [123].

First, the short-range forces are controlled by the expression of receptors at the cell surface that bind specifically to adhesion molecules in another cell or extracellular matrix. The integrins are α - β heterodimeric proteins that are the main mediators of cell-matrix adhesion in all tissues. Because cell-matrix adhesion is not a static process but undergoes continuous remodelling, integrin-mediated adhesion is a dynamic process characterised by the perpetual breakage and reformation of bonds with extracellular

binding partners [122]. The cell adhesion molecules are randomly distributed within the plasma membrane and the formation of tight adhesion areas by receptor segregation is a diffusion controlled process [123].

Secondly, the non-specific forces include: 1) attractive van der Waals interactions, 2) electrostatic interactions, which can be mediated by cell surface receptors exhibiting large number of acidic sialic acid residues (such as Gly-CAM), 3) repulsive undulation forces due to thermally excited bending undulations of lipid protein bilayer, 4) diverse polymer induced forces which may include steric repulsion forces between molecules of the glycocalix, such as cell adhesion molecules exhibiting long extracellular chains but also interactions mediated by extracellular matrix proteins such as hyaluronic acid and fibronectin, which are bound to their respective receptors and integrin [123].

Finally, from theoretical studies of cell-adhesion process, the deformation of the cell and the mobility of the membrane components are expected to affect the rate at which bonds between the cell and adhesion surface form, the number of bonds, and the probability of cell adhesion. For the bond formation to occur the cell and the surface must approach within a short distance of each other. The elasticity of the cell membrane allows the membrane to deform to fit the contours of an adhesion surface it encounters [50]. Besides, the adhesion strength is closely related to the receptor-cytoskeleton coupling. A drastic reorganization of the membrane-coupled actin-base cytoskeleton is induced by receptor-ligand recognition [123]. In general, integrin receptors mediate mechanical force transfer across the cell surface and the cytoskeleton, whereas other transmembrane receptors do not [52]. For example, Potard et al. [52] compared RGD-coated with HECD-1 (anti-E-cadherin antibody) in confluent epithelial cell line (MCF7) and found that the stiffness of the cytoskeleton through integrins was significantly higher than E-cadherins.

An integrating understanding of cell structure and mechanics is necessary for elucidating many fundamental aspects for cell behaviour, from motility to differentiation and development. The cytoskeleton, a biopolymer network formed by filamentous actin, intermediate filaments and microtubules, together with filament cross-linker, motor and regulatory proteins determine the mechanical properties of cells [53]. Several approaches to model the cell structure have been proposed. The cortical shell-liquid core models which are widely applied for suspended cells, the solid model for adherent cells, the power-law structural damping model which is more suitable for studying dynamic behaviour of adherent cells, and the biphasic model which has been

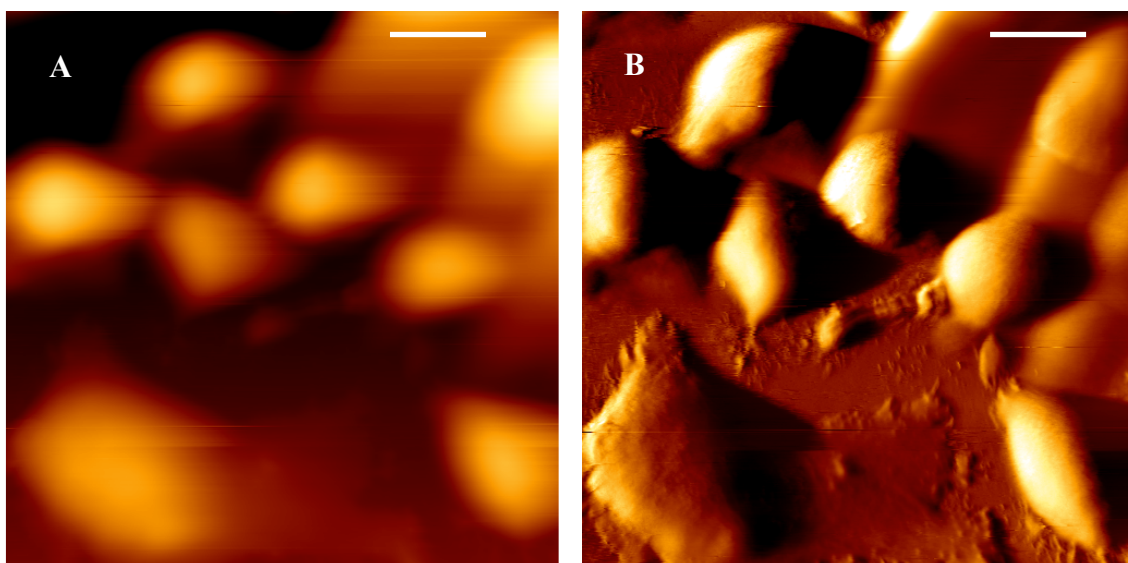
used to study musculoskeletal cell mechanics. These models are derived using either the micro/nano-structural approach or the continuum approach. The former deems the cytoskeleton as the main structural component. The continuum approach treats the cell as comprising materials with certain continuum material properties. Even when the continuum approach does not provide insight into detailed molecular mechanical events, it is a simple approach and more straightforward to use in computing mechanical properties of the cells if the biomechanical response at the cell level what is needed. In particular, the elastic model is a simplification of the viscoelastic model where the time factor has been neglected [54].

In this work, AFM was used to compare the interaction of cells with polyelectrolytes (PEI and PSS), to study the cell shape and mechanical properties when growing on PE coated surfaces, and to investigate the adhesion of coated tip to cells.

V.2. Results

V.2.1. Measurements with Si_3N_4 tip

Cell imaging using contact mode AFM and force vs. distance curves were performed on living HepG2 cells in PBS buffer. Figure V-1 shows the image obtained of the cells seeded on glass after 48 hours culture.



V-1: AFM image of HepG2 cells on a glass slide after 48 hours culture. The scan size was $100\mu\text{m}$ with a line rate of $40\mu\text{m/s}$. A) High image after line plane subtraction. B) Deflection image of the figure A. The scale bar represent $15\mu\text{m}$.

In figure 1A the height-measured image is shown and in figure 1B the deflection image is presented. The deflection image shows details of the cell, specially the extensions on the surface are defined. The cell dimensions are similar to the ones measured by optical microscopy, and since no morphological changes were observed during the experiments, it seems that were not affected during the scanning.

Force spectroscopy maps on cells growing on glass coated with PEI and multilayer ending on PSS were done. A grid size of $1.5 \times 1.5\mu\text{m}$ squares was defined and each force-distance curve was done in the middle of each square. Each force curve is a round trip, from an initial tip resting position to the sample surface (approach or trace) and its way back to the resting position (retraction or retrace). From both part of the force curve different information can be extracted. From the trace we extract height and slope at contact, and from retrace the relaxation and adhesion.

In figures V-2 and V-3 height measurements from cells growing on PSS and PEI coated surfaces are shown.

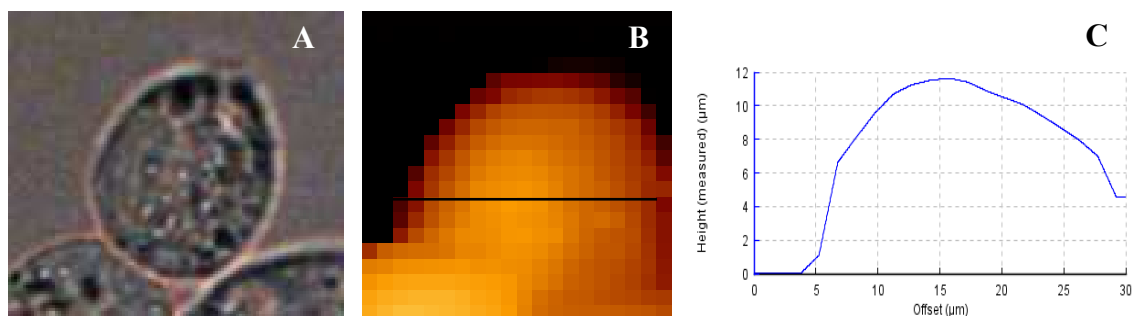


Figure V-2: Cells growing on PEM ending with PSS. Optical image and force map spectroscopy with Si_3N_4 tip. A) Optical image, B) high measured trace, C) cross section of figure B.

As observed with the optical microscope, the cells growing on PSS had an spherical like shape. The diameter parallel to the surface was about 20-25 µm, and the height was of approximately 12 µm.

The cells growing on PEI spread so the height decreased and the borders look less sharp as seen in figure V-2C. The cell had more than 30 µm length and 9 µm height.

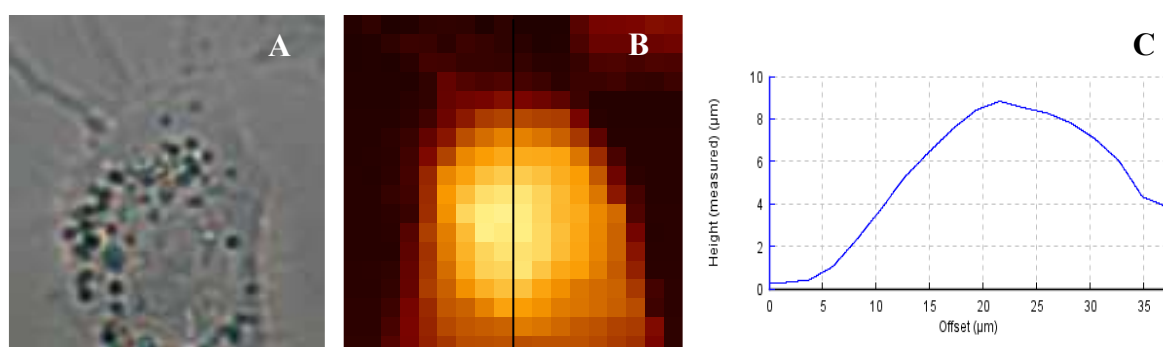


Figure V-3: Cells growing on PEI. Optical image and force map spectroscopy with Si_3N_4 tip. A) Optical image, B) high measured trace, C) cross section of figure B.

The major aim of the force-distance curves is to give information about mechanical properties and interactions between the cell surface of the tip and the specimen under study. Different surface characteristics that lead to different cell shapes could also involve different mechanical properties of the cells [52].

The cell response to local deformation is reflected in the slope of the force distance curves at contact. The trace slope maps of cells growing on PEI and PSS are presented in figure V-4A and V-4B respectively. In both images it is clearly defined when the tip is on the substrate surface, very hard surface with a high trace slope, in contrast when it is on the cell with a less steep trace slope. In figures V-4C and V-4D two examples of

force distance curves on cells growing on PSS and PEI are shown. In this graphs, the vertical deflection (or force) is presented vs. piezo displacement. This data was converted to force vs. indentation curves using the following relation.

$$\delta = h - h_{\text{contact}} - \frac{F}{k}$$

with : δ : indentation, h : height measured, h_{contact} : h when the tip reach the surface, F : force and k : cantilever constant.

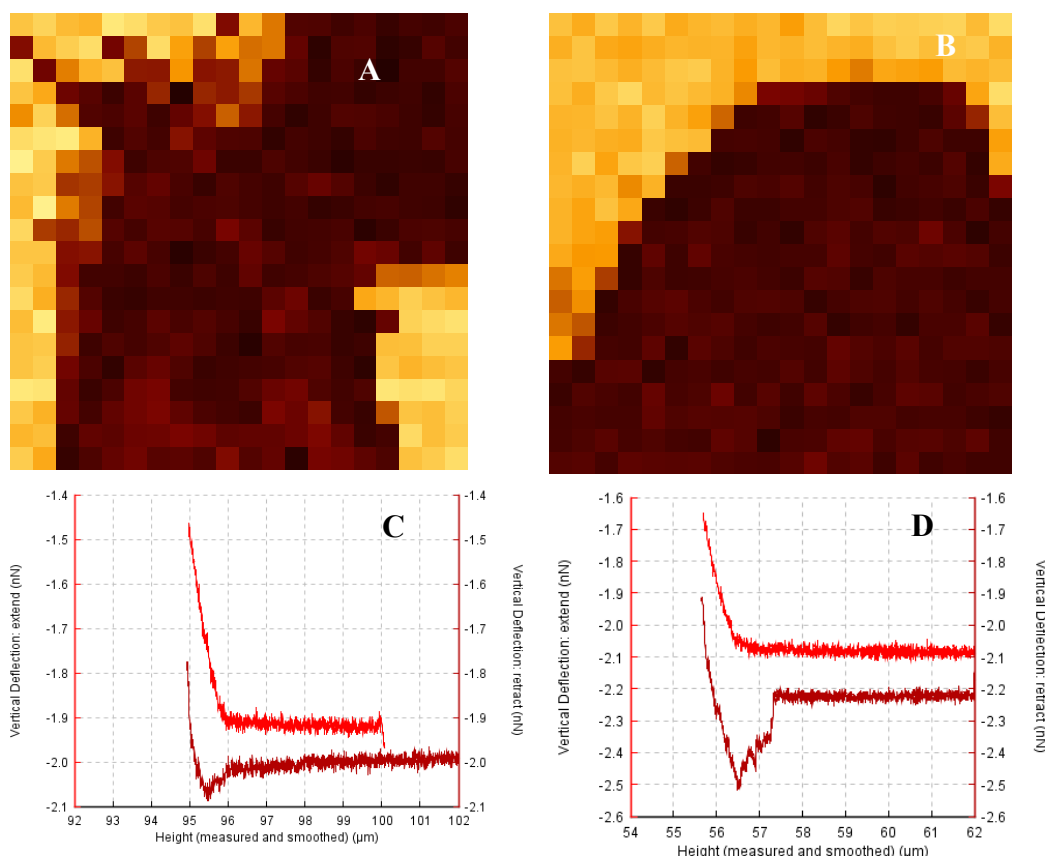


Figure V-4: Force-distance mapping of cell growing on PEI and PSS with Si_3N_4 tip for a 500 pN force set point. The slopes in the images A and B were automatically calculated by JPK imaging program using the last 50 nm of the trace curve. A) Trace slope map of a cell growing on PEI, B) trace slope map of a cell growing on PSS, C) force distance curve on a cell of the map in A, D) force distance curve on a cell of the map in B.

All the force curves were done at the same trace-retrace speed ($10 \mu\text{ms}^{-1}$) and at a maximum force set point of 500 pN. Once the tip reached the set point, it immediately returned to its resting position or remained at a constant height for 3 seconds. In each case it is said that the delay was of 0 and 3 seconds respectively.

When the maximum load was reached, the average indentation value obtained was for the cells growing on PSS was $\delta = 1.3 \pm 0.3 \times 10^{-6}$ m and on PEI $\delta = 0.6 \pm 0.2 \times 10^{-6}$ m.

This means that applying the same force, the deformation obtained for cell on PSS was larger than on PEI. The cells seemed to be “softer” on PSS than on PEI. This was also observed when comparing slope traces $6 \pm 2 \times 10^{-4}$ and $11 \pm 5 \times 10^{-4} \text{ Nm}^{-1}$, respectively.

Several researches studying the mechanical properties of different cells report the corresponding elastic modulus. The elastic moduli were calculated applying the Hertz model and assuming that the tip geometry can be approximated to a cone [119]. Then,

$$F = \frac{\pi \cdot \tan \alpha \cdot E}{1 + \nu^2} \delta^2$$

with $\alpha = 35^\circ$ and Poisson ratio $\nu = 0.3-0.5$ [124]

Fitting each curve to this equation, an elastic modulus could be calculated for each position where the force curve was performed as shown in figure V-5.

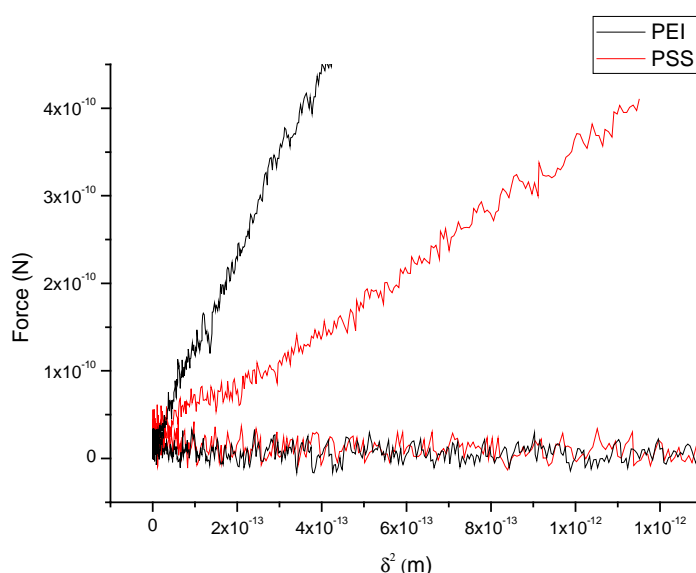
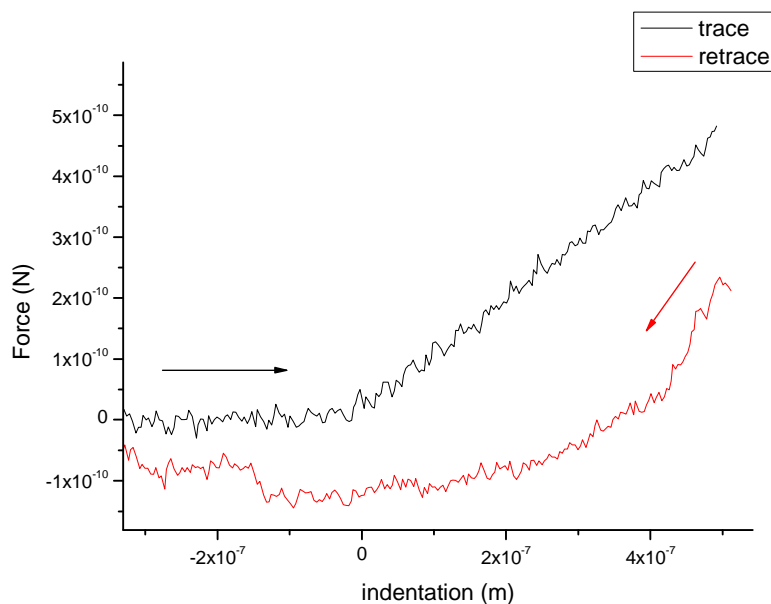
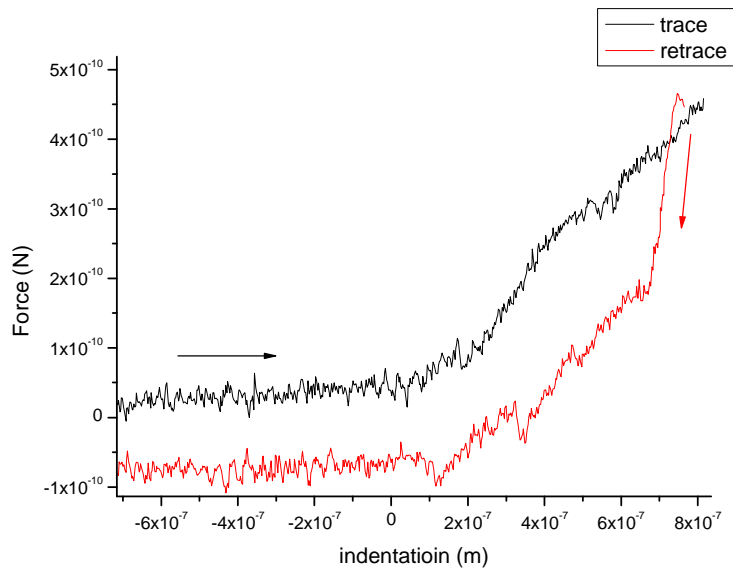


Figure V-5: Hertz model fitting of approaching curves for cell growing on PEI and PSS coated surfaces. The elastic modulus is directly proportional to the slope. The calculated E for cells growing on PEI was higher than when growing on PSS.

The average values obtained at the central part of the cell were $330 \pm 20 \text{ Nm}^{-2}$ and $1600 \pm 200 \text{ Nm}^{-2}$ for cells on PSS and PEI, respectively.

Until now, only the trace parts of the force curves were analysed. For cells growing on PEI coated surface, if the retrace curves are studied, a different behaviour is observed comparing the experiments with 0 and 3 seconds delay. The origin of the retrace curve almost coincide with the end of the retrace curve as shown in figure V-6A, but when

retracting the path was different from the trace. In figure V-6B there was a 3 seconds delay and it is observed that the origin of the retrace curve has a lower value of force, and the retraction path also followed different path. It seems that during the 3 seconds the tip remained pressing the cell at a constant height, part of the stress is relaxed.



V-6: Tip relaxation for cells on PEI. A) Force curves with 0s delay; B) force curves with 3 s delay. After 3 seconds delay there is a clear relaxation of the initial stress.

The relaxation was of 240 ± 15 pN. Since the area under the trace and retrace curves represent the work done during approaching and retracting, respectively; the area within both curves represents the energy lost in the process. For PEI, at 0s delay the energy loss was of $6 \pm 2 \times 10^{-7}$ J that represents the 60% of the approaching work. When the delay was 3 s, the energy loss was of $1.2 \pm 0.2 \times 10^{-6}$ J, and represents the 90% of the approaching work.

For cells growing on PSS, only experiments with 3 seconds delay were carried out. A similar behaviour was observed with a relaxation of 120 ± 15 pN and energy loss of 1.3×10^{-6} J that represents the 86 % of the initial work.

V.2.2. Tip functionalised with PEs

To compare the interactions of the polyelectrolytes with the cells, the tips were functionalised with PEI and PSS, and after incubation with cell culture medium, were ready to use. They were calibrated in PBS against glass using the built in calibration procedure of the JPK software, determining the cantilever sensitivity and spring constant. In the approaching curves during calibration, it was observed that the tip coated with PSS, presented higher repulsion in comparison with the tip coated with PEI.

Force distance curves on different parts of the cell were carried out with both functionalised tips at loads of 250, 500 and 750 pN, at $10 \mu\text{ms}^{-1}$, and with 0 and 3 seconds delay on the cell surface using the constant high mode.

Figure V-7 and V-8 shows the approaching curves of few force-distance curves taken with both tips. For the PEI tip, no significant repulsion was observed between the tip and the cell surface. The distance at which the tip contacts the surface is assumed to occur when the slope of the approaching curve significantly changed (distance=0). For the PEI, this change is of two orders of magnitude. The slope after 0 distance is comparable with the slope obtained with clean tip at the same set point, which was of $8 \pm 3 \times 10^{-4}$ N/m which seems to correspond to the response of the tip pressing the cells.

Figure V-7 shows the PSS tip approaching the cell surface. Higher repulsion between the tip and the cell surface was observed, and due to that, the moment at which the tip contact the surface is not so clear. In spite of that, if a lineal fit is performed before and after the slope change, in the steepest region the slope obtained was of $13 \pm 4 \times 10^{-4}$ N/m, similar to the PEI and clean tip.

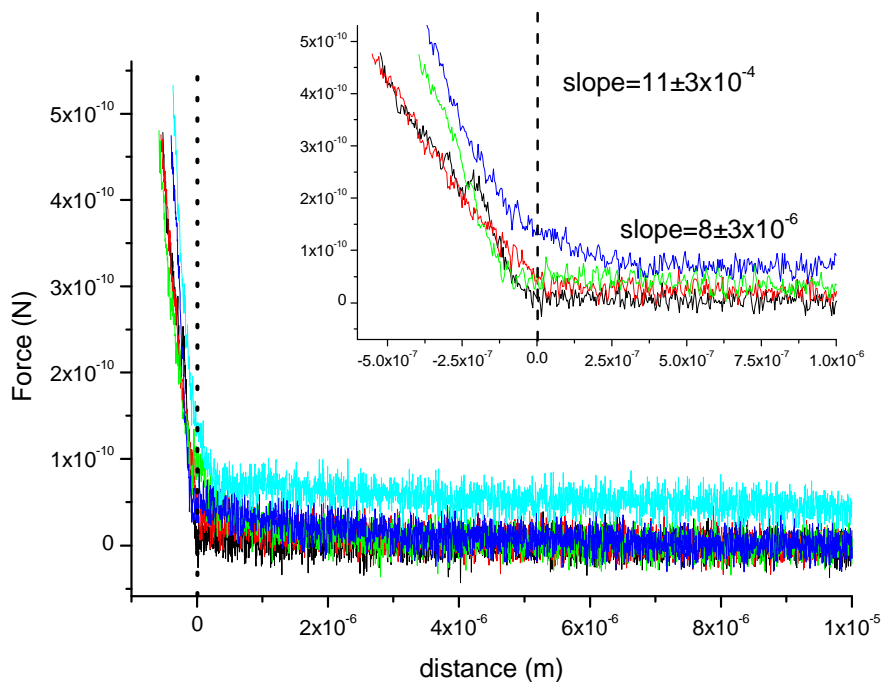


Figure V-7: Approaching part of force vs. distance curves of PEI tip on cells (n=5). Before contact the cell surface there is a slight repulsion measured as an increase in the slope of 8×10^{-6} N/m.

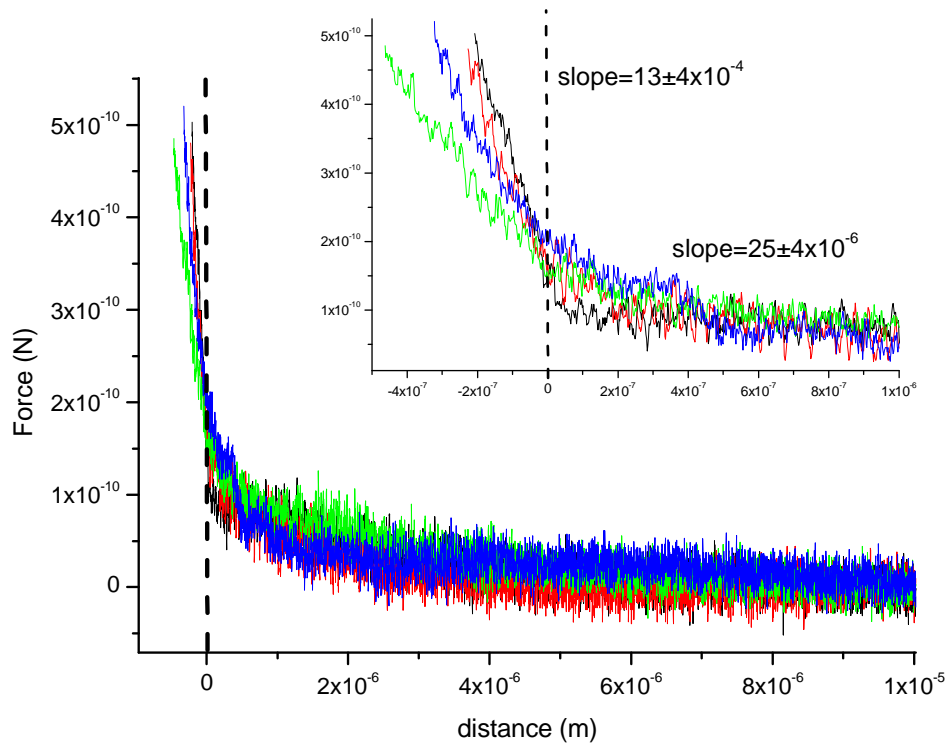


Figure V-8: Approaching part of force vs. distance curves of PSS tip on cells (n=5). The tip contact with the surface is not as clear due to higher repulsion, and presented a slope of 25×10^{-6} N/m.

When the lineal fit of the trace curve is performed before contact, the slope was of $25 \pm 4 \times 10^{-6}$ N/m. The crossing of both curves determines the defined distance 0.

Studying the retraction curve, the adhesion of the tip to the cell surface can be studied. During retraction, a wide variety of curves were observed, with several peaks of adhesion that show elastic behaviour at shorter distances, and flat regions behaving in a step-wise manner showing no elastic behaviour.

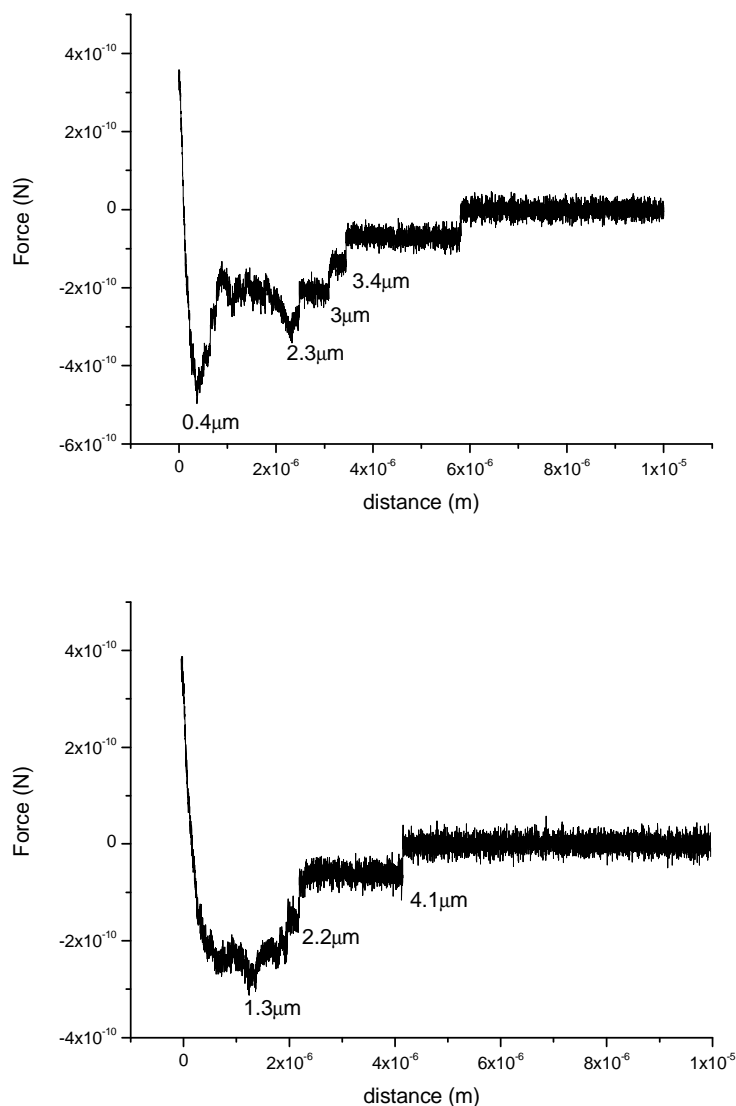
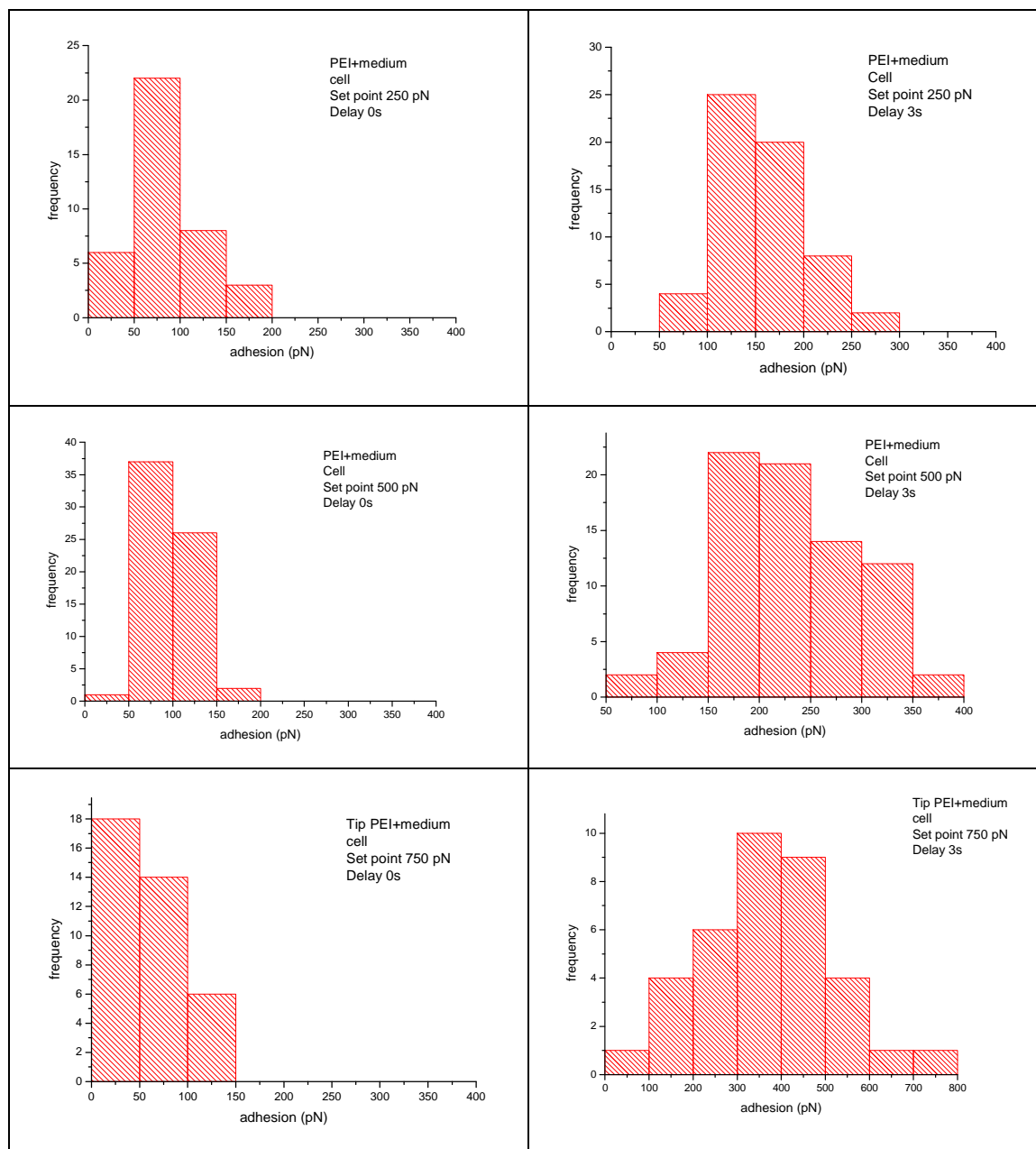
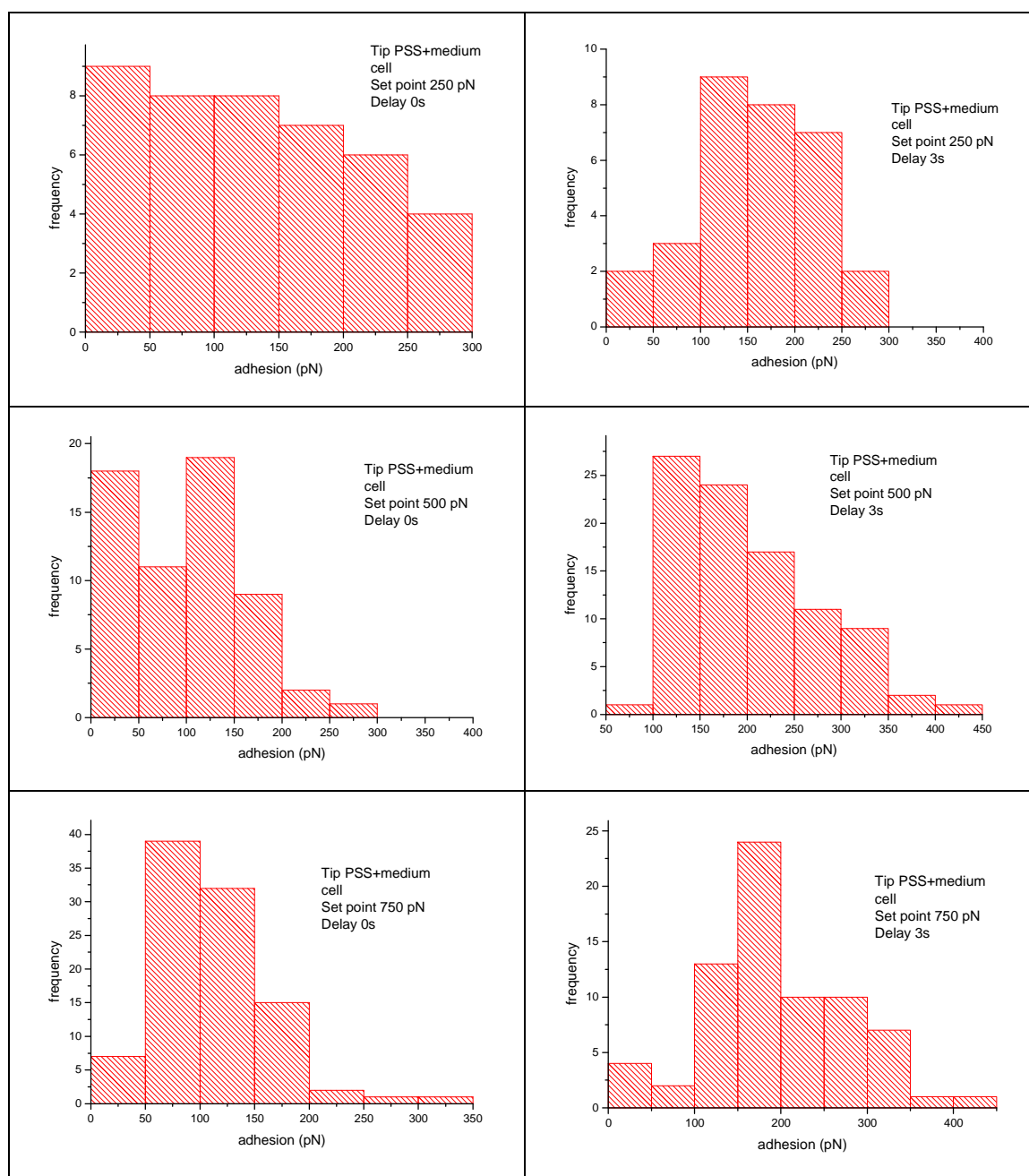


Figure V-9: Retracting curves for PEI tip with a set point 750 pN and 3s delay. Different shapes were obtained with multiple peaks showing elastic and non-elastic behaviour.

In the following histograms of figure V-10 the values of the maximum adhesion are reported for both tips at different set points and delay times. Besides in the table V-1, the average values with their standard error are reported to facilitate the comparison.





V-10: Histograms of the adhesion of coated tips on cells at different set points with 0 and 3 s delay.

Tabla V-1: Maximum adhesion values (average \pm se)

<i>PEI</i>	<i>Set point</i>		
Delay	250 pN	500 pN	750 pN
0s	80 \pm 6	90 \pm 3	50 \pm 7
3s	150 \pm 7	230 \pm 7	360 \pm 35
<i>PSS</i>	<i>Set point</i>		
Delay	250 pN	500 pN	750 pN
0s	120 \pm 13	80 \pm 9	110 \pm 5
3s	150 \pm 15	190 \pm 10	190 \pm 15

It is observed that when the delay on the surface is 0s, adhesion values obtained at different set points and PE are in the range of 50-100pN (noise is of 50pN). When the tip remained on the surface for 3 seconds, a significant increase in the average value of maximum adhesion was observed for the tip covered with PEI. However, for the PSS, even when there is an increase in the average adhesion when the set point rose from 250 to 500 pN, no furthermore difference was observed when the set point was 750 pN.

Due to the fact that the retracting curves are complex, with several adhesion peaks, not only the maximum adhesion, but also the separation work as proposed by Kim et al. was determined in order to compare the interactions of cell with the PEI and PSS tips [121]. The separation works were calculated only for the experiments with 3 seconds of delay on the surface of the cell and are presented in table 2. Similarly as with the maximum adhesion, the separation work increased with the set point for the PEI, but was very similar for the PSS. If we compare the values for the PEI and PSS, the separation work did not differ much until reaching the 750 pN set point. This trend was also observed for the maximum adhesion.

Table V-1: Separation work

<i>PEI</i>	<i>Set point</i>		
	250 pN	500 pN	750 pN
Separation work			
Average ± se	$1.2 \pm 0.2 \times 10^{-16}$	$3.0 \pm 0.3 \times 10^{-16}$	$7.0 \pm 0.7 \times 10^{-16}$
range	$1 \times 10^{-17} - 3.3 \times 10^{-16}$	$4.5 \times 10^{-17} - 8 \times 10^{-16}$	$2 \times 10^{-16} - 1.2 \times 10^{-15}$
<i>PSS</i>	<i>Set point</i>		
	250 pN	500 pN	750 pN
Separation work			
Average ± se	$2.0 \pm 0.4 \times 10^{-16}$	$3.0 \pm 0.3 \times 10^{-16}$	$3.0 \pm 0.7 \times 10^{-16}$
range	$0 - 6 \times 10^{-16}$	$7 \times 10^{-17} - 7 \times 10^{-16}$	$1 - 7 \times 10^{-16}$

In figure V-11, the separation work was plotted vs. the adhesion. At low maximum loads, the values obtained with PEI tip and PSS are similarly distributed. But for the PEI at 750 pN, it seems to reach a maximum in separation work with higher values of adhesion.

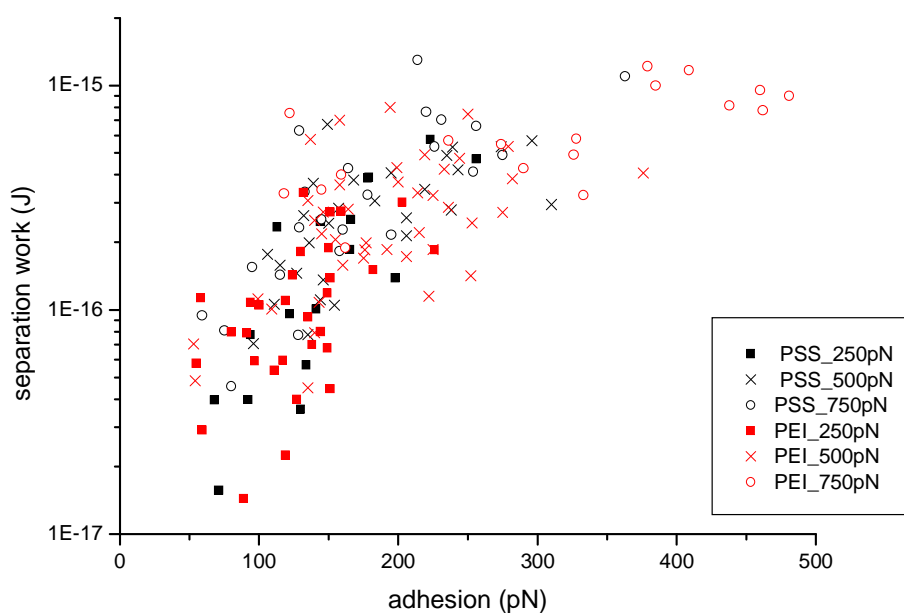


Figure V-11: Separation work vs. maximum adhesion at three maximum loads with PEI and PSS coated tips. At maximum loads of 250 and 500 pN the distribution the distribution of the points is similar, but at 750 pN with PEI coated tip the adhesion was higher but similar with separation works.

V.3. Discussion

The AFM experiments carried on the cells seemed not to affect them, and they remained apparently alive during the experiments (5-6 hours). For cell imaging, contact AFM was done. At low magnification scan size ($100\mu\text{m}^2$), the relevance of the tip height was observed when imaging groups of cells, due to the inability to reach the area in-between them. In spite of that, when the cells were separated enough, the cells could be resolved as is shown in figure V-1.

Considering that the cells adhered less strongly to PSS coated substrates, and in order to measure the cell height on PEI and PSS, a force-distance map was done for cells attached on both substrates. This avoided the constant scanning on the cells, which could lead to cell detachment. It was confirmed that the cells growing on PSS are higher ($12\mu\text{m}$) than the ones attached to PEI ($9\mu\text{m}$), without significant membrane spreading on the surface.

From the force maps performed on cells growing on PEI coated surface, it was observed that the time that the tip remained on the cells affected the value of force relaxation and the energy loss. First, when there was no delay, it was not possible to measure any relaxation. In spite of that, there were energy losses in that process due to the viscoelastic characteristic of the cells. When the tip delay was of 3 seconds, a significant relaxation was observed as well as a bigger energy loss (hysteresis).

If the values obtained for cells on PEI and PSS are compared, it can be concluded that cells on PSS are “softer”, since a lower trace slope and larger indentation (at the same force set point and tip speed) was obtained for the cells on PSS. Besides, the elastic moduli obtained follow the same tendency, higher elastic moduli for the cells on PEI. Besides, reported values of elasticity of cells such as macrophages and fibroblast are in the same range, from 100-2000 Pa [116; 124].

Even it was observed that the cells are not elastic bodies, the lack of a simple model to evaluate the mechanical properties the cells, and the fact that under low deformation it could be a valid approximation, no further viscoelastic modelling is attempted. In spite of that, the results obtained give several hints about different parameter that could be useful for the cell mechanics characterisation to be developed in future work.

When functionalised tips were used, it was observed that the PSS coated tip presented more repulsion, probably due to the fact that generally it is believed that the cell surface

is negatively charge due to the presence of sialic acid residues in the glycocalix of the cell.

Another explanation to the repulsion is the generation of long-range repulsion forces by large protein filaments of the extracellular matrix due to steric repulsion.

To compare the interaction of the tip coated with polyelectrolyte with the cells, the adhesion of the different tips with the cells was studied. Due to the multiple interactions that are established during retraction, the cantilever deflexion shows complex adhesive interactions [121]. Force steps characterised by a nearly linear increase in force before the point of rupture are considered to represent the unbinding of discrete adhesive units under load. Rupture events preceded by force plateau regimes are interpreted as the extraction of cytoskeleton-free membrane tubes (tethers) from the cell membrane [122]. Because the detachment process is not the result of only one type of interaction, the area under the force-extension curve has been proposed as a better measure of interaction than the rupture force. This parameter could be a better estimate of the magnitude of interaction and is referred to as “separation work” [121].

First, considering the maximum adhesion values, when the delay of the tip on the surfaces was 0 s, there was very low adhesion, in spite of increasing the set point with both tips. In order to have adhesion, the molecules of the polyelectrolyte coating the tip have to interact with the cell glycocalyx (50-100 nm thick) and with molecules on the membrane. It is observed that when the delay on the surface is 0s, the adhesion is very low, and there is no difference among the adhesion values obtained at different set points. In order to increase the adhesion values, the tip remained at a constant height on the surface for 3 seconds. An increase in the average value of maximum adhesion was clearly observed for the tip covered with PEI. However, for the PSS, even when there is a slight increase in the average adhesion when the set point rise from 250 to 500 pN, is not present for 750 pN. Looking at the force histograms, it is possible to see, that the relative frequency of lower adhesion values decreased when the set point increased. Then, both tips had a similar behaviour when increasing the set point. The average values for both tips are similar. However, at 750 pN, the adhesion for the PEI is higher, when the tip is functionalize with PEI. Looking at the histograms it is possible to see that the majority of the maximum adhesion events were in the 300-500pN range for the PEI, while for the PSS ranged from 150 to 200 pN.

Due to the fact that the retracting curves are complex, with several adhesion peaks, not only the maximum adhesion, but also the separation work as proposed by Kim et al. was determined in order to compare the interactions of cell with the PEI and PSS tips [121]. In our experiment the results obtained comparing the maximum adhesion and the separation works were similar. Then it seems that the tip coated with PEI has stronger interaction than the PSS tip, when it is on the cell surface for 3 seconds and the force set point is of 750 pN.

V.4. Conclusion

It was confirmed that the cells spread on PEI and have a maximum height of $\approx 9 \mu\text{m}$, in contrast to the rounded shape of the cells on PSS with a maximum height of $\approx 12 \mu\text{m}$. Besides, due to a different interaction with the surface, different cell mechanical properties resulted. Cells attached on PSS were “softer” than cells growing on PEI. The mechanical cell response to the applied load was time dependent. Force-distance curves showed higher hysteresis (dissipated energy) for longer tip residence time on the cell surface.

During the study of the interaction of functionalised tips with the cell, it was observed that the PSS-tip experienced more repulsion to the cell surface. Besides, the maximum adhesion of the tip to the cell surface was independent of the set point and tip coating when the tip did not stop on the surface. The highest adhesion (360 pN) was obtained when the tip was functionalised with PEI at loads of 750 pN with a 3 seconds delay on the surface.

Chapter VI

Conclusion and outlook

Different biocompatible surfaces with defined functionalities have been engineered with synthetic polyelectrolytes, using the layer-by-layer technique and soft lithography. In this way, we have immobilised proteins and cells preserving their function, increasing the degree of complexity of the system.

The first important result was the adsorption of the enzyme laccase, which was covalently immobilised on a gold/PEI/GA layer. We have proved that the enzyme conserved its catalytic activity in the presence of ABTS. Furthermore, the adsorption of PAH and PSS on immobilised laccase was achieved. However, the effect of the polyelectrolyte on the activity of the enzyme is still a question that will be addressed in the future work, since the ABTS also interacts with the polyelectrolytes.

Soft-lithography (combining polyelectrolyte and PDMS stamps) was used to build micro-patterned surfaces, which hosted 2-D crystalline protein layers, generating a nanobiofunction inside the macrostructure. This could be achieved using the protein passivating PEG. Three types of bacterial proteins were patterned, each of them with different biological properties. The wild type protein SbpA, which acts in nature as a protective wall keeping the bacterial shape (and also antibacterial surface) maintained its square crystalline structure (similar as the structure found in bacteria). The second protein, the recombinant rSbpA-EGFP, preserved its fluorescent properties after adsorption on the patterned surface as shown by fluorescent microscopy. Finally, the heterotetramer S-layer fusion protein (rSbpA-STV) showed specific affinity for (labelled) biotin. It has to be pointed out that the ability to manipulate protein distribution at the micro-scale is a basic requirement for biosensor development.

Concerning cell/surface interaction, it was found that HepG2 cells adopted different morphologies depending on the hosting underlying polyelectrolyte. While positive polyelectrolytes (PEI, PAH) adsorbed molecules that triggered cell spreading,

PLL-g-PEG (neutral and highly hydrated interface) and anionic PSS did not favour cell spreading. Taking the advantage of the lower cell affinity for PLL-g-PEG, both cell attachment and confinement on PLL stamped strips was achieved. Spreading of the cells was monitored with QCM-D and light transmission microscopy, and assayed with crystal violet. An interesting question that should be further investigated is the relation between change in conformation and local adhesion points. For example QCM-D measurements have revealed that cells “do not weight” when deposited on PSS (the opposite happens when cell adsorb on PEI), although they remained attached to the surface.

Atomic force microscopy offered some clarity at this point and confirmed that the cells spread on PEI had a maximum height of ca. 9 μm , in contrast to the rounded shape of the cells on PSS with a maximum height of ca. 12 μm . This was also reflected in the cell mechanical properties: cells on PSS were “softer” than cells growing on PEI.

Functionalised tips with polyelectrolytes showed that the (negative) PSS-tip experienced larger repulsion than the (positive) PEI-tip when they approached the cell surface. It was found that the maximum adhesion of the tip to the cell surface was independent of the applied load and tip coating when the residence time of the tip at the cell surface was zero. The highest adhesion (750 pN) was observed for a PEI coated tip, after remaining on the cell surface for three seconds.

Some questions still remain concerning the engineering and nanocontrol of biosurfaces as well as cell mechanical properties and cell manipulation. This work has shown that functional proteins can be deposited on surfaces preserving their function. A near challenge in the future in this direction is the manipulation of protein and peptide deposition to achieve different functionalities on the surface. Much work concerning cell mechanical properties remains to be done, since there are no clear physical models to address such question due to the complexity of the cell. Another ambitious question to be investigated is the link between cell mechanics and the cell living cycle.

References

- [1]M. Tirrell, E. Kokkoli, and M. Biesalski, The role of surface science in bioengineered materials. *Surface Science* 500 (2002) 61-83.
- [2]D.G. Castner, and B.D. Ratner, Biomedical surface science: Foundations to frontiers. *Surface Science* 500 (2002) 28-60.
- [3]T.M. Cooper, Biomimetic thin films. in: H.S. Niiwa, (Ed.), *Handbook of Nanostructured materials and nanotechnology*, Academic Press, London, 2000, pp. 711-768.
- [4]A.S. Rudolph, Biomaterial technology using self assembled lipid microstructures. *J. Cellular Biochem.* 56 (1994) 183-187.
- [5]M. Pomerantz, A. Segmuller, L. Netzer, and J. Sagiv, Coverage of Si substrates by self-assembling monolayers and multilayers as measured by IR, wettability and X-ray diffraction *Thin Solid Films* 132 (1985) 153-162.
- [6]C.D. Bain, E.B. Troughton, Y.-T. Tao, J. Evall, G.M. Whitesides, and R.G. Nuzzo, Formation of monolayer films by the spontaneous assembly of organic thiols from solution onto gold. *J. Am. Chem. Soc.* 111 (1989) 321-335.
- [7]D. Pum, and U.B. Sleytr, The application of bacterial S-layers in molecular nanotechnology. *Trends in Biotechnology* 17 (1999) 8-12.
- [8]G. Decher, J.D. Hong, and J. Schmitt, Buildup of Ultrathin Multilayer Films by a Self-Assembly Process .3. Consecutively Alternating Adsorption of Anionic and Cationic Polyelectrolytes on Charged Surfaces. *Thin Solid Films* 210 (1992) 831-835.
- [9]G. Decher, Polyelectrolyte Multilayers, an Overview. in: G. Decher, and J.B. Schlenoff, (Eds.), *Multilayer Thin Films*, Wiley-VCH, 2003, pp. 1-46.
- [10]D.L. Elbert, C.B. Herbert, and J.A. Hubbell, Thin polymer layers formed by polyelectrolyte multilayer techniques on biological surfaces. *Langmuir* 15 (1999) 5355-5362.
- [11]R. Heuberger, G. Sukhorukov, J. Vörös, M. Textor, and H. Möhwald, Biofunctional polyelectrolyte multilayers and microcapsules: control of non-specific and bio-specific protein adsorption. *Advanced Functional Materials* 15 (2005) 357-366.
- [12]M. Schönhoff, Self-assembled polyelectrolyte multilayers. *Current Opinion in Colloid and Interface Science* 8 (2003) 86-95.
- [13]G.B. Sukhorukov, H. Möhwald, G. Decher, and Y.M. Lvov, Assembly of polyelectrolyte multilayer films by consecutively alternating adsorption of polynucleotides and polycations. *Thin Solid Films* 284-285 (1996) 220-223.

- [14] M.T. Thompson, M.C. Berg, I.S. Tobias, M.F. Rubner, and K.J.V. Vliet, Tuning compliance of nanoscale polyelectrolyte multilayers to modulate cell adhesion. *Biomaterials* 26 (2005) 6836-6845.
- [15] M. Delcea, R. Krastev, T. Gutbetlet, D. Pum, U.B. Sleytr, and J.L. Toca-Herrera, Mapping bacterial surface layers affinity to polyelectrolytes through the building of hybrid macromolecular structures. *Journal of Nanoscience and Nanotechnology* 7 (2007) 4260-4266.
- [16] F. Caruso, and C. Schuler, Enzyme multilayer on colloid particles: Assembly, stability, and enzymatic activity. *Langmuir* 16 (2000) 9595-9603.
- [17] S. Rodríguez-Couto, J. F. Osmá, V. Saravia, G.M. Gübitz, and J.L. Toca-Herrera, Coating of immobilised laccase for stability enhancement: A novel approach. *Applied Catalysis A* 329 (2007) 156-160.
- [18] J.E. Wong, A.K. Gaharwar, D. Muller-Schulte, D. Bahadur, and W. Richtering, Layer-by-layer assembly of a magnetic nanoparticle shell on a thermoresponsive microgel core. *Journal of Magnetism and Magnetic materials* 311 (2007) 219-223.
- [19] J. Ji, and J. Shen, Electrostatic self-assembly and Nanomedicine, 27th Annual International Conference of the Engineering in Medicine and Biology Society, IEEE-EMBS 2005, pp. 720-722.
- [20] D. Falconnet, G. Csucs, H.M. Grandin, and M. Textor, Surface engineering approaches to micropattern surfaces for cell-based assays. *Biomaterials* 27 (2006) 3044-3063.
- [21] D.A. Stenger, J.H. Georger, C.S. Dulcey, J.J. Hickman, A.S. Rudolph, T.B. Nielsen, S.M. McCort, and J.M. Calvert, Coplanar Molecular Assemblies of Aminoalkylsilane and Perfluorinated Alkylsilane - Characterization and Geometric Definition of Mammalian-Cell Adhesion and Growth. *Journal of the American Chemical Society* 114 (1992) 8435-8442.
- [22] C.B. Herbert, T.L. McLernon, C.L. Hypolite, D.N. Adams, L. Pikus, C.C. Huang, G.B. Fields, P.C. Letourneau, M.D. Distefano, and W.S. Hu, Micropatterning gradients and controlling surface densities of photoactivatable biomolecules on self-assembled monolayers of oligo(ethylene glycol) alkanethiolates. *Chemistry & Biology* 4 (1997) 731-737.
- [23] A. Folch, and M. Toner, Microengineering of cellular interactions. *Annu. Rev. Biomed. Eng.* 2 (2000) 227-56.
- [24] Y.N. Xia, and G.M. Whitesides, Soft lithography. *Angewandte Chemie-International Edition* 37 (1998) 551-575.
- [25] G.M. Whitesides, E. Ostuni, S. Takayama, X.Y. Jiang, and D.E. Ingber, Soft lithography in biology and biochemistry. *Annual Review of Biomedical Engineering* 3 (2001) 335-373.

- [26]J. Tien, and C.S. Chen, Patterning the cellular microenvironment. *Ieee Engineering in Medicine and Biology Magazine* 21 (2002) 95-98.
- [27]M. Mrksich, L.E. Dike, J. Tien, D.E. Ingber, and G.M. Whitesides, Using microcontact printing to pattern the attachment of mammalian cells to self-assembled monolayers of alkanethiolates on transparent films of gold and silver. *Experimental Cell Research* 235 (1997) 305-313.
- [28]J.S. Hovis, and S.G. Boxer, Patterning and composition arrays of supported lipid bilayers by microcontact printing. *Langmuir* 17 (2001) 3400-3405.
- [29]J.L. Tan, J. Tien, and C.S. Chen, Microcontact printing of proteins on mixed self-assembled monolayers. *Langmuir* 18 (2002) 519-523.
- [30]X.P. Jiang, H.P. Zheng, S. Gourdin, and P.T. Hammond, Polymer-on-polymer stamping: Universal approaches to chemically patterned surfaces. *Langmuir* 18 (2002) 2607-2615.
- [31]G. Csucs, R. Michel, J.W. Lussi, M. Textor, and G. Danuser, Microcontact printing of novel co-polymers in combination with proteins for cell-biological applications. *Biomaterials* 24 (2003) 1713-1720.
- [32]B. Alberts, *Molecular Biology of the Cell*, Garland, New York, 1994.
- [33]M. Wahlgren, and T. Arnebrant, Protein adsorption to solid surfaces. *TIBTECH* 9 (1991) 201-208.
- [34]U.B. Sleytr, H. Bayley, M. Sara, A. Breitwieser, S. Kupcu, C. Mader, S. Weigert, F.M. Unger, P. Messner, B. JahnSchmid, B. Schuster, D. Pum, K. Douglas, N.A. Clark, J.T. Moore, T.A. Winningham, S. Levy, I. Frithsen, J. Pankovc, P. Beale, H.P. Gillis, D.A. Choutov, and K.P. Martin, Applications of S-layers. *Fems Microbiology Reviews* 20 (1997) 151-175.
- [35]U.B. Sleytr, M. Sara, D. Pum, and B. Schuster, Characterization and use of crystalline bacterial cell surface layers. *Progress in Surface Science* 68 (2001) 231-278.
- [36]S. Moreno-Flores, A. Kasry, H.-J. Butt, C. Vavilala, M. Schmittl, D. Pum, U.B. Sleytr, and J.L. Toca-Herrera, From native to non-native two-dimensional protein lattices via underlying hydrophilic/hydrophobic nanoprotusion. *Angewandte Chemie-International Edition* (2008).
- [37]A. Martin-Molina, S. Moreno-Flores, E. Perez, D. Pum, U.B. Sleytr, and J.L. Toca-Herrera, Structure, surface interactions, and compressibility of bacterial S-layer through scanning force microscopy and the surface force apparatus. *Biophysical Journal* 90 (2006) 1821-1829.
- [38]J.L. Toca-Herrera, R. Krastev, V. Bosio, S. Kupcu, D. Pum, A. Fery, M. Sara, and U.B. Sleytr, Recrystallization of bacterial S-layers on flat polyelectrolyte surfaces and hollow polyelectrolyte capsules. *Small* 1 (2005) 339-348.

- [39]N. Ilk, S. Kupcu, G. Moncayo, S. Klimt, R.C. Ecker, R. Hofer-Warbinek, E.M. Egelseer, U.B. Sleytr, and M. Sara, A functional chimaeric S-layer-enhanced green fluorescent protein to follow the uptake of S-layer-coated liposomes into eukaryotic cells. *Biochemical Journal* 379 (2004) 441-448.
- [40]D. Moll, C. Huber, B. Schlegel, D. Pum, U.B. Sleytr, and M. Sara, S-layer-streptavidin fusion proteins as template for nanopatterned molecular arrays. *Proceedings of the National Academy of Sciences of the United States of America* 99 (2002) 14646-14651.
- [41]M. Pleschberger, A. Neubauer, E.M. Egelseer, S. Weigert, B. Lindner, U.B. Sleytr, S. Muyldermans, and M. Sara, Generation of a functional monomolecular protein lattice consisting of an S-layer fusion protein comprising the variable domain of a camel heavy chain antibody. *Bioconjugate Chemistry* 14 (2003) 440-448.
- [42]C. Vollenkle, S. Weigert, N. Ilk, E. Egelseer, V. Weber, F. Loth, D. Falkenhagen, U.B. Sleytr, and M. Sara, Construction of a functional S-layer fusion protein comprising an immunoglobulin G-binding domain for development of specific adsorbents for extracorporeal blood purification. *Applied and Environmental Microbiology* 70 (2004) 1514-1521.
- [43]N. Ilk, C. Vollenkle, E.M. Egelseer, A. Breitweiser, U.B. Sleytr, and M. Sara, Molecular characterization of the S-layer gene, *sbpA*, of *Bacillus sphaericus* CCM 2177 and production of a functional S-layer fusion protein with the ability to recrystallize in a defined orientation while presenting the fused allergen. *Applied and Environmental Microbiology* 68 (2002) 3251-3260.
- [44]N. Durán, M.A. Rosa, A. D'Annibale, and L. Gianfreda, Applications of laccases and tyrosinases (phenoloxidases) immobilized on different supports: a review. *Enzyme and Microbial technology* 31 (2002) 907-931.
- [45]A.I. Yaropolov, O.V. Skorobogat'ko, S.S. Vartanov, and S.D. Varfolomeyev, Laccase. Properties, catalytic mechanism, and applicability. *Appl. Biochem. Biotechnol.* 49 (1994) 257-80.
- [46]S. Rodriguez-Couto, and J.L. Toca-Herrera, Industrial and biotechnological applications of laccases: A review. *Biotechnology Advances* 24 (2006) 500-513.
- [47]P. Roy, J. Washizu, A.W. Tilles, M.L. Yarmush, and M. Toner, Effect of flow on the detoxification function of rat hepatocytes in a bioartificial liver reactor. *Cell Transplantation* 10 (2001) 609-614.
- [48]J.F. Cabrita, L.M. Abrantes, and A.S. Viana, N-Hydroxysuccinimide-terminated self-assembled monolayers on gold for biomolecules immobilisation. *Electrochimica Acta* 50 (2005) 2117-2124.
- [49]M.D. Ward, and D.A. Hammer, A theoretical analysis for the effect of focal contact formation on cell-substrate attachment strength. *Biophysical Journal* 64 (1993) 936-959.

- [50] J.W. Roos, and M.A. Hjortso, Kinetic of ligand-receptor bond formation. in: M.A. Hjortso, and J.W. Roos, (Eds.), Cell adhesion: fundamentals and biotechnology applications, Marcel Dekker, Inc, New York, 1994.
- [51] M.R. Koller, and E.T. Papoutsakis, Cell adhesion in animal cell culture: Physiological and fluid-mechanical implications. in: M.A. Hjortso, and J.W. Ross, (Eds.), Cell adhesion: Fundamentals and Biotechnological applications, New York, 1994.
- [52] W.H. Goldmann, Mechanical aspects of cell shape regulation and signaling. *Cell Biology International* 26 (2002) 313-317.
- [53] K.E. Kasza, A.C. Rowat, J. Liu, T.E. Angelini, C.P. Brangwynne, G.H. Koenderink, and D.A. Weitz, The cell as a material. *Current Opinion in Cell Biology* 19 (2007) 101-107.
- [54] C.T. Lim, E.H. Zhou, and S.T. Quek, Mechanical models for living cells- a review. *Journal of Biomechanics* 39 (2006) 195-216.
- [55] C.M. Dipersio, D.A. Jackson, and K.S. Zaret, The Extracellular-Matrix Coordinately Modulates Liver Transcription Factors and Hepatocyte Morphology. *Molecular and Cellular Biology* 11 (1991) 4405-4414.
- [56] G.-X. Zhang, Z.-Q. Zhao, H.-D. Wang, and B. Hao, Enhancement of osteopontin expression in HepG2 cells by epidermal growth factor via phosphatidylinositol 3-kinase signaling pathway. *World J Gastroenterol* 10 (2004) 205-208.
- [57] W.M. Becker, L.J. Klenismith, and J. Hardin, *The world of the cell*, Benjamin/Cummings, San Francisco, 2000.
- [58] N.B. Javitt, HepG2 cells as a resource for metabolic studies: lipoprotein, cholesterol, and bile acids. *Faseb Journal* 4 (1990) 161-168.
- [59] Y. Dai, and A.I. Cederbaum, Cytotoxicity of Acetaminophen in Human Cytochrome P450e1-Transfected Hepg2 Cells. *Journal of Pharmacology and Experimental Therapeutics* 273 (1995) 1497-1505.
- [60] M. Pinti, L. Troiano, M. Nasi, R. Ferraresi, J. Dobrucki, and A. Cossarizza, Hepatoma HepG2 cells as a model for in vitro studies on mitochondrial toxicity of antiviral drugs: which correlation with the patient? *Journal of Biological Regulators and Homeostatic Agents* (2003) 166-171.
- [61] S. Wilkening, F. Stahl, and A. Bader, Comparison of primary human hepatocytes and hepatoma cell line HEPG2 with regard to their biotransformation properties. *Drug Metabolism and Disposition* 31 (2003) 1035-1042.
- [62] T. Miyashita, S. Enosawa, S. Suzuki, A. Tamura, H. Tanaka, H. Amemiya, T. Matsumura, T. Omasa, K. Suga, T. Aoki, and Y. Koyanagi, Development of a bioartificial liver with glutamine synthetase-transduced recombinant human hepatoblastoma cell line, HepG2. *Transplantation Proceedings* 32 (2000) 2355-2358.

- [63]S. Enosawa, T. Miyashita, S. Suzuki, X.K. Li, M. Tsunoda, H. Amemiya, M. Yamanaka, S. Hiramatsu, N. Tanimura, T. Omasa, K. Suga, and T. Matsumura, Long-term culture of glutamine synthetase-transfected HepG2 cells in circulatory flow bioreactor for development of a bioartificial liver. *Cell Transplantation* 9 (2000) 711-715.
- [64]L. Damelin, S. Choudhury, S. Coward, M. Hubank, H. Hodgson, and C. Selden, HepG2 cells in 3-dimensional culture exhibit elevated expression of genes associated with lipid metabolism - Further evidence that cells cultured in alginate can provide the cellular component of a bioartificial liver. *Hepatology* 38 (2003) 678A-678A.
- [65]U.B. Sleytr, M. Sara, Z. Kupcu, and P. Messner, Structural and Chemical Characterization of S-Layers of Selected Strains of *Bacillus-Stearothermophilus* and *Desulfotomaculum-Nigrificans*. *Archives of Microbiology* 146 (1986) 19-24.
- [66]C. Huber, J. Liu, E.M. Egelseer, D. Moll, W. Knoll, U.B. Sleytr, and M. Sara, Heterotetramers formed by an S-layer-streptavidin fusion protein and core-streptavidin as a nanoarrayed template for biochip development. *Small* 2 (2006) 142-150.
- [67]S. Linko, Production of lignin peroxidase by immobilized *Phanerochaete chrysosporium*, University of Helsinki 1991.
- [68]M.M. Bradford, *Analytical Chemistry* 72 (1976) 248-254.
- [69]M.L. Niku-Paavola, L. Raaska, and M. Itävaara, Detection of white-rot fungi by a non-toxic stain. *Mycological Research* 94 (1990) 27-31.
- [70]F. Höök, J. Vörös, M. Rodahl, R. Kurrat, P. Böni, J.J. Ramsden, M. Textor, N.D. Spencer, P. Tengvall, J. Gold, and B. Kasemo, A comparative study of protein adsorption on titanium oxide surfaces using in situ ellipsometry, optical waveguide lightmode spectroscopy, and quartz crystal microbalance/dissipation. *Colloids and Surfaces B-Biointerfaces* 24 (2002) 155-170.
- [71]J. Malmström, H. Agheli, P. Kingshott, and D.S. Sutherland, Viscoelastic modeling of highly hydrated laminin layers at homogeneous and nanostructured surfaces: Quantification of protein layer properties using QCM-D and SPR. *Langmuir* 23 (2007) 9760-9768.
- [72]J. Redepenning, T.K. Schlesinger, E.J. Mechalke, D.A. Puleo, and R. Bizios, Osteoblast attachment monitored with a quartz crystal microbalance. *Analytical Chemistry* 65 (1993) 3378-3381.
- [73]M. Rodahl, F. Hook, A. Krozer, P. Brzezinski, and B. Kasemo, Quartz crystal microbalance setup for frequency and Q-factor measurements in gaseous and liquid environments, *AIP*, 1995, pp. 3924-3930.
- [74]P. Schwinté, V. Ball, B. Szalontai, Y. Haikel, J.C. Voegel, and P. Schaaf, Secondary structure of proteins adsorbed onto or embedded in polyelectrolyte multilayers. *Biomacromolecules* 3 (2002) 1135-1143.

- [75]J. Tien, A. Terfort, and G.M. Whitesides, Microfabrication through electrostatic self-assembly. *Langmuir* 13 (1997) 5349-5355.
- [76]M. Nolte, and A. Fery, Coupling of individual polyelectrolyte capsules onto patterned substrates. *Langmuir* 20 (2004) 2995-2998.
- [77]R. Michel, S. Pasche, M. Textor, and D.G. Castner, Influence of PEG architecture on protein adsorption and conformation. *Langmuir* 21 (2005) 12327-12332.
- [78]N.P. Huang, R. Michel, J. Voros, M. Textor, R. Hofer, A. Rossi, D.L. Elbert, J.A. Hubbell, and N.D. Spencer, Poly(L-lysine)-g-poly(ethylene glycol) layers on metal oxide surfaces: Surface-analytical characterization and resistance to serum and fibrinogen adsorption. *Langmuir* 17 (2001) 489-498.
- [79]D.S. Salloum, and J.B. Schlenoff, Protein adsorption modalities on polyelectrolyte multilayers. *Biomacromolecules* 5 (2004) 1089-1096.
- [80]K.C. Dee, D.A. Puleo, and R. Bizios, Protein-Surface Interactions. in: I. John Wiley & Sons, (Ed.), *An Introduction to Tissue-Biomaterial Interactions*, 2002, pp. 37-51.
- [81]E.P. Diamandis, and T.K. Christopoulos, The bitoin-(strept)avidin system: Principles and applications in Biotechnology. *Clin. Chem.* 37 (1991) 625-636.
- [82]D.S. Salloum, S.G. Olenych, T.C.S. Keller, and J.B. Schlenoff, Vascular smooth muscle cells on polyelectrolyte multilayers: Hydrophobicity-directed adhesion and growth. *Biomacromolecules* 6 (2005) 161-167.
- [83]L. Richert, P. Lavalle, D. Vautier, B. Senger, J.F. Stoltz, P. Schaaf, J.C. Voegel, and C. Picart, Cell interactions with polyelectrolyte multilayer films. *Biomacromolecules* 3 (2002) 1170-1178.
- [84]S.Y. Yang, J.D. Mendelsohn, and M.F. Rubner, New class of ultrathin, highly cell-adhesion-resistant polyelectrolyte multilayers with micropatterning capabilities. *Biomacromolecules* 4 (2003) 987-944.
- [85]M. Chanana, A. Gliozzi, A. Diaspro, I. Chodnevskaja, S. Huewel, V. Moskalenko, K. Urlichs, H.J. Galla, and S. Krol, Interaction of polyelectrolytes and their composites with living cells. *Nano Letters* 5 (2005) 2605-2612.
- [86]C. Boura, P. Menu, E. Payan, C. Picart, J.C. Voegel, S. Muller, and J.F. Stoltz, Endothelial cells grown on thin polyelectrolyte multilayered films: an evaluation of a new versatile surface modification. *Biomaterials* 24 (2003) 3521-3530.
- [87]M.d. Rosa, M. Carteni, O. Petillo, A. Calarco, S. Margarucci, F. Rosso, A.d. Rosa, E. Farina, P. Grippo, and G. Peluso, Cationic polyelectrolyte hydrogel fosters fibroblast spreading, proliferation, and extracellular matrix production: Implications for Tissue Engineering. *Journal of Cellular Physiology* 198 (2004) 133-142.

- [88]U.B. Sleytr, P. Messner, D. Pum, and M. Sara, Crystalline bacterial cell surface layers (S layers): From supramolecular cell structure to biomimetics and nanotechnology. *Angewandte Chemie-International Edition* 38 (1999) 1035-1054.
- [89]D. Pum, G. Stangl, C. Sponer, W. Fallmann, and U.B. Sleytr, Deep UV patterning of monolayers of crystalline S layer protein on silicon surfaces. *Colloids and Surfaces B-Biointerfaces* 8 (1997) 157-162.
- [90]D. Pum, G. Stangl, C. Sponer, K. Riedling, P. Hudek, W. Fallmann, and U.B. Sleytr, Patterning of monolayers of crystalline S-layer proteins on a silicon surface by deep ultraviolet radiation. *Microelectronic Engineering* 35 (1997) 297-300.
- [91]E.S. Gyrovary, A. O'Riordan, A.J. Quinn, G. Redmond, D. Pum, and U.B. Sleytr, Biomimetic nanostructure fabrication: Nonlithographic lateral patterning and self-assembly of functional bacterial S-layers at silicon supports. *Nano Letters* 3 (2003) 315-319.
- [92]J.S. Xu, M.W. Ma, and W.M. Purcell, Characterisation of some cytotoxic endpoints using rat liver and HepG2 spheroids as in vitro models and their application in hepatotoxicity studies. I. Glucose metabolism and enzyme release as cytotoxic markers. *Toxicology and Applied Pharmacology* 189 (2003) 100-111.
- [93]S.M. Notley, M. Eriksson, and L. Wagberg, Visco-elastic and adhesive properties of adsorbed polyelectrolyte multilayers determined in situ with QCM-D and AFM measurements. *Journal of Colloid and Interface Science* 292 (2005) 29-37.
- [94]A.P. Ngankam, G. Mao, and P.R.V. Tassel, Fibronectin adsorption onto polyelectrolyte multilayer films. *Langmuir* 20 (2004) 3362-3370.
- [95]J. Schmitt, T. Grunewald, G. Decher, P.S. Pershan, K. Kjaer, and M. Lösche, *Macromolecules* 26 (1993) 7058-7063.
- [96]K. Glasmästar, C. Larsson, F. Höök, and B. Kasemo, Protein adsorption on supported phospholipid bilayers. *Journal of Colloid and Interface Science* 246 (2002) 40-47.
- [97]C. Huber, N. Ilk, D. Runzler, E.M. Egelseer, S. Weigert, U.B. Sleytr, and M. Sara, The three S-layer-like homology motifs of the S-layer protein SbpA of *Bacillus sphaericus* CCM 2177 are not sufficient for binding to the pyruvylated secondary cell wall polymer. *Molecular Microbiology* 55 (2005) 197-205.
- [98]M.M. Stevens, and J.H. George, Exploring and engineering the cell surface interface. *Science* 310 (2005) 1135-1138.
- [99]P. Vadgama, Surface biocompatibility. *Annu. Rep. Prog. Chem., Sect C* 101 (2005) 14-52.
- [100]F. Grinell, Cellular adhesiveness and extracellular substrates. *Int. Rev. Cytol.* 53 (1978) 65.

- [101]B.-K. Katz, E. Zamir, A. Breshadsky, K. Kam, K.M. Yamada, and B. Geiger, Physical state of the extracellular matrix regulates the structure and molecular composition of cell-matrix adhesions. *Molecular Biology of the Cell* 11 (2000) 1047-1060.
- [102]W.J. Koa, J.A. Hubbel, and J.M. Anderson, Protein-mediated macrophage adhesion and activation on biomaterials: a model for modulating cell behavior. *Journal of Material Science: Materials in Medicine* 10 (1999) 601-605.
- [103]M. Wahlgren, and T. Arnebrant, Protein Adsorption to Solid-Surfaces. *Trends in Biotechnology* 9 (1991) 201-208.
- [104]J. Wegener, A. Janshoff, and H.-J. Galla, Cell adhesion monitoring using a quartz crystal microbalance: comparative analysis of different mammalian cell lines. *Eur Biophys J* 28 (1998) 26-37.
- [105]D.M. Gryte, M.D. Ward, and W.-S. Hu, Real-time measurement of anchorage-dependent cell adhesion using a quartz crystal microbalance. *Biotechnology Progress* 9 (1993) 105-108.
- [106]C. Fredriksson, S. Khilm, B. Kasemo, and D.M. Steel, In vitro real-time characterization of cell attachment and spreading. *Journal of Material Science: Materials in Medicine* 9 (1998) 785-788.
- [107]K.A. Marx, T. Zhou, M. Warren, and S.J. Braunhut, Quartz crystal microbalance study of endothelial cell number dependent differences in initial adhesion and steady-state behavior: Evidence for cell-cell cooperativity in initial adhesion and spreading. *Biotechnology Progress* 19 (2003) 987-999.
- [108]C. Fredriksson, S. Kihlman, M. Rodahl, and B. Kasemo, The piezoelectric quartz crystal mass and dissipation sensor: a means of studying cell adhesion. *Langmuir* 14 (1998) 248-251
- [109]C. Modin, A.-L. Strane, M. Foss, M. Duch, J. Justesen, J. Chevallier, L.K. Andersen, A.G. Hemmersam, F.S. Pedersen, and F. Besenbacher, QCM-D studies of attachment of differential spreading of pre-osteoblastic cells on Ta and Cr surfaces. *Biomaterials* 27 (2006) 1346-1354.
- [110]A.-S. Cans, F. Höök, O. Shupliakov, A.G. Ewing, P.S. Eriksson, L. Brodin, and O. Orwan, Measurement of the dynamics of exocytosis and vesicle retrieval at cell populations using a quartz crystal microbalance. *Analytical Chemistry* 73 (2001) 5805-5811.
- [111]J. Wegener, J. Seebach, A. Janshoff, and H.-J. Galla, Analysis of the composite response of shear wave resonators to the attachment of mammalian cells. *Biophysical Journal* 78 (2000) 2821-2833.

- [112] M.S. Lord, C. Modin, M. Foss, M. Duch, A. Simmons, F.S. Pedersen, B.K. Milthorpe, and F. Besenbacher, Monitoring cell adhesion on tantalum and oxidised polystyrene using quartz crystal microbalance with dissipation. *Biomaterials* 27 (2006) 4529-4537.
- [113] D. Fotiadis, S. Scheuring, S.A. Muller, A. Engel, and D.J. Muller, Imaging and manipulation of biological structures with the AFM. *Micron* 33 (2002) 385-397.
- [114] M. Arnold, M. Fritz, E. Bäuerlein, M. Radmacher, E. Sackmann, and A. Boulbitch, Bacterial turgor pressure can be measured by atomic force microscopy. *Physiological Reviews* E 62 (2000) 1034-1044.
- [115] G.T. Charras, P.P. Lehenkari, and M.A. Horton, Atomic force microscopy can be used to mechanically stimulate osteoblast and evaluate cellular strain distribution. *Ultramicroscopy* 86 (2001) 85-95.
- [116] S. Leporatti, A. Gerth, G. Köhler, B. Kohlstrunk, S. Hauschildt, and E. Donath, Elasticity and adhesion of resting and lipopolysaccharide-stimulated macrophages. *FEBS Letters* 580 (2006) 450-454.
- [117] P. Hinterdorfer, H.J. Gruber, F. Kienberger, G. Kada, C. Riener, C. Borken, and H. Schindler, Surface attachment of ligands and receptors for molecular recognition force spectroscopy. *Colloids and Surfaces B-Biointerfaces* 23 (2002) 115-123.
- [118] A. Razatos, Y.-L. Ong, F. Boulay, D.L. Elbert, J.A. Hubbel, M.M. Sharma, and G. Georgiou, Force measurements between bacteria and poly(ethylen glycol)-coated surfaces. *Langmuir* 16 (2000) 9155-9158
- [119] H.-J. Butt, B. Cappella, and M. Kappl, Force measurements with atomic force microscope: Technique, interpretation and applications. *Surface Science Reports* 59 (2005) 1-152.
- [120] D. Leckband, Novel recognition mechanisms in biological adhesion. *Current Opinion in Colloid and Interface Science* 6 (2001) 498-505.
- [121] H. Kim, A. Hideo, O. Toshiya, and I. Atsushi, Quantification of fibronectin and cell surface interactions by AFM. *Colloids and Surfaces B-Biointerfaces* 25 (2002) 33.
- [122] C.M. Franz, A. Taubenberger, P.-H. Puech, and D.J. Müller, Studying integrin-mediated cell adhesion at the single-molecule level using AFM force spectroscopy. *Science STKE* 406 (2007) 1-16.
- [123] E. Sackmann, and R.F. Bruinsma, Cell adhesion as wetting transition? *ChemPhysChem* 3 (2002) 262-269.
- [124] S. Park, D. Koch, R. Cardenas, J. Käs, and C.K. Shih, Cell motility and local viscoelasticity of fibroblasts. *Biophysical Journal* 89 (2005) 4330-4342.

CURRICULUM VITAE

Name: **María Verónica Saravia Silvera**

Date of birth: 25/12/75

Nationality: Uruguayan

Personal e-mail: verosasi@hotmail.com

Education

Oct. 2003- Sept. 2005 **Rovira i Virgili University.** Degree of advanced studies.
Title: Hepatocyte aggregates: Methods of preparation in the microgravity simulation bioreactor. Supervised by Dr. Petros Lenas and Dr. José Luis Toca-Herrera

March 1995- Dec. 2001 **Universidad de la República, Uruguay**
Degree: Chemical Engineer

Research stays

July 2005-August 2005 **Max Planck Institute of Colloids and interfaces, Golm, Germany** (Interfaces Dept., Dr. Andreas Fery's Laboratory)

I applied micro-contact printing to pattern surfaces with polyelectrolytes. The surfaces were characterized with fluorescence microscopy and atomic force microscopy.

June 2006-Sept. 2006 **Max Planck Institute of Colloids and interfaces, Golm, Germany** (Interfaces Dept., Dr. Andreas Fery's Laboratory)

I applied micro-contact printing to pattern SbpA, SbpA-EGFP and SbpA-Streptavidin on surfaces coated with polyelectrolytes. The surfaces were characterized with fluorescence microscopy, contact angle and atomic force microscopy. Beads with

different biotin surface density were prepared and characterized with fluorescence spectroscopy (not included in this work).

May 2007-June 2008 **CIC biomaGUNE, San Sebastián, Spain** (Biosurfaces Unit, Dr. José Luis Toca-Herrera's Laboratory)

I used QCM-D and AFM to study the adhesion and affinity of HepG2 cells to different polyelectrolytes. Force measurements were used to study cell mechanics.

Technical skills

Quartz crystal micro-balance (QCM-D)

Atomic force microscopy (AFM), imaging and force spectroscopy.

Fluorescence and optical microscopy

Scanning electron microscopy

Micro-contact printing

Layer-by-layer technique

Cell and bacterial culture

Scholarships granted

DAAD: Short stay research scholarship for a 3-month stay in Max Planck Institute of Colloids and Interfaces, Golm, Germany

Universidad Rovira i Virgili scholarship for PhD studies during 2003-2007

Congresses and conferences

(* thesis work)

* V. Saravia, J. Folch, J. L. Paternain, J. L. Toca Herrera. Oral: "Monitoring cell adhesion on polyelectrolytes with QCM-D", Q-Sense meeting, Toulouse, France, October 2007.

* V. Saravia, S. Küpcü, D. Pum, U. B. Sleytr and J. L. Toca-Herrera. Poster: "Cell attachment and patterning on polyelectrolytes and bacterial proteins", NanoSpain 2007, Sevilla, Spain, March 2007.

* V. Saravia, M. Nolte, S. Küpcü, A. Fery, D. Pum, U. B. Sleytr and J. L. Toca-Herrera. Poster: “Protein patterning through Micro-contact printing and Layer-by-Layer technique”, XXXI Reunión Iberoamericana de Adsorción, Tarragona, 23 de septiembre de 2006.

* V. Saravia, M. Nolte, A. Fery, D. Pum, U. B. Sleytr, J. L. Toca-Herrera. Poster: “Micro-contact printing of polyelectrolyte for protein patterning”, 6th European Symposium on Biochemical Engineering Science, Salzburg, Austria, August 2006.

* Summer School, International University of Bremen: Complex materials: Cooperative projects of the Natural, Engineering and Bioscience. 24 June- 1 July 2006. Poster: “Surface chemistry and geometrical constrains: Implication in protein adsorption and functionality”, authors: V. Saravia, M. Nolte, S. Küpcü, A. Fery, D. Pum, U. B. Sleytr and J. L. Toca-Herrera

L. Loperena, V. Saravia, D. Murro, M. D. Ferrari, C. Lareo, “Butter oil as model substrate to Evaluate Milk Fat Degrading Microorganisms Used in Bioaugmentation Strategies”, VII Seminário de hidrólise enzimática de biomassas, VII SHEB, Maringá, Paraná, Brazil, 2002

V. Saravia, D. Murro, M. D. Ferrari, C. Lareo, L. Loperena, “Uso del butter oil como substrato modelo para evaluar la degradación microbiana de la grasa de leche”, V Feria – Congreso Latinoamericano de Biotecnología, I Congreso Uruguayo de Biotecnología, Place: Montevideo, Uruguay, 2002

M. D. Ferrari, C. Lareo, C. Lima, L. Loperena, D. Murro, V. Saravia, C. Scapiello, “Bioaumentación de sistemas de tratamiento biológico de efluentes: uso y producción de inóculos especializados”, V Feria – Congreso Latinoamericano de Biotecnología, I Congreso Uruguayo de Biotecnología, Montevideo, Uruguay, 2002

V. Saravia, L. García, M. D. Ferrari, C. Lareo, L. Loperena, “Evaluación de un inóculo comercial para el tratamiento biológico de un efluente de lactería”, V Encuentro Nacional de Microbiólogos, Montevideo, Uruguay, 2001

Publication list

(* thesis work)

* Bacterial protein patterning by micro-contact printing of PLL-g-PEG. V. Saravia, S. Küpcü, M. Nolte, C. Huber, D. Pum, A. Fery, U. B. Sleytr, and J. L. Toca-Herrera. *Journal of biotechnology*, 130 (3), p.247-252, Jun 2007

* Coating of immobilised laccase for stability enhancement: A novel approach. S. Rodriguez Couto, J. F. Osma, V. Saravia, G. M. Gubitz, and J. L. Toca Herrera. *Applied Catalysis A, General*, 329, p.156-160, Oct 2007

* Sunflower seed shells: A novel and effective low-cost adsorbent for the removal of the diazo dye Reactive Black 5 from aqueous solutions. J. F. Osma, V. Saravia, J. L. Toca-Herrera, and S. Rodríguez Couto. *Journal of Hazardous Materials*, 147 (3), p.900-905, Aug 2007

* Mandarin peelings: The best carbon source to produce laccase by static cultures of *Trametes pubescens*. J. F. Osma, V. Saravia, J. L. Toca-Herrera, and S. Rodríguez Couto. *Chemosphere*, 67 (8), p.1677-1680, Apr 2007

Performance of a commercial inoculum for the aerobic biodegradation of a high fat content dairy wastewater. L. Loperena, M. D. Ferrari, V. Saravia, D. Murro, C. Lima, L. Ferrando, A. Fernandez, and C. Lareo. *Bioresource Technology*, 98 (5), p.1045-1051, Mar 2007

Kinetic properties of a commercial and a native inoculum for aerobic milk fat degradation. L. Loperena, V. Saravia, D. Murro, M.D. Ferrari and C. Lareo, *Bioresource Technology*, Volume 97, Issue 16, November 2006, 2160-2165.

Butter oil as model substrate to evaluate milk fat degrading microorganisms used in bioaugmentation strategies, V. Saravia, D. Murro, M.D. Ferrari, C. Lareo and L. Loperena, *FEB*, 13, 2004, 353-355

Uso de inóculos diseñados para la bioaumentación de sistemas biológicos de tratamiento de efluentes conteniendo grasas. M.D. Ferrari, C. Lareo, L. Loperena, D. Murro, and V. Saravia. *Revista de la Asociación de Ingenieros Químicos del Uruguay*, 22, 2002, 21-27.